



THE HONG KONG
POLYTECHNIC UNIVERSITY

香港理工大學

Pao Yue-kong Library

包玉剛圖書館

Copyright Undertaking

This thesis is protected by copyright, with all rights reserved.

By reading and using the thesis, the reader understands and agrees to the following terms:

1. The reader will abide by the rules and legal ordinances governing copyright regarding the use of the thesis.
2. The reader will use the thesis for the purpose of research or private study only and not for distribution or further reproduction or any other purpose.
3. The reader agrees to indemnify and hold the University harmless from and against any loss, damage, cost, liability or expenses arising from copyright infringement or unauthorized usage.

IMPORTANT

If you have reasons to believe that any materials in this thesis are deemed not suitable to be distributed in this form, or a copyright owner having difficulty with the material being included in our database, please contact lbsys@polyu.edu.hk providing details. The Library will look into your claim and consider taking remedial action upon receipt of the written requests.

**MAGNETIC-FIELD INDUCED
LUMINESCENCE VIA STRAIN-MEDIATED
COUPLING**

WONG MAN CHUNG

M. Phil

The Hong Kong Polytechnic University

2016

The Hong Kong Polytechnic University

Department of Applied Physics

**Magnetic-Field Induced Luminescence via
Strain-Mediated Coupling**

Wong Man Chung

**A thesis submitted in partial fulfillment of the requirements
for the degree of Master of Philosophy**

Jan, 2016

CERTIFICATE OF ORIGINALITY

I hereby declare that this thesis is my own work and that, to the best of my knowledge and belief, it reproduces no material previously published or written, nor material that has been accepted for the award of any other degree or diploma, except where due acknowledgement has been made in the text.

_____ (Signed)

_____ **Wong Man Chung** _____ (Name of student)

Abstract

Compared to photoluminescence (PL) and electroluminescence (EL), little work is reported on magnetoluminescence, because magnetoluminescence effects typically occur under extreme conditions of high magnetic field and low temperature. Owing to the excellent magneto-mechanical coupling property, magneto elastomer has been extensively used in magnetic sensors and actuators. It can be foreseen that the combination of phosphor materials and magneto elastomer is not only an alternative solution to direct magnetic-luminescence but also paving a way to better understanding of the relationship between magnetic field and luminescence.

In this study, novel magnetic-induced luminescence (MIL) phenomenon has first been observed from the flexible magnetic composite laminates via strain-mediated coupling. Red-green-blue (RGB) and white light emissions were observed by the naked eyes from the magnetic composite laminates. The fabrication and morphology, magnetic, and elastic characterizations of the magneto composite laminates will be given. The basic luminescent mechanism, measurement of optical characters and emission modulation will be briefly introduced.

Firstly, the magnetic composite laminates were fabricated by consisting of the metal-ion-doped ZnS microparticles phosphor mixed to polydimethylsiloxane (PDMS)

and another phase consists of Fe–Co–Ni alloy particles mixed to PDMS to form magneto elastomer. In this work, ZnS is chosen as phosphor host because of its non-central symmetric wurtzite structure, which can result in piezoelectric potential when applying strain. On the other hand, the designed magnetic composite can response to external magnetic field and then exhibit large deformation, which can serve as a magnetic actuator to stimulate the doped ZnS in the hybrid system. Magnetization of the magneto elastomer was measured from vibrating sample magnetometer (VSM) at room temperature. The magnetic behavior of the composite can be approximately considered as linear behavior with no significant hysteresis because of negligible coercive field ($H_c \approx 9$ Oe). The Young's modulus for the magnetic elastomer is calculated to be 70 MPa under a zero magnetic field. Measurement shows that both strain and stress of the magnetic elastomer increase monotonically and reproducible after many cycles of operation when the static magnetic field increases from 1.5 to 6 kOe, making it durable and reliable for MIL application.

Secondly, MIL phenomenon has been observed from the phosphor composites via strain-mediated coupling. The pattern of the green colored logo and white color light emission can be seen by the naked eyes from the magnetic composite laminates under an AC magnetic field of $H_{rms} = 3.5$ kOe and frequency of 30 Hz. Interestingly, the achieved

light emissions of the material systems can be modulated in reversible and dynamical manners under the control of low magnetic field at room temperature. The hybrid device performance parameters, including CIE, CCT, luminance, and power efficiency have been tested. The CIE coordinates are found to be (0.3462, 0.3735) and hence the CCT is determined to be 5027 K, indicating the obtained MIL phosphor composite emits a somewhat cool white color.

Finally, optimization design has been done with the structure of magnetic composite laminates and measurement conditions. Therefore, RGB colors were observed with ZnS: Cu, Al and $(\text{Ca}_{1-x}\text{Sr}_x)\text{S}:\text{Eu}$ co-doped phosphor composite laminates under 3.5 kOe AC magnetic fields. Tunable white color was also realized with ZnS: Cu, Al and YAG: Ce co-doped phosphor composite laminates. In this work, the display and light source drive by a magnetic field, providing a new insight and possibility for display and solid state lighting applications in any specific situation where alternating magnetic fields are applicable. The hybrid magnetic composite laminates possess flexible, contactless and free of electric power features, which are attractive for future magnetic sensing and energy harvesting applications.

List of publications

1. Man-Chung Wong, Li Chen, Ming-Kiu Tsang, and Jianhua Hao, “Magnetic-induced luminescence from flexible composite laminates by coupling magnetic field to piezophotonic effect”, **Advanced Materials**, 2015, **27**, 4488-4495. (IF: 17.49) (Featured in Frontispiece, and highlighted as "Materials: Magnetic opportunities" by Chief Editor, Dr. Oliver Graydon in "News and Views", *Nature Photonics*, 9, 558 (2015)).
2. Li Chen, Man-Chung Wong, Gongxun Bai, Wenjing Jie and Jianhua Hao, “White and green light emissions of flexible polymer composites under electric field and multiple strains”, **Nano Energy**, 2015, 14, 372-381. (IF: 10.355)
3. Long-Biao Huang, Gongxun Bai, Man-Chung Wong, Zhibin Yang, Wei Xu, and Jianhua Hao, "Magnetic-assisted noncontact triboelectric nanogenerator converting mechanical energy into electricity and light-emissions", **Advanced Materials**, 2016, 28, 2744. (IF: 17.49)

Acknowledgements

I would like to express my appreciation to my supervisor Dr. J. H. Hao for his excellent guidance and constant encouragement throughout the whole period of my research work.

Moreover, I would like to thank Dr K. W. Kwok and Dr C. W. Leung for their encouragement, technical support in synthesis and characterizations. I would also like to thank the support of Miss L. Chen, Mr. M. K. Tsang and Mr. W. J. Fong for discussion and testing. Also, I would like to thank Mr. C.Y. Tang for giving useful advices, guidance in fabrication and VSM measurement. In addition, I would like to thank Dr. T. L. Wong for teaching me the operation of the SEM.

I gratefully acknowledge the financial support from the Research Grants Council of Hong Kong (GRF No. PolyU 5005/13P) and technical support provided by University Research Facility in Materials Characterization and Device of the Hong Kong Polytechnic University.

Last but not least, I would like to thank my parents and girlfriend for their understanding, constant support and encouragement.



Table of contents

| | |
|--|------------|
| Abstract | I |
| List of publications | IV |
| Acknowledgements | V |
| Table of contents | VII |
| List of Figures and Table..... | XII |
| | |
| CHAPTER 1 INTRODUCTION | 1 |
| 1.1 Luminescence | 1 |
| 1.2 Mechanoluminescence | 4 |
| 1.2.1 Mechanism of mechanoluminescence | 7 |
| 1.2.2 ZnS based phosphor | 11 |
| 1.2.3 Examples of mechanoluminescence | 14 |
| 1.3 Photoluminescence | 18 |
| 1.3.1 Mechanism of photoluminescence | 19 |
| 1.3.2 YAG: Ce PL phosphor | 20 |
| 1.3.3 Long persistence luminescence phosphor | 23 |
| 1.3.4 Mechanism of the long persistence phosphor | 25 |



| | |
|--|-----------|
| 1.3.5 (Ca _{1-x} Sr _x) S: Eu long persistence phosphor | 26 |
| 1.4 Magnetic responsive material | 28 |
| 1.4.1 Theory of magnetic field | 28 |
| 1.4.2 Magnetic material classification | 30 |
| 1.4.3 Soft magnetic materials | 32 |
| 1.5 Magnetorheological elastomer | 36 |
| 1.5.1 Characteristic of dopant in MR elastomer | 38 |
| 1.5.2 Characteristics of polymer packaging MR elastomer | 41 |
| 1.5.3 Mechanism of MR elastomer | 44 |
| 1.6 Motivation of research | 48 |
| 1.7 Scope of work | 50 |
| CHAPTER 2 EXPERIMENTAL TECHNIQUES | 52 |
| 2.1 Composite fabrication | 52 |
| 2.1.1 Spin coating | 52 |
| 2.1.2 3D printing | 56 |
| 2.2 Characterization | 58 |
| 2.2.1 Scanning electron microscopy | 59 |
| 2.2.2 Vibrating sample magnetometer | 60 |
| 2.2.3 Luminescent spectroscopy | 62 |



| | |
|--|-----------|
| 2.2.4 Spectrometer | 64 |
| 2.2.5 Spectroradiometer | 66 |
| 2.2.6 AC magnetic field system | 67 |
| CHAPTER 3 OBSERVATION OF MAGNETIC INDUCED LUMINESCENCE | 68 |
| 3.1 Mechanism of MIL | 69 |
| 3.2 Fabrication of flexible MIL composite laminates | 74 |
| 3.3 Results and discussion | 76 |
| 3.3.1 Relationship between MIL and frequency of magnetic field | 76 |
| 3.3.2 Relationship between MIL and magnetic field strength | 86 |
| 3.3.3 Transient response of MIL | 89 |
| 3.3.4 CIE of MIL | 93 |
| CHAPTER 4 MIL COUPLING WITH PHOTOLUMINESCENCE | 95 |
| 4.1 Composite fabrication | 96 |
| 4.1.1 White MIL composites fabrication | 96 |
| 4.1.2 RGB MIL composite fabrication | 97 |
| 4.1.3 RGB MIL wafer sized composite display fabrication | 97 |
| 4.2 Results and discussion | 98 |
| 4.2.1 Morphology of MIL multicolor display composite | 99 |



| | |
|--|------------|
| 4.2.2 Mechanism for persistence luminescence via MIL | 102 |
| 4.2.3 Transient response | 105 |
| 4.2.4 High frequency AMF induced white MIL | 111 |
| 4.2.5 Demonstration of MIL | 115 |
| 4.2.6 Performance and efficiency | 118 |
| CHAPTER 5 CONCLUSION AND FUTURE WORK | 120 |
| 5.1 Conclusion | 120 |
| 5.2 Suggestions for future work | 124 |
| References | 127 |



List of Figures and Table

| | |
|--|-----------|
| Figure 1-1 Classification of luminescence..... | 1 |
| Figure 1-2 Example of mechanoluminescence, (a) Image and photograph of application of compressional load and ultrasound induced ML, [16] (b) Wind driven ML, [17] (c) white color ML display [18] and (d) the luminescence response of a sputtered ML thin film. [19] | 5 |
| Figure 1-3 (a) Schematic diagram for the mechanism of the dislocation electrostatic interaction model of the EML of crystals. (b) Schematic diagram showing the mechanism of EML emission in a typical EML crystal (1-detraping of the electron and its movement in the conduction band, 2-electron-hole recombination, 3- excitation of dopant, ion. 4- light emission). | 8 |
| Figure 1-4 Energy level diagrams of trivalent lanthanide ions: (a) Er³⁺, (b) Yb³⁺, (c) Tm³⁺ and (d) Eu³⁺. The black-solid, colored-solid, dash-dotted and dashed lines represent energy absorption, light emission, energy transfer and multiphonon relaxation respectively. [31]..... | 10 |
| Figure 1-5 Schematic represents the two crystal structures of ZnS..... | 12 |
| Figure 1-6 Diagram of energy level ZnS: Al, Cu, Mn phosphor..... | 13 |
| Figure 1-7 Schematic diagram shows a typical photoluminescence process..... | 20 |
| Figure 1-8 Emission from (YAG: Ce) phosphor by a blue laser excitation. | 21 |
| Figure 1-9 Energy level diagram of YAG: Ce phosphor under 470 nm excitation. | 21 |
| Figure 1-10 (a) PL and PLE spectrum of a typical YAG: Ce phosphor dealing a | |



photoluminescence process. (b) Its corresponding color temperature.
.....23

Figure 1-11 Bologna stone.25

**Figure 1-12 Energy band diagram showing the persistence luminescence from
photoexcitation.27**

Figure 1-13 Excitation and emission spectra of the CaS,SrS: Eu.....28

**Figure 1-14 Spin alignments of two types of magnetic materials and corresponding
coercive field.32**

**Figure 1-15 Comparison of coercive field of soft with hard ferromagnetic material.
.....34**

**Figure 1-16 Schemes depicting the different types of magnetic responsive materials
obtained from the doping of various polymers with magnetic particles
and illustrations of their response when exposed to a static magnetic
field or AMF.37**

**Figure 1-17 Room temperature magnetization of the Fe-Ni-Co doped magnetic
elastomer versus magnetic field measured by VSM.40**

**Figure 1-18 Mechanical response of a typical MR elastomer under various magnetic
field strength.43**

**Figure 1-19 Various respond of MR elastomer in different structural forms and
composition, (a) Soft, Magnetic Field-Driven hydrogel actuators with
muscle-Like flexibility. (b) MR silicone loaded with soft iron pre-
aligned under a field. (c) Deflection of different membranes, under the
same magnetic field under increasing weight ratios of magnetic
polarizable particle and membrane (weight ratio = 2) for increasing**



| | |
|--|----|
| field strength (right). [75] | 47 |
| Figure 2-1 Schemes depicting the spin coating process. | 55 |
| Figure 2-2 A photograph of the in house 3D printer. | 57 |
| Figure 2-3 A photograph of the SEM in the laboratory. | 59 |
| Figure 2-4 A photograph of the VSM in the laboratory. | 61 |
| Figure 2-5 A photograph of the PL measurement system in the laboratory. | 63 |
| Figure 2-6 A photograph of the spectrometer in the laboratory. | 64 |
| Figure 2-7 A photograph of the spectroradiometer in the laboratory. | 66 |
| Figure 2-8 A schematic of the AC magnetic field system in the laboratory. | 68 |
| Figure 3-1 Frontispiece of Advanced Materials and highlighted by Nature Photonics. | 69 |
| Figure 3-2 Schematic diagram illustrating the field of piezophotonics and MIL. | 69 |
| Figure 3-3 MIL effect based on strain-mediated magnetoluminescent coupling in two phases of magnetic elastomer and mechanoluminescence phosphor. | 70 |
| Figure 3-4 3-D printed ABS mold. | 74 |
| Figure 3-5 PMMA mold for fabrication of the MIL phosphor phase. | 75 |
| Figure 3-6 Emission spectra of ZnS: Al, Cu phosphor based MIL composite under AMF of various frequencies. | 78 |
| Figure 3-7 Emission spectra of ZnS: Al, Cu, Mn phosphor based MIL composite under AMF of various frequencies. | 79 |
| Figure 3-8 A linear relation between luminescence intensity of ZnS: Al, Cu phosphor based MIL and low frequency of magnetic field. | 80 |



Figure 3-9 Emission spectra of ZnS: Al, Cu phosphor based MIL under a high frequency of AMF.....81

Figure 3-10 Intensity of ZnS: Al, Cu phosphor based MIL under a high frequency of AMF.....83

Figure 3-11 Emission spectra of ZnS: Al, Cu phosphor coupled MIL under a high frequency AMF.84

Figure 3-12 Emission spectra of ZnS: Al, Cu, Mn phosphor coupled MIL under various strength of AMF.88

Figure 3-13 Intensity of ZnS:Al, Cu phosphor coupled MIL under various strength of AMF.....89

Figure 3-14 Transient response of green MIL from the Al, Cu-doped ZnS phosphor composite.....90

Figure 3-15 Enlarged graphs of a single cycle. The rising and falling edges of MIL can be fitted to exponential growth (red) and decay (green) functions.92

Figure 3-16 CIE diagram showing the green and white lights of the obtained MIL-based pattern and light source.....94

Figure 3-17 CIE diagram showing the green and tunable blue lights of the obtained MIL-based pattern and light source.....94

Figure 4-1 SEM images of the synthesized PDMS polymer composite laminate consisted of Fe–Co–Ni alloy particle-based magnetic elastomer, metal-ion-doped ZnS microparticle-based mechanoluminescence phosphor and Persistence phosphor.99

Figure 4-2 Schematic showing the coupling between MIL with simultaneous



| | |
|--|------------|
| persistence luminescence. | 103 |
| Figure 4-3 Emission spectra of persistence luminescence excited by MIL under a low frequency of AMF..... | 104 |
| Figure 4-5 Transient characteristics of persistence luminescence via MIL excitation from the Al, Cu-doped ZnS green-phosphor based composite. | 107 |
| Figure 4-6 The rising and falling edges of MIL and persistence luminescence. The Blue line is when the AMF activated. | 109 |
| Figure 4-7 CIE diagram showing the red lights of the obtained persistence luminescence via MIL excitation | 111 |
| Figure 4-8 Emission spectra of YAG: Ce phosphor coupled with MIL excitation under a high frequency AMF. | 112 |
| Figure 4-9 Normalized intensity of YAG: Ce phosphor coupled MIL excitation under a high frequency AMF | 114 |
| Figure 4-10 Displaying green colored logo “PU” representing the abbreviation for the Hong Kong Polytechnic University from MIL materials driven by low magnetic field without (upper) and with a magnetic field (lower), White color emission of MIL light source. [35] | 115 |
| Figure 4-11 Photograph of MIL light source under uniaxial magnetic field of the red color logo representing the Hong Kong Polytechnic University (left) and displaying red, green and blue colored MIL matrix under high frequency AMF (right)..... | 117 |
| Figure 4-12 Photographs of the MIL for color tuning under various AMF frequencies and field strength of 2 kOe..... | 118 |



Table 1 Performance parameters of the emissions based on MIL composite..... 118

Figure 5-1 Schematic showing the prospect of future MIL investigation. 125



Chapter 1 Introduction

1.1 Luminescence

Luminescence is defined as the emission of light by a substance that is supplied with some form of energy rather than heat; so it is a form of cold body radiation. [1-5]

Luminescence can be caused by photon excitation, the passage of a strong electric field, electron beam excitation, or stress on a crystal.

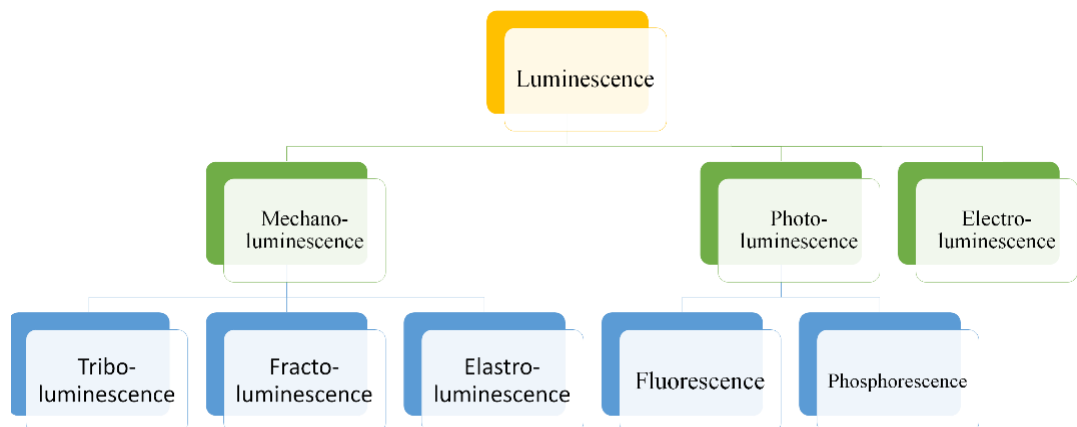


Figure 1-1 Classification of luminescence.

Luminescent has been extensively investigated because of its interesting physics and widespread applications. The past several decades have witnessed a rapid growth in research and development of various forms of luminescent materials.[6]

Luminescence can be distinguished by the method of excitation sources shown in

Figure 1-1. For instance, photoluminescence (PL) is excited by photon,



mechanoluminescence (ML) is stimulated by mechanical stress,[7] and electroluminescence (EL) is emissions of light in response to electric field.[8, 9] Luminescence has a variety of applications such as display, light-emitting capacitor (LEC), laser and biosensor. [10]

Luminescent material is also called phosphors. By means of phosphor, it is a substance that exhibits the trend of luminescence under various stimuli.[11] The types of stimulus that cause luminescent from phosphor depended on the phosphor's crystal structure and its electronic configuration. [12, 13]

By far the most common application of luminescence in daily life is PL in the fluorescent light bulb. A fluorescent bulb consuming the same amount of power as an incandescent bulb will but produce three to five times more light. By using a phosphor coats the inside surface of a fluorescent lamp can absorb ultraviolet light emitted by excited mercury atoms. It re-emits at longer wavelengths visible light. A fluorescent lamp gives off much more light than an incandescent one, and does so without producing heat.

In contrast to the nearly instantaneous activation of fluorescence, phosphorescence involves a delayed emission of radiation after absorption. The delay



may take as much as several minutes, on the other hand phosphorescence continues to appear after the energy source has been removed. For example, the hands and numbers on a watch that glows in the dark, as well as any number of other items, are coated with phosphorescent materials. Television tubes also use phosphorescence. The tube itself is coated with phosphor, and a narrow beam of electrons causes excitation in a small portion of the phosphor. The phosphor then emits the primary colors of light, red, green, or blue light and continues emission after the electron beam has moved on to another region of phosphor on the tube. As it scans across the tube, the electron beam is turned rapidly on and off, creating an image made up of thousands of glowing, colored dots.

EL devices are fabricated using either organic or inorganic electroluminescent materials. The active materials are generally semiconductors of wide enough bandwidth to allow exit of the light. These devices have low power consumption compared to competing lighting technologies, such as neon or fluorescent lamps. And unlike neon and fluorescent lamps, EL lamps are not negative resistance devices so no extra circuitry is needed to regulate the amount of current flowing through them. This, together with the thinness of the material, has made EL technology valuable to the



advertising industry. Relevant advertising applications include electroluminescent billboards, wires and signs. EL manufacturers are able to control precisely time and areas of an electroluminescent sheet illuminate. This has given advertisers the ability to create more dynamic advertising that is still compatible with traditional advertising spaces. It's also used as an application for public safety identification involving alphanumeric characters on the roof of vehicles for clear visibility from an aerial perspective. Electroluminescent lighting, especially electroluminescent wire (EL wire), owing to its flexibility and safety, EL wires have also made its way into clothing as many designers have brought this technology to the entertainment and nightlife industry

1.2 Mechanoluminescence

ML is the emission of light originated from fracture or deformation during the application of mechanical stress on a solid. [14] The phenomenon of ML has attracted more attention because of its potential application in sensing structure damage, fracture, and deformation. ML was first reported by Boyle in 1664 that a particular



diamond produced a very vivid, but exceedingly short-lived splendor when pressed on with a steel bodkin. [15] Waller in 1684 reported that when substances such as white sugar, loaf sugar and rock salt were crushed in mortar, they gave such intense light the sides of the mortar and the shape of the pestle could distinctly be displayed.

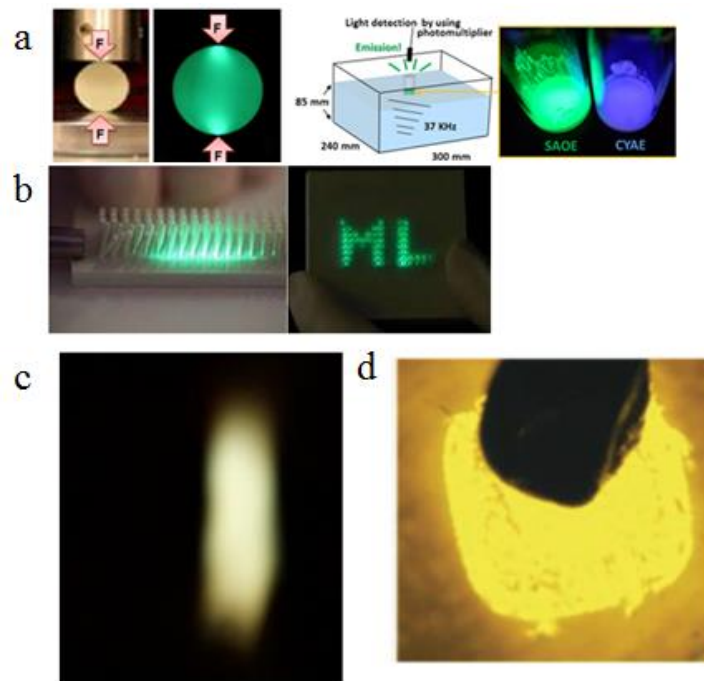


Figure 1-2 Example of mechanoluminescence, (a) Image and photograph of application of compressional load and ultrasound induced ML, [16] (b) Wind driven ML, [17] (c) white color ML display [18] and (d) the luminescence response of a sputtered ML thin film. [19]

ML can convert the local mechanical energy into light emission with the



application of various stresses, such as deformation, friction, impact, and vibration.[14, 18] Figure 1-2 gives some example of mechanoluminescence from previous studies.

On the whole, the physical processes involved in ML indicate that there are two types of ML, including deformation ML (DML) and tribo-ML (TML). DML is produced owing to the physical processes induced during deformation of solids, whereas the TML is produced due to the contact phenomenon during the contact or separation of two dissimilar materials initially intact. DML is independent of the material used to produce the deformation and the contact phenomenon, but depends only on the material under deformation. This DML may further be divided into three types, elastic ML (EML) induced by elastic deformation, plastic ML (PML) induced by plastic deformation and fracto-mechanoluminescence (FML), in which the ML is induced by fracture of solids. TML may further be subdivided as electrically induced TML, chemically induced TML and thermally induced TML, in which the TML is induced by triboelectrification, tribochemical reaction and tribothermal generation, respectively. [20]



1.2.1 Mechanism of mechanoluminescence

The mechanism of elastic ML emission can be explained as follows, which utilizes the piezoelectrically-stimulated electron detrapping model. When applied a mechanical stress on the crystals with a non-symmetric structure, deformation produces an inner piezoelectric field. This non-symmetrical structure either arises from the substantial defect of doped ions or the special phases of the host lattice. Owing to the decrease of the trap-depth caused by piezoelectric field, electrons detrapped from filled-electron traps and reached the conduction band. Then detrapped electrons may recombine with the holes trapped in the defect centers or they may jump to the valence band subsequently energy released non-radiatively. During the recombination process of electron and hole pairs, the energy transferred to doped ions and light emitted. As the piezoelectric field is also produced during the release of pressure, ML happens when the pressure is released. The mechanism of ML occurrence during the release of pressure should be similar to pressure arising. These two theories were demonstrated in the Figure below. [15]



theory of trapping and de-trapping of charge carriers in the semiconductor can be studied using ML intensity. They also concluded the values of the relaxation time of surface charges, the quadratic relation of pressure, and the threshold pressure for illumination to take place can be deduced from the measurement of the time-dependence of ML. Z. L. Wang gives rise and demonstrated that a field of piezophotonic and give its mechanism. [23, 24]

Nearly 50% of all inorganic salts and organic molecular solids exhibit the phenomenon of ML/FML. Only a few limited cases of non-destructive ML materials have been found. Rare earth doped aluminate or silicate crystals and metal ions doped ZnS crystals ML phosphors, have been reported exhibit EML. [23, 25, 26] To date more than a dozen kinds of inorganic materials with excellent EML performance have been successfully developed. These inorganic materials include common silicate, titanate, aluminate and phosphate systems, together with traditional red phosphors $\text{BaTiO}_3\text{-CaTiO}_3$: Pr, [27] green phosphors SrAl_2O_4 : Eu, [28] and blue phosphor CaYAl_3O_7 : Eu were developed. [29] By screening various ML compounds, SrAl_2O_4 and ZnS are widely accepted as the most effective candidates for ML. It is basically due to their relatively high stability such that they are able to render high ML efficiency.



Another reason for the appeal of these two compounds for ML is the high solubility of various lanthanide and transition-metal dopants. Figure 1-4 gives the typical examples of energy level diagrams of trivalent lanthanide ions. [30] The doped ions can generate additional energy levels that transform the deformation generated excitation energy against non-radiative relaxations; thereby maximizing optical emissions at various wavelengths that are dependent on the dopant composition concentration and intensity.

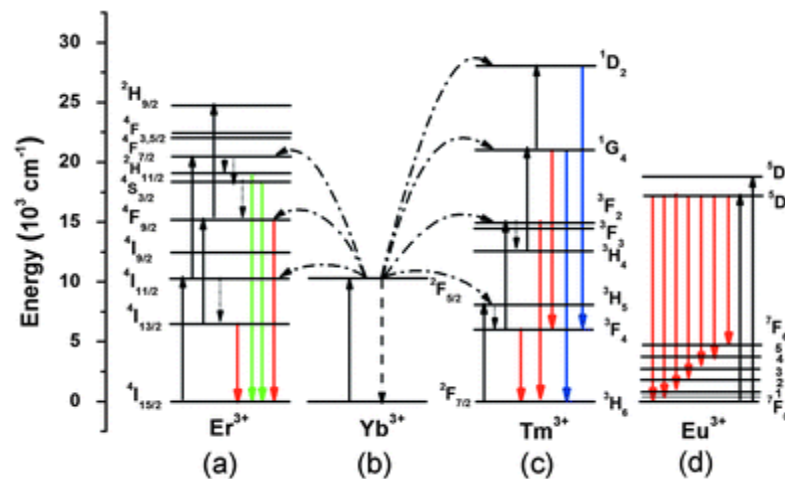


Figure 1-4 Energy level diagrams of trivalent lanthanide ions: (a) Er^{3+} , (b) Yb^{3+} , (c) Tm^{3+} and (d) Eu^{3+} . The black-solid, colored-solid, dash-dotted and dashed lines represent energy absorption, light emission, energy transfer and multiphonon relaxation respectively. [31]



1.2.2 ZnS based phosphor

The in deep study of ML from doped ZnS can be regarded since 1960s. [32] However, early studies did not attract much attention owing to the weak ML emissions. In 1999, Xu and co-workers found that an appropriate amount of Mn^{2+} dopants led to strong orange ML luminescence of ZnS crystals under a relatively small mechanical stimulus. [33] On the basis of this discovery, they sputtered a Mn^{2+} -doped ZnS films on various ceramic substrates. An elevated substrate temperature resulted in bright ML emissions that were one magnitude brighter than those of its bulk counterparts. The study conducted by the group of Xu has stimulated interest in developing type II–VI semiconductor-based ML phosphors. In parallel efforts, Jeong and co-workers demonstrated composite ML films composed of a PDMS matrix incorporated with commercial Cu^{2+} -doped ZnS phosphors. The flexible film displays bright and consistent ML emissions when subjected to repeated mechanical stress, demonstrating high durability. [17, 34] They employed a combination of different types of ML phosphors, ZnS: Cu, ZnS: Mn, incorporated into the same polymer matrix, which enables one to tune the optical characteristics via doping in hosting matrix.

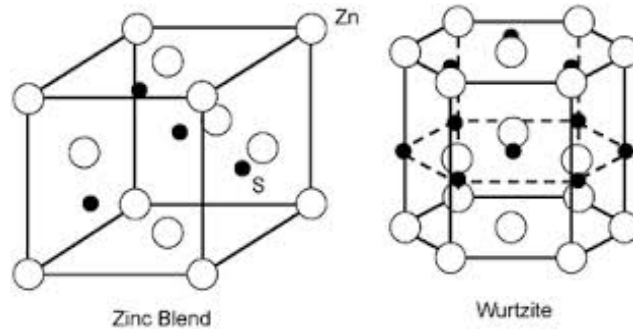


Figure 1-5 Schematic represents the two crystal structures of ZnS.

The ML mechanism beneath ZnS; Al, Cu, and ZnS: Cu ML should be the same, consider ML from ZnS: Mn as an example. Owing to its non-centrosymmetric structure, the deformation of ZnS: Mn crystals produced a piezoelectric field. Take Mn doped ZnS for example. The piezoelectric field near the Mn^{2+} ions increased owing to the change in local crystal structure. The trap-depth is decreased due to the piezoelectric field or due to the band bending the de-trapping of electrons from filled-electron traps takes place, as proposed by Wang et al. [23] As the crystal structure deform and formed a piezoelectric field, electrons reach the conduction band. The electrons may be reaching the conduction band and recombine with the holes trapped in the defect centers. Figure 1-6 show the whole energy band diagram of ZnS:Al, Cu, Mn. In order ML to commence, electrons may jump to the valence band and subsequently energy may be released non-radiative. These non-radiative energy



released during electron–hole recombination may be transferred to the Mn^{2+} , Cu^+ , Al^+ ions whereby these ions may get excited. The de-excitation of excited ions gives rise to the light emission characteristic of the doping ions. The Mn^{2+} metal-ions doped ZnS peaked at 588 nm (2.11 eV) is due to the radiation energy transition between 4T_1 and 6A_1 .

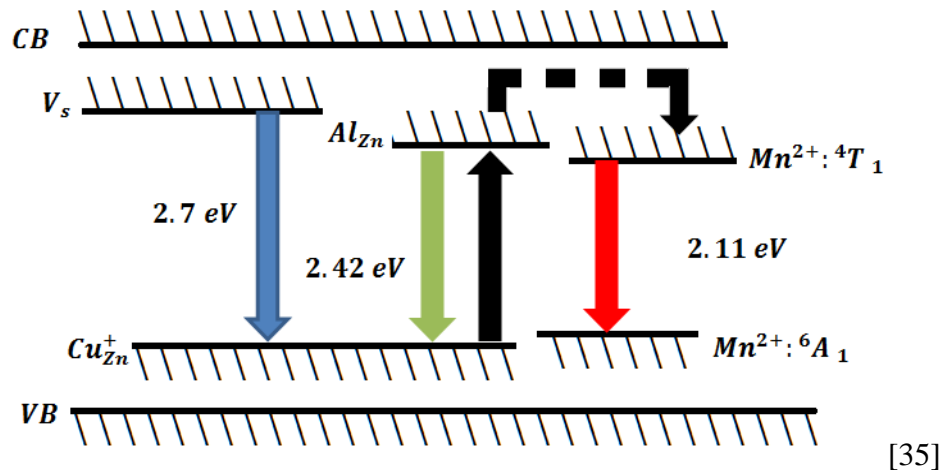


Figure 1-6 Diagram of energy level ZnS: Al, Cu, Mn phosphor.

To understand the emissions of green and blue process, schematic illustrates a band diagram also shown in Figure 1-6. Similarly, the ZnS compound trap electrons to form shallow donor levels in sulfur vacancies (V_s), while taking blue and green emissions from the Al^{3+} , Cu^+ . They also create another donor levels and substitutional occupies the Zn^{2+} site (Al_{Zn}), and substituted for (Cu_{Zn}) and generate acceptor level which can trap holes. The energy level diagram indicates, there can be two light-



emission peaks, an intense light emission at 2.42 eV originates from the D–A pairs and recombination between $Al_{Zn} \rightarrow Cu_{Zn}$.

1.2.3 Examples of mechanoluminescence

In order to apply the ML material as a light source, the surface of the ML composite should have the most efficiency of mechanical-optical coupling with the strongest luminescence intensity. A hybrid material that combined ML material and photo-reactant material proves a new way for photo-coupling. As Terasaki et al. reported a preparation method for a hybrid material consisting of the ML material and TiO_2 photo catalytic nano particles. [16] By using the surface sol gel method, they succeeded in coating the TiO_2 photo catalytic nano particles on the surface of the ML material, thus preparing a hybrid material where the nanoparticles took over the emitted ML and commerce photocatalysis activities.

Zhang et al. revealed that another semiconductor $Ca_2MgSi_2O_7: Eu$ micro-particles emit green light under the mechanical stress. [36] The ML showed a similar spectrum as PL implies that ML is emitted from the same center of Eu^{2+} ions as PL. So a visible ML green light emitted when pressing the sample. They also quantify



using lab-made Atomic-force microscope (AFM) ML investigation system, to investigate the ML of single micro-particle under the application of micro force, they conclude each particle require a 10 μN force to emit a signal.

Impulsive excitation of ML of gamma ray irradiated CaSO_4 : Eu phosphors have been studied by Kher et al. [37] ML was impulsively emitted by dropping a load onto the sample. Three distinct ML emission peaks have been observed. For CaSO_4 : Eu the ML intensity increases with the increasing concentration of the Eu dopant. The effect of temperature on the FWHM, spectra and peak ML intensity was discussed. On the basis of the result obtained they deduced that ML excitation is related to the movement of dislocation with defect centers, or dopant caused defect centers, the increase in ML with temperature is due to the enhancement in these dislocation capture probability.

A technique of cultivating and measure ultrasonic power with a ML sensing film was studied by Zhan et al. [38] A linear relationship was observed between the ultrasonic power and the ML intensity induced by ultrasonic vibration, indicating that ultrasonic power can be evaluated by measuring ML intensity.

The parameters affecting impact ML of the SrAl_2O_4 : Eu film and ZnS: Mn coating is determined by Chandra. [39] The ML technique can be used to determine



the impact parameters in the elastic deformation and plastic region deformation as well as fracture ML can also be used to determine the impact parameters for the collision between solid and liquid. The ML material was coated on the surface of a solid. The measurement of fracto-ML in microsecond and nanosecond range may provide a tool for studying the fragmentations in solids by the impact. Using a CCD camera, the sizes of contact area, the depth of compression can be determined for different intervals of time.

Ballistic impacts of the tribo-ML properties of ZnS: Mn doped sample is studied by Fontenot et al [40] using ballistic impacts of specially prepared rounds manufactured in two different calibers. The tribo-ML emission spectrum was then recorded as the rounds impacted the target. Results show a ~1 nm shift in the emission spectrum with increased impact energy.

Terasaki and co-workers first proposed the concept of utilizing ML phosphors as signal sources for bioimaging and phototherapy application. They investigate the emission of light from the ML phosphor composite under stimulation from an ultrasonic wave. The investigation was nondestructive and noninvasive. [16] When compared with labeling techniques reliant on PL, this method avoids photonic damage



to tissues and does not suffer from strongly as compare with attenuation of excitation radiation owing to tissue absorption and scattering. Recently, Jeong and co-workers reported a patterned ML device composed of PDMS elastomer incorporated with ZnS microparticles. [34] By using a combination of doped ZnS phosphors at various weight ratio, they demonstrated light emission of tunable colors following excitation by an air flow. The study highlights the viability of constructing wind-driven display devices. [17] However, the generation of sufficiently bright emission by natural wind alone that lacks a harmonic frequency remains an arduous task to solve before this technology can be put into practice. ML phosphors have also been employed as a light source to drive photocells. In one example, Terasaki and co-workers constructed a system combining an epoxy pellet containing $\text{SrAl}_2\text{O}_4:\text{Eu}$ phosphors and a silicon solar cell. [41] The photocurrent was successfully observed by compressing the sample coupled into the solar cell. This photocell composite system is capable of enduring in certain extreme environment, such as deep sea and arctic regions.

Wang et al [42] developed the world's first ML for a practical use in the sensing information region in a ML handwriting system consisting a ML material and a PET thin film. The ML material developed in their laboratory was a ML composite, an



epoxy doped with efficient ML materials of ZnS:Mn used as a light source, and a photolithography used as the patterning . With the application of compressive stress via handwriting on the ML composite in the system, the photocurrent arise from to ML by a sensor was successfully recorded for further analysis.

1.3 Photoluminescence

Photoluminescence (PL) is the light emission from material after the absorption of photons. It is one of many forms of luminescence (light emission) and is initiated by photoexcitation (excited by photons). Following excitation, various relaxation processes typically occur in which other photons are re-radiated. The time interval between absorption and emission vary. The ground state is defined as the state with the lowest energy; states of higher energy are called excited states. An emission center possesses several distinct reservoirs of energy levels, including electronic, vibrational, rotational, transitional, and those associated with a nuclear and electron spin. Modifying the photon energy with luminescent materials has provided exciting opportunities for applications in photonics, photovoltaics, diagnostics, and therapeutics. [30]



1.3.1 Mechanism of photoluminescence

PL comprises both fluorescence and phosphorescence processes and originates from an absorption/emission process between different electronic energy levels in the material. The intensity and emission of PL depends on which material under illumination and which wavelength of excitation employed. Aforementioned, the luminescence of phosphors is extremely important in controlling and processing light for active components of light sources, optical sensing, and display devices. Short wavelength light is possible to obtain yellow, red, as a secondary light from a suitable phosphor, such that it can complement the emission to yield a white light.

The absorption of a photon, which is used to excite the luminescence, takes place by either the host lattice or by doped impurities. This process involves transport of energy through the luminescent materials. After both radiative transition and light emission from host lattice, or non-radiative transition from host to dopant, the emission takes place on the impurity ions, which generate the desired emission. Quite frequently, the emission color can be adjusted by choosing the proper impurity ion, without changing the host lattice in which the impurity ions are incorporated.

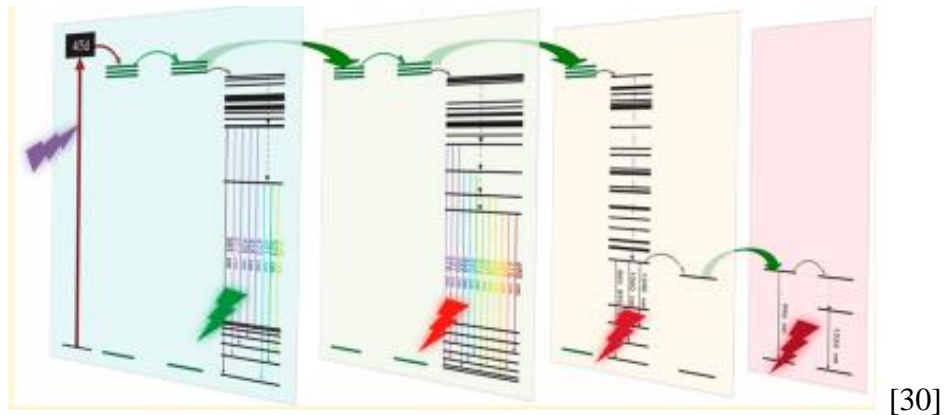


Figure 1-7 Schematic diagram shows a typical photoluminescence process.

1.3.2 YAG: Ce PL phosphor

Yttrium aluminum garnet ($Y_3Al_5O_{12}$, YAG) is a synthetic crystalline material of the garnet group, it have been widely studied in the application of displays because of their stability at the conditions of high irradiance. YAG is used as the host material of full-color phosphors by changing of the doping materials, namely Ce, Tb, Eu, and Tm. Especially YAG: Ce is regarded as an efficient phosphor for converting the blue radiation into a very broad yellow emission band. Such that, the corresponding yellow emission from YAG: Ce is intense enough to complement excitation blue light which escapes through the phosphor in order to produce a white light. As shown in Figure 1-8.



Figure 1-8 Emission from (YAG: Ce) phosphor by a blue laser excitation.

The mechanism beneath this excitation of the YAG: Ce phosphor to produces a tunable white luminescence. As in Figure 1-9, excitation and emission bands can be ascribed to the transitions of Ce^{3+} ions between the 4f and 5d levels.

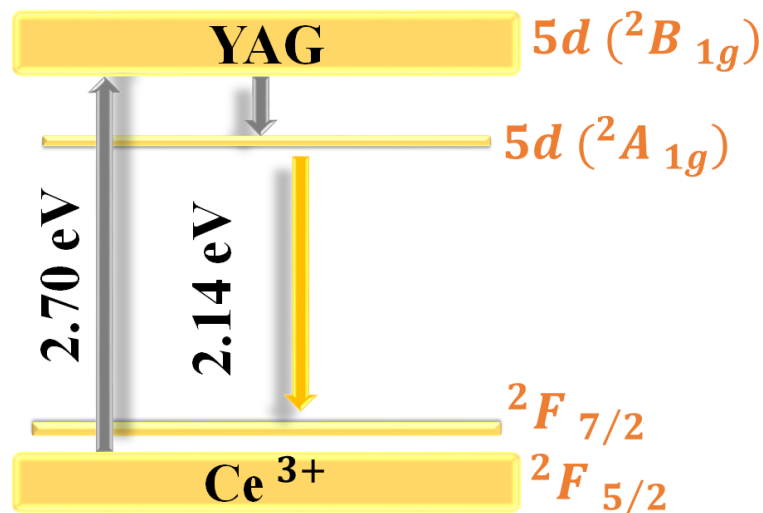


Figure 1-9 Energy level diagram of YAG: Ce phosphor under 470 nm excitation.

The energy level diagram of Ce^{3+} with the demonstrate that Ce^{3+} has a $4f_1$



configuration, the spin-orbit interaction causes the ground state electron orbit 2F splits into a $^2F_{7/2}$ excited state and a $^2F_{5/2}$ ground state. According to the radial wave function for the excited 5d electron extends spatially beyond the closed $5s^25p^6$ shells, the 5d levels are strongly perturbed by the ligand field of the host. Thus, the 4f-5d transitions are easily influenced by the ligand field around Ce^{3+} . As in YAG crystals, part of the Ce^{3+} ions replace the Y^{3+} ions, and the 5d configuration of Ce^{3+} deduced a strong crystal field cause a large crystal-field splitting. This splitting causes lowering of the position of the lowest 5d level and the 4f-5d transition of Ce^{3+} shifts to the visible emission region. The excitation band centered at 452 nm attributed to the first allowed 4f-5d transition of Ce^{3+} ions, from the Ce^{3+} 4f level ($^2F_{5/2}$) to its lowest 5d ($^2A_{1g}$) level. The emission band centered at 535 nm is consigned as the combination of the emission centered at 580 and 520 nm, which are attributed to the transition of Ce^{3+} : 5d ($^2A_{1g}$) \rightarrow 4f ($^2F_{7/2}$) and Ce^{3+} : 5d ($^2A_{1g}$) \rightarrow 4f ($^2F_{5/2}$), respectively. Figure 1-9 give the energy band gap diagram. [43]

The dopant, trivalent Ce, ion has one electron in the 4f state. The ground state of Ce^{3+} is divided into $^2F_{7/2}$ and $^2F_{5/2}$ with an energy difference of 2200 cm^{-1} . The next higher state begins from the 5d state and such that the 4f-5d transitions are parity



allowed. The 5d state is splitted by crystal field and hence is more than one Ce^{3+} absorption bands in the excitation spectrum in the board region between 200 and 500 nm. And there are three broad bands with maxima at 233, 340 and 463 nm because in the YAG host, Ce^{3+} occupies a distorted cube. The excitation band covering from 400 to 500 nm is the most intense band and provides grounds to apply the phosphor to blue ML. The emission wavelength of Ce^{3+} is very sensitive to the crystallographic environment it exposed to, acting as the basis for the red or blue shift of Ce^{3+} emission. Unlike the $4f$ electron with the shielding effect of outer shell $6s$ and $5p$ electrons, the shift of the $5d$ and hence the d–f emission band of Ce^{3+} ion is heavily dependent on the local crystal field surrounding the Ce^{3+} ions.

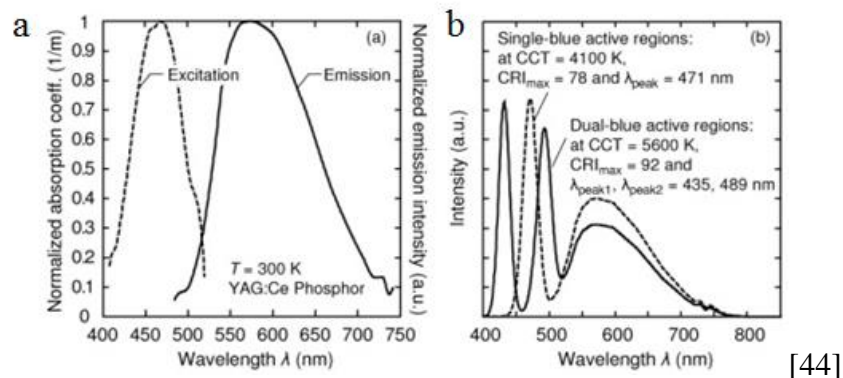


Figure 1-10 (a) PL and PLE spectrum of a typical YAG: Ce phosphor dealing a photoluminescence process. (b) Its corresponding color temperature.

1.3.3 Long persistence luminescence phosphor

Commonly referred as phosphorescence, persistent luminescence is the



phenomenon encountered in materials which make them glow in the dark after the end of an excitation with UV or visible light for a long period of time. [45, 46] In some cases luminescence can last for hours after the stoppage of the excitation. Phosphors with persistent luminescence have been rapidly developed in the past decades, largely stimulated by the green persistent phosphors have already been commercialized and are being widely used as night-vision materials in various important fields. Because of their sufficiently strong and long-lasting (>10 h) persistent luminescence and their ability to be excited by either sunlight or the visible spectrum.[47] During the 1600 century following the discovery of the bright emission from the (reduced) Bologna stone, Figure 1-11. The phenomenon did not cease to arouse the interest of both scientists and laymen, persistent luminescence mechanisms have somewhat converged in what is known now, though there is not really any widespread agreement on the details.[48]

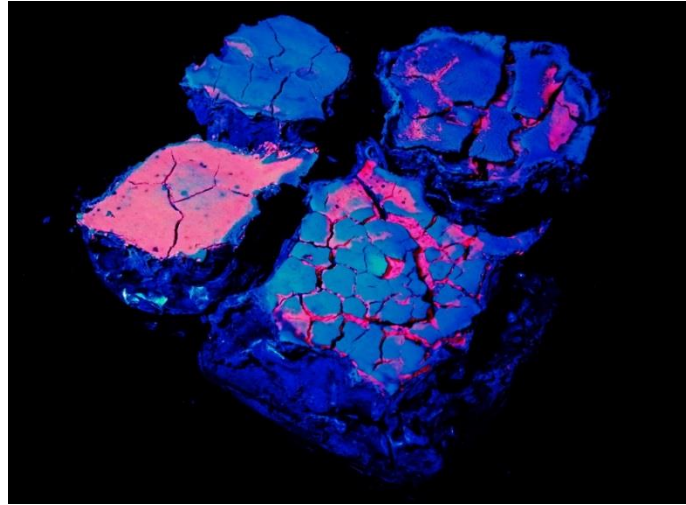


Figure 1-11 Bologna stone.

1.3.4 Mechanism of the long persistence phosphor

In persistent phosphors, two kinds of active center are involved emitters and traps. [49] Emitters are centers capable of emitting radiation after being excited. Traps usually do not emit radiation, but store excitation energy and release it gradually to the emitters owing to thermal or other physical stimulations. Whereas the emission wavelength of a persistent phosphor is mainly determined by the emitter, the persistence intensity and time are determined by the trapping states. [47] Whereas significant achievements have been made in visible persistent phosphors, the research and development of persistent phosphors in the NIR region have been greatly interested recently.



1.3.5 (Ca_{1-x}Sr_x) S: Eu long persistence phosphor

As a highly efficient red emitting simultaneous persistence luminescence phosphors, strontium sulfide, calcium sulfide doped Europium (Ca_{1-x}Sr_x) S: Eu, has been attracting a lot of investigation. The inorganic phosphors typically consist of a host lattice doped with activator ions in small concentrations. There are two types of activator ions can be such that these rare-earth phosphors can be separated into two types: broadband emitting owing to the transition between the 5d and 4f of Eu²⁺. As shown in Figure 1-12, the activator ion in the first type strongly interacts with the host lattice, when these d electrons are involved. The strong coupling of the electronic states with the vibrational modes of the lattice mainly leads to more or less broad bands in the spectrum. The emission spectrum arises from the d-f transition of 4f⁶ 5d¹ (T_{2g}) to 4f⁷ ⁸S_{2/7}, where there is no shield of active electronic level against the surrounding ligands. The position and width of the emission band are strongly dependent on the lattice the co-dopant, which is incorporated into the degree of splitting of the 4f⁶ 5d¹ level into the terms T_{2g} and E_g and increasing field strength of the ligand. This all result a lowering of the gap between (T_{2g}) and E_g, hence, a red-shift of the emission band.

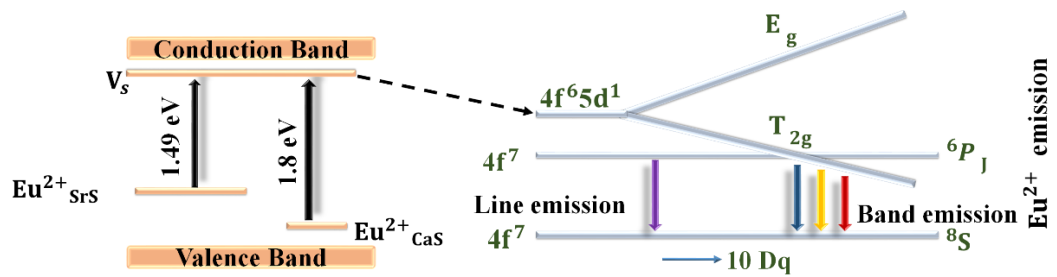


Figure 1-12 Energy band diagram showing the persistence luminescence from photoexcitation.

The excitation spectra of this red phosphor consist of two broad bands, one is low-energy green excitation band (400–550 nm) and the other is high-energy UV excitation band (250–350 nm). The emission is practically independent of the excitation wavelength. The origin of these excitation bands from previous report stated it has been related to the multiplicity of defect levels arising between valence and conduction band due to the non-statistical distribution of cations in the solid solution, especially for the calcium-rich material. [50] Such that the stoichiometric ratio between calcium and strontium played a strong role in here, the other is the doping level/molar ratio of europium. As a result, the single emission band at 600–750 nm is practically independent of excitation wavelength. The peak of the emission band shown in this work is found to be 645 nm.

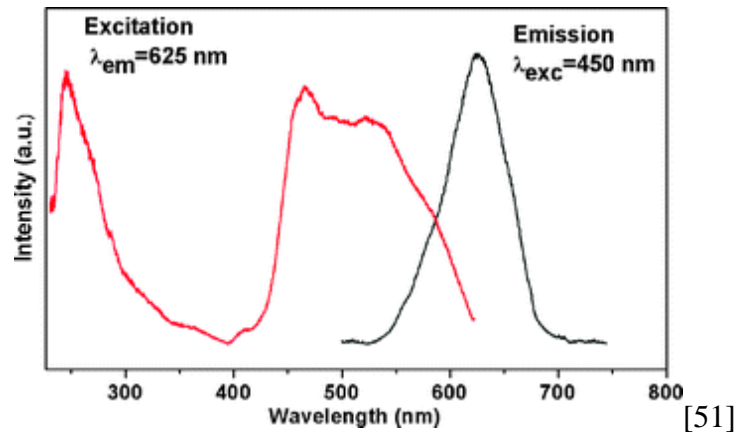


Figure 1-13 Excitation and emission spectra of the CaS,SrS: Eu.

1.4 Magnetic responsive material

1.4.1 Theory of magnetic field

Magnetic field lines can reach a certain density within a material, quantified by the material's magnetic permeability. The definition of the magnetic flux density describes as the number of field lines per unit area. The flux density decreases quickly with increasing distance from a magnetized surface.

Elements that exhibit magnetism at room temperature include iron, nickel and cobalt. Some of the strongest magnetic fields can be achieved with alloys such as samarium cobalt (SmCo) or neodymium iron boron (NdFeB). On the other hand, magnetic fields are generated around any current carrying wire explained by the theory



of special relativity from electron moving at relativistic speed related to other. Such fields can be switched on and off and tuned depending on the applied current.

A magnetic field can be from a magnet or an electromagnetic. And a magnetic field can be regarded as two types of field, namely a homogeneous and an inhomogeneous magnetic field. By combining magnets into arrays, complex magnetic field patterns can be achieved even on the micron-size scale. [52] In a homogeneous magnetic field, ideally the density of flux lines is constant over a distance there is no gradient in the flux density. In an inhomogeneous magnetic field, however, there is a gradient in the density of flux lines over distance from the magnetized surface.

Homogeneous fields are required for numerous high end application such as NMR spectroscopy and magneto-hydrodynamic pumping or traditional nuclear power plant NaK circulation. [53] The method usually involves utilizing large size magnets respect to the fluid volume employed.

A time varying magnetic field used to provide a dynamic response that can be achieved by using an electromagnet with a highly permeable core material such as soft iron or the famous mu-Metal. It can be rather challenging to achieve a desired magnetic field pattern, strength and gradient over a confined space. Especially with



low or moderated frequency when considering how quickly the flux density decreases with distance from the magnet surface and the time response for a ML. For manipulation at room temperature, two approaches can be taken: electromagnets or conventional permanent magnets. The chosen conventional permanent magnets are placed close to volume considered, as having the advantages of ease of fabrication, low temperature and ease of fabrication.

1.4.2 Magnetic material classification

According to their magnetic susceptibility, materials are classified as diamagnetic, paramagnetic and ferromagnetic.

Diamagnetic materials, with its susceptibility smaller than 0, are repelled from magnetic fields, as diamagnetic material have only paired electrons, such that they are instinct drive towards minima of magnetic field strength. Most materials are weakly diamagnetic, including all elements of group 5 and 7 and all noble gas, water, proteins, DNA, cells, polymers, wood and glass. Although the response is quite interesting, the magnitude of response is often weak.

Paramagnetic materials have at least one unpaired electron in their atom, which



is unable to magnetize, but having magnetic response. As their magnetic susceptibility equal to zero, aligned with a magnetic field and experience a small force towards magnetic field maxima, as they are attracted to magnetic fields. Overall, their magnetization is linearly proportional to the magnetic field. They can be candidates for MIL. Examples of paramagnetic materials include oxygen, platinum and manganese (II) salts. Natural ferromagnetic materials consist of cobalt, iron and nickel, which are strongly attracted to magnetic fields in room temperature. Their magnetization is strong in the magnetic field with coercive field after sufficient external magnetic field, and a much greater response under the same magnetic field as compare with a paramagnetic material, which is more appreciable to induce macroscopic luminescence.

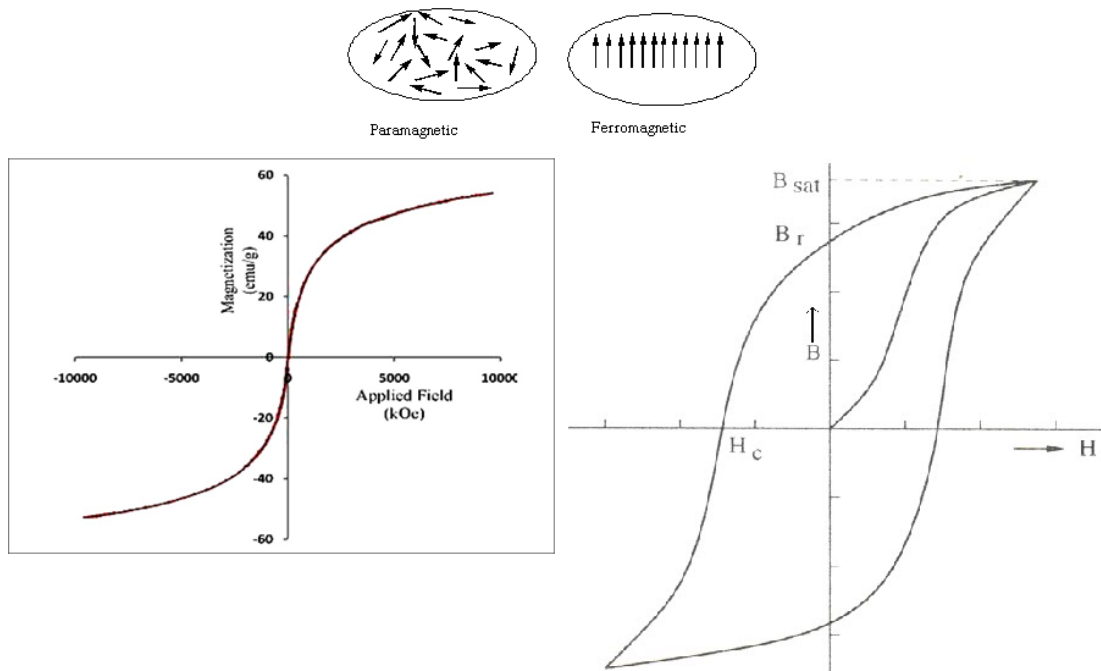


Figure 1-14 Spin alignments of two types of magnetic materials and corresponding coercive field.

1.4.3 Soft magnetic materials

The soft magnetic material is a special type of ferromagnetic material, which has the properties like higher magnetic permeability and saturation induction, with low coercivity. [54, 55] Improvements in these properties have resulted in power-handling electrical devices with reduced size and weight and increased efficiency. They are essential constituents of magnetic-mechanical and electrical device in the modern advancement because of the connection with ordinary steels between mechanical



softness and ease of magnetization reversal. [56] These materials perform the vital task of concentrating and shaping magnetic flux. The continuing development of better materials resulting both in improved efficiencies of key building blocks of present technology-motors, generators, transformers, inductors, and sensors-and in novel devices and applications.

Soft magnetic material has few remanence and high saturation magnetization, that in the absence of external magnetic field, the net moment of these domains is almost zero. As soon as an external field is applied, the particles react similar to a ferromagnetic with their magnetic susceptibility is much larger than that of paramagnetic material. Several investigated particles of Fe-Co, Fe-Ni and Co-Ni alloys and found that the particles of these binary alloys can be successfully obtained with uniform particle size, desired compositions and superior magnetic properties. Its amorphous alloys exhibit such a property owing to the disordered atomic configurations. [57]

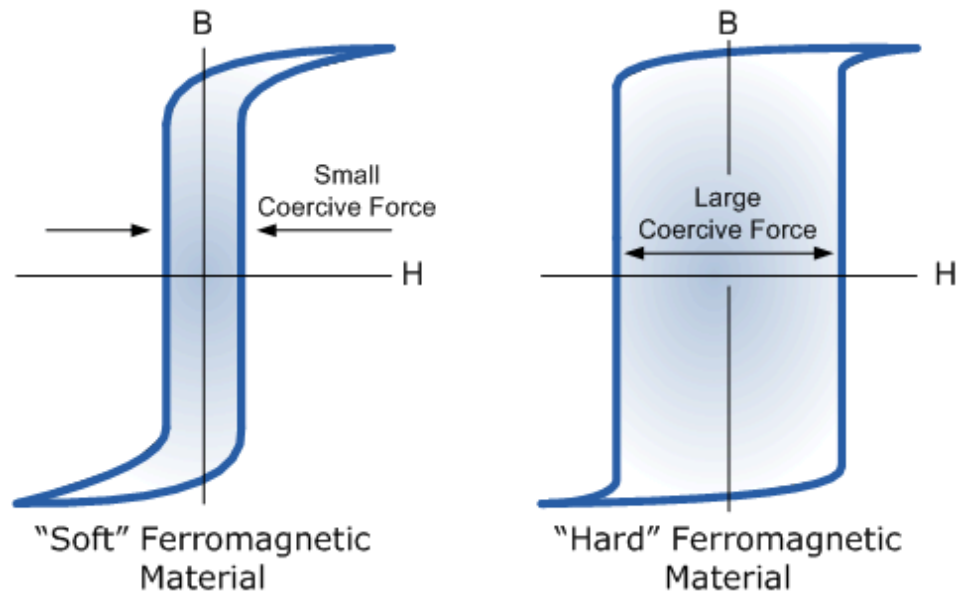


Figure 1-15 Comparison of coercive field of soft with hard ferromagnetic material.

The types of applications for soft magnetic materials fall into two main categories: alternative magnetic field (AMF) and static magnetic field. In static magnetic field applications the material is magnetized in order to perform an operation and then demagnetized at the conclusion of the operation, as an example the electromagnet on a crane at a scrap yard will be switched on to attract the scrap metal and then switched off to drop. In AMF applications the material will be continuously cycled from being magnetized in one direction to the other, throughout the period of operation. A high permeability will be desirable for each type of application but the significance of the



other properties such as remanence.

For AMF applications the important consideration is how much energy is lost in the system as the material is cycled around its hysteresis and the time delay of response.

[58] The energy loss can originate from three different sources: hysteresis loss, which is related to the area contained within the hysteresis loop where the remanence of such a material; it can be reduced by the reduction of the intrinsic coercive field, with a consequent reduction in the area contained within the hysteresis loop. The anomalous losses can be reduced by having a completely homogenous material, single crystal, for example, within which there will be no hindrance to the motion of domain walls. [59] The final one is eddy current loss, which is related to the generation of electric currents in the magnetic material and the associated resistive, thermal and anomalous loss, which is related to the movement of domain walls within the material.

The magnetic moment of a soft magnetic particle generally is smaller than that of large ferromagnetic microparticle under the same external field strength. Resulting the magnetic force acted on a soft magnetic particle will be smaller, which will result in slower magnetic inducing processes. However, the advantage of soft magnetic particles is the possibility to simply “switch off” the magnetic effects by removing the



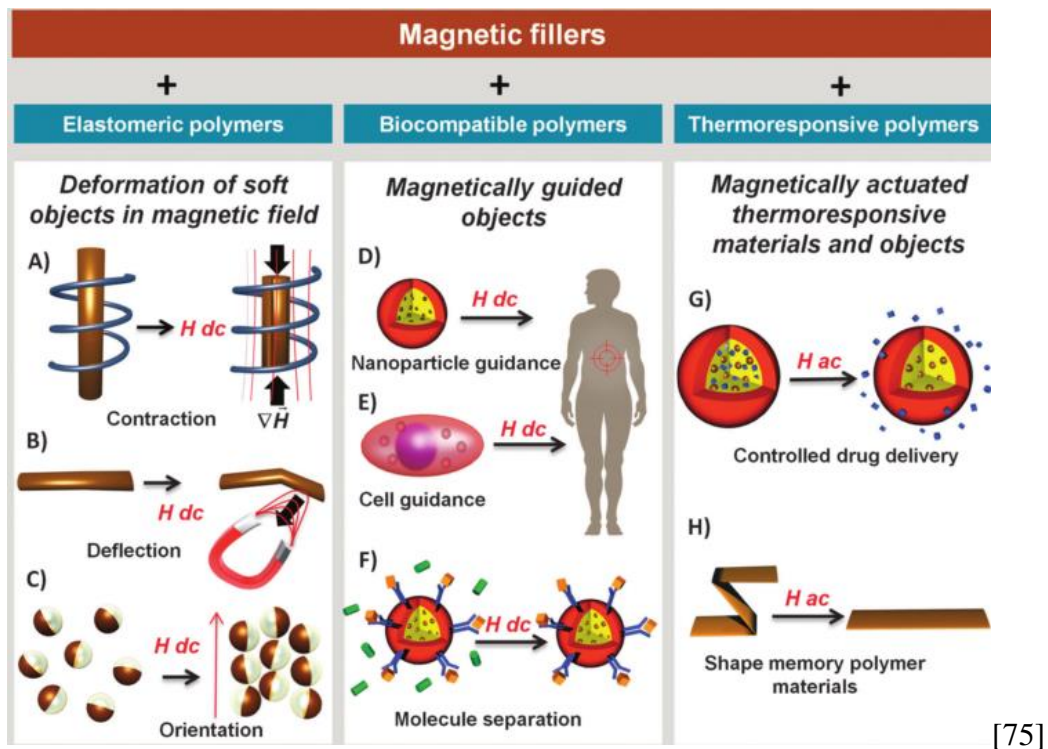
magnetic induction field as the particles are considered to be non-interacting. [60]

1.5 Magnetorheological elastomer

Materials whose properties vary considerably, or coupling strongly with, in the presence of an external stimulus are known as smart materials. [61, 62] Various magnetic smart materials have been identified and studied intently. The most important are magnetic suspensions, ferrofluids, magnetostrictive materials and magnetic shape-memory alloys. [63-70] Magnetic suspensions are complex fluids whose rheological characteristics, viscosity, shear rate change significantly in the presence of a magnetic field. [71, 72]

Materials whose mechanical and rheological properties can be varied by the application of external magnetic field can be divided into three major groups: solid hard bodies, magnetic fluids or suspensions, and MR elastomers. [73] A MR elastomer is defined as a material composed of magnetic particles aligned in a polymer medium by exposure to a magnetic field, thus having elastic and/or magnetic anisotropic properties. [74] It has drawn a lot of interest owing to their dynamic response and their potential usage in smart composite or devices. These devices depend heavily on their

ability to respond to magnetic field changes, which is fascinating and crucial for maintaining and regulating normal functions. Composites consist of magnetically 'hard' or 'soft' particles embedded in polymeric scaffolding were employed in a remarkably wide range of applications. Including media magnetic data storage, magnetic position sensors, flexible magnets, electromagnetic shielding drug delivery, tissue engineering, biosensors, many forms of active diagnosis, microelectronics, micromagnetic dynamic actuators, and magneto-mechanics. [75-82]



[75]

Figure 1-16 Schemes depicting the different types of magnetic responsive materials obtained from the doping of various polymers with magnetic particles



and illustrations of their response when exposed to a static magnetic field or

AMF.

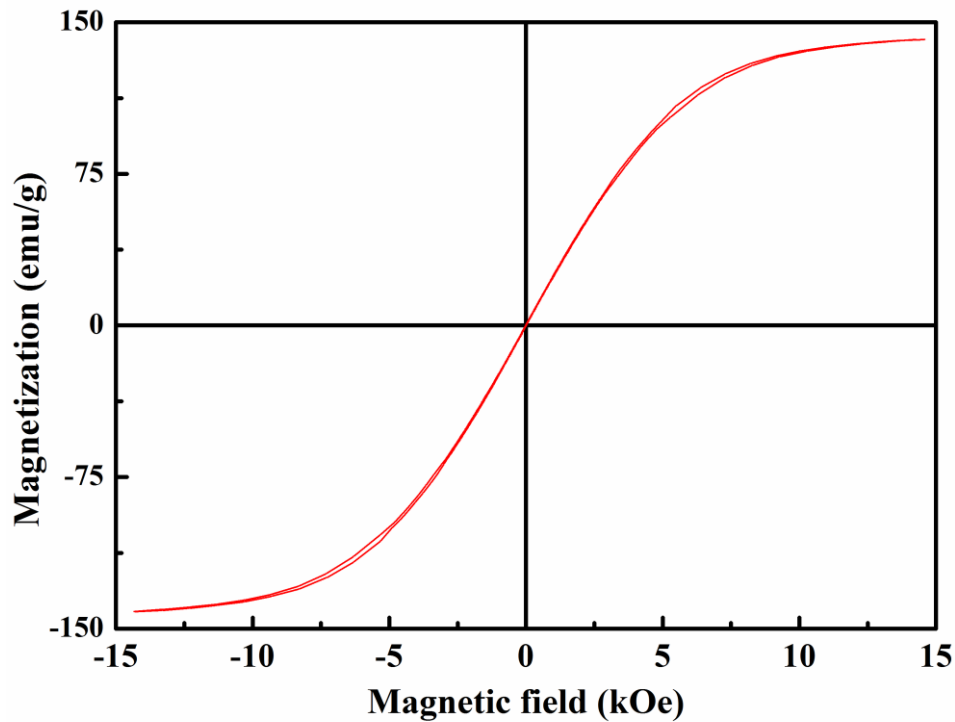
1.5.1 Characteristic of dopant in MR elastomer

Under the stimulation of a magnetic field upon fabrication of these composites can possess anisotropic mechanical, [83] electrical transport, [84] and magnetic properties due to the chain-like particle structures that result from the magnetic dipole interactions between particles. [85] It consists of soft composite materials which comprise of magnetically polarizable particles like iron in a soft polymer matrix. Under magnetic field stimulates, the mechanical behavior of the composite is dictated by superposition of these magnetic particle interactions and elastic forces of the elastomer matrix. It has led to vast research opportunities in the field of mechanical actuation.

Typically, carbonyl iron particles are added to the polymer material prior to crosslinking of elastomer. The fabrication methods involved preventive ways of aggregation of magnetized particles. Usually prior to and during crosslinking, a strong external field (magnetic or electrical) is applied to the composite. Changing these magnetic polarizable particle properties: size, surface area, solubility, permeability,



shape of magnetize results a desired mechanical properties. Typical micron-sized magnetic polarizable particles will support hundreds of magnetic domains, maximum inter-particle attraction and the maximum magnetorheological effect is increased by choosing a particle material with high saturation magnetization Fe, Co and Ni are the most important metals as magnetic materials since they are unique ferromagnetic elements at room temperature. Although generally particles with spherical shape obtained from the thermal decomposition of iron pentacarbonyl are commonly used. Alloys of iron and cobalt are known to have a slightly higher saturation magnetization (up to 2.4 Tesla) and low conceive field. It has also been used in MR elastomer. Typical particle volume fractions are between 0.1 and 2.5. Figure 1-17 show the relationship the typical magnetization response of a MR elastomer under external magnetic field.



[35]

Figure 1-17 Room temperature magnetization of the Fe-Ni-Co doped magnetic elastomer versus magnetic field measured by VSM.

The combination of the magnetic and the elastic properties leads to a number of striking phenomena that are exhibited in response to imposed magnetic field. Giant deformational effect, tunable elastic modulus, non-homogeneous deformation and quick response to the magnetic field are required.



1.5.2 Characteristics of polymer packaging MR elastomer

A material which is intended for use as a magnetic actuator must be both flexible and have a large magnetic permeability. However, as a rule of thumb, adding high-modulus magnetic particles to a composite to achieve higher magnetic permeability generally increases the modulus of the composite, resulting in a less flexible structure. A method for determining the response of a composite for optimal loading of magnetic particles will result in the most responsive material.

Attempts to fabricate MR materials have been performed using soft materials such as synthetic polymer gels, [86] silicone elastomers, [86] and rubbers. The advantages of the process ability of polymer host are that they can be formed into objects with numerous forms or dimension. Many details of the past investigations about MR gels and elastomers have been reviewed in the literatures. [87, 88] The stability of magnetic particles in MR elastomer is superior to that in MR fluids because of the high viscosity of MR solids, as the sedimentation of magnetic particles does not take place easily in MR solids. However, the MR elastomer's response via strain induction is generally small compared to that of fluids. This originates mainly because the magnetic particle is difficult to move and form a chain structure in the solid



polymer agglomeration. Large macromolecule polymer-based materials are the most developed and studied, owing to their high versatility and ability to dramatically alter their intrinsic properties as a function of small environmental changes. [89, 90] Indeed, the huge development of synthesis and successes in polymer chemistry allows a proper design of well-defined macromolecules that can incorporate stimuli-responsive building blocks for most of the magnetic mechanical coupling application. Combined effects of magnetic orientation, and temperature induced phase transition, such as from nematic to isotropic phase as magnetic particles co-operated with a polymer material having its own properties, [91] they can produce a large variety of magnetic responsive polymer composites. Polymer matrix incorporated with magnetic particles combine the favorable properties of magnetic material with simple and economical processing sequences of polymers with low Young' s modulus to achieve large deflections, or extension. [60]

In many cases for MR elastomer, the relative change in the storage modulus (the ratio of storage modulus at magnetic field to off-fields) was several times or less. Consequently a better colloidal stability favors their usage, stability upon fabrication or homogeneous dispersion within a typical polymer matrix. A highly elastic magnetic



composite with a homogeneous distribution of magnetic particles has been shown that the magnetic properties of these materials are similar to those of magnetic powders that are fillers of composites. The introduction concept with highly reliable, and robust, modular automated composite. Such systems generate a minimum of consumables.

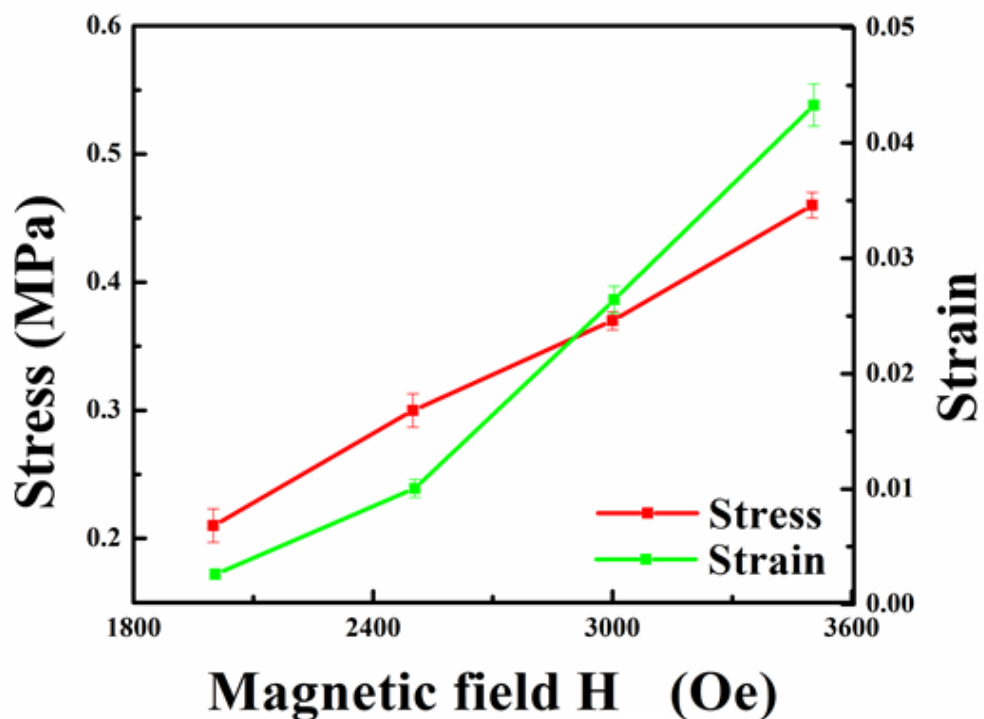


Figure 1-18 Mechanical response of a typical MR elastomer under various magnetic field strength.

The MR elastomer is not highly sensitive to contaminants or impurities that are commonly encountered during manufacture and usage. Further, because the magnetic



polarization mechanism is basically not affected by the surface morphogen chemistry of surfactants and additives, it is usually straightforward to stabilize. Organic polymer materials such as silicone elastomer and Polyimide can also be used to achieve larger deflections in various forms due to their low Young's modulus and high Poisson's ratio. Silicone elastomer is especially promising because of the extremely low stiffness and high tear tolerance. This work employs magnetic elastomers reported in the literature targets at the tuning of optical properties with a magnetic field, while numerous instances of iron particles dispersed in a silicone elastomer have been reported. [92, 93] Magnetic elastomers can also be obtained from soft magnetic particles dispersed in poly (dimethylsiloxane) (PDMS) owing to the prior functionalization of the particle surface with PDMS chain silicone polymer would be absorbed directly onto the surface of these magnetic particles, [93], with the ability to low cost mass production.

1.5.3 Mechanism of MR elastomer

When magnetic polarizable particles are incorporated into elastomeric polymer scaffolds, controlled deformations can be obtained, such as stretching or contraction



of a cylinder, bending of an elongated sample, deflection of a membrane, chaining of microparticles, rotation of anisotropic objects, or rupture of a capsule. [75]

Unlike ferrofluid, carrier liquid could lead to the formation of a network of particles agglomerates throughout the suspension. This result the magnetorheological fluid reversibly changes from a liquid state to a semi-solid state in the presence of a magnetic field with a weak stress and low strain induction. Elastic characteristics of MR elastomer such as yield stress and apparent strain can quickly be controlled by applying a magnetic field. In the presence of an external magnetic field, MR elastomer was characterized by a field-dependent yield stress and an increase in elastic modulus.

Consider its structure, magnetic field responsive elastomers can be thought as solid that analogs to a magnetic field responsive fluid. Like many field responsive fluids, field responsive elastomers are composed of magnetic polarizable particles dispersed in a polymer medium. Its physical response and field sensitivity of these elastomers is very similar with ferrofluid. However, there are some distinct differences in the way in which these two classes of materials are typically intended to operate. The most noteworthy is that the particle chains within the magnetic elastomer are intended to always operate in the pre-yield regime, the operation simultaneously



commerce with the application of magnetic field. While ferrofluid typically operate within a post-yield continuous shear and flow regime, this is due to the response time required to form chains or agglomerates in quiescent conditions for ferrofluid. The responsibility of field responsive fluids is defined as their field dependent yield stress while the strength of field responsive elastomers is typically characterized by their field dependent modulus. The formation of chains is in the order of milliseconds. [94] If the AMF has a high frequency, the stresses generated by MR elastomers also appear on milliseconds. Except in highly viscous host materials, the ubiquitous chains of particles eventually aggregate into multichain columns or stripes. The aggregates typically vary with time with the magnetic field strength applied. [95] The nature of the short range of the magnetic force dominates both the microscopic and macroscopic mechanics of magnetized MR materials, which act as brittle viscoelastic solids under dynamic mechanical loading, exhibiting mechanical nonlinearity even at very small strains. [96]

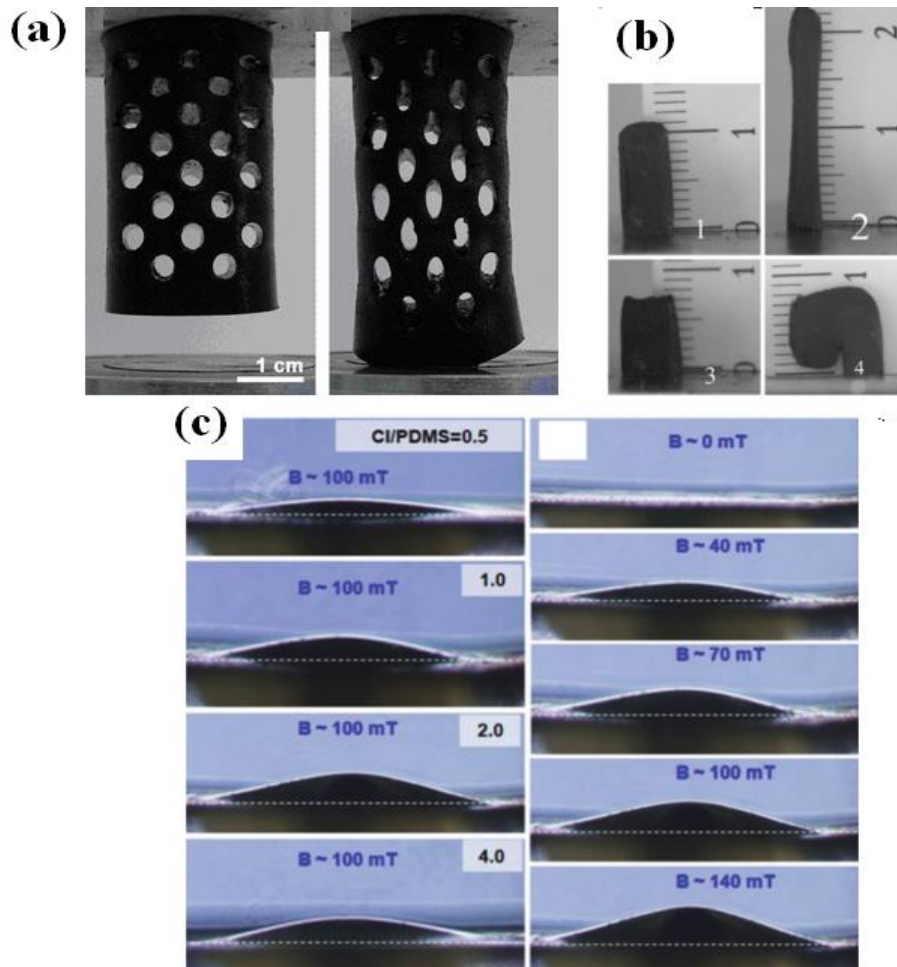


Figure 1-19 Various responds of MR elastomer in different structural forms and composition, (a) Soft, Magnetic Field-Driven hydrogel actuators with muscle-Like flexibility. (b) MR silicone loaded with soft iron pre-aligned under a field. (c) Deflection of different membranes, under the same magnetic field under increasing weight ratios of magnetic polarizable particle and membrane (weight ratio = 2) for increasing field strength (right). [75]



Typically, magnetic fields are applied to the polymer composite during crosslinking in order to form a chained columnar magnetic responsive particle structure has come locked in place after curing of the elastomer. Such processing has been used for some time to impart special anisotropic properties of viscoelastic materials. [96]

The resulting structure would itself be useful in a variety of applications ranging from biocompatible magnetic hyperthermia agents to magneto-mechanical actuation, with huge advantages such as larger change in dimensions, no contact actuation, lower power consumption, and the avoidance of the high voltages needed for ER fluids.

1.6 Motivation of research

In most reports, the term of magneto luminescence occurred under the influence of externally applied magnetic field, which does not mean the magnetic-induced luminescence (MIL). Magneto luminescence has previously been observed in some luminescence systems, such as semiconductor nanostructures and organic compounds under various special effects. Notably, the ML effects typically occur under extreme



conditions of high magnetic field and low temperature. By comparison, the realization of light-emission stimulated by magnetic field faces an even greater challenge and hence the phenomenon of intrinsic MIL is extremely rare. The long-standing problem limits hindering potential applications of both magnetic and luminescent materials. It is worthy of attention that the availability of various types of laminate structures with great flexibility of design makes it possible to tailor their properties via interfacial coupling. By considering that the direct magnetic–luminescence coupling is exceptionally difficult to realize in a single phase, the development of composite laminates may be an alternative solution to tackle the major problem at this stage, particularly the practical approach based on composite laminates should be favorable for many magnetic applications. In the real world, magnetic fields exist in many systems, and therefore the detection of magnetic field is essential for environmental surveillance, mineral exploring, and safety monitoring. For example, the large magnetic flux generated from a grid-connected power wire can be used to monitor power consumption of electric appliances in the power industry. It is known that conventional magnetic sensing materials and devices are restricted to employing the conversion from magnetic field input to electric signal output, such as Hall,



magneto-resistive, and magneto-electric effects, as well as recently developed magnetic Tribo-nanogenerator. Therefore, it would be very attractive if MIL-based laminate materials and devices are conceived, which are capable of showing the ability of responding and harvesting energy from magnetic fields. In contrast to conventional magnetic sensors, the MIL-based devices enjoy competitive advantages, the major advantages of magnetic induction is the possibility of having a non-contact remote control including real-time visualization, remote sensing without making electrical contact, nondestructive and noninvasive detection.

1.7 Scope of work

This thesis describes the experimental investigation of magnet induced luminescence by laminated composite and alternative magnetic field. The objectives of this research are to realize and control the luminescence intensity and wavelength of metal ions doped zinc sulfide, to study the luminescent properties of the phosphor and explore the possibility to be used practically in MIL applications.

This thesis consists of five chapters. Chapter 1 gives an introduction on the ML, magnetic material, fundamental concept and overview of PL, photoluminescence and



magnetic elastomer. Some literature review is also given on the luminescent mechanism of ML. The development and status of ML phosphors are discussed.

In Chapter 2, all the characterization techniques that have been used in the present study are addressed. In view of fabrication, a brief description of the fundamental mechanisms of 3D printing, spin coating is provided. The working principles of some primary characterization equipment, for example, vibrating sample magnetometer (VSM) and scanning electron microscopy (SEM) are also included.

In Chapter 3, the property of magnetic induced luminescence is a critical issue. Fabrication and characterization of Al, Cu and Mn doped ZnS phosphor in PDMS introduced. An emphasis is placed in the parameter of the magnetic field applied to the properties of light emitted from various phosphor.

Chapter 4 presents the ideas of various applications of MIL, including the further tuning of MIL emission with doping of YAG: Ce phosphor and Eu doped Ca, SrS phosphor. The results and discussion on the persistence photoluminescent spectra are explained.

The conclusions of the thesis with a summary of the significant results of the present investigation and future work are presented in Chapter 5.



Chapter 2 Experimental techniques

The composites fabrication, structural and luminescent characterization of the MIL will be introduced in this chapter.

2.1 Composite fabrication

The phosphors presented were bought from Lonco Company Limited. They were synthesized by Osram Sylvania, a worldwide supplier of electroluminescent phosphor which supplies the phosphor used in cell phones, pagers, automotive interiors, handheld computers. Or any means which requires a thin and cold lighting background. These phosphors are comparatively better than the traditional phosphor in terms of particle size, morphology, crystallinity, reaction temperature and duration. The thin films were prepared by spin coating or 3D printing, which is recognized as a powerful technique for growing high-quality complicated-structure macroscopic films on different types of substrates. The laminates composite were prepared by dip coating.

2.1.1 Spin coating

Spin coating is a procedure used to deposit uniform thin films to flat substrates.



Usually a small amount of coating material is applied at the center of the substrate, which is either spinning at low speed or not spinning at all.

Spin coating has been used for years for the fabrication of thin films. A typical process involves depositing a small puddle of a fluid resin onto the center of a substrate and then spinning the substrate at high RPM. Centripetal acceleration will cause the resin to spread to, and eventually off, the edge of the substrate leaving a thin film of resin on the surface. Final film thickness and other properties will depend on the nature of the resin (viscosity, drying rate, percent solids, surface tension, etc.) and the parameters chosen for the spin process. Factors such as final rotational speed, acceleration, and fume exhaust contribute to how the properties of coated films are defined.

A typical spin process consists of a dispense step in which the resin fluid is deposited onto the substrate surface, a high-speed spin step to thin the fluid, and a drying step to eliminate excess solvents from the resulting film. Two common methods of dispense are static dispenses, and dynamic dispenses. As most of the spin coating process is static dispense. Here give a brief discussion on the process.

Static dispense is depositing a small puddle of fluid in the center of the substrate.



This can range from 1 to 10 ml depending on the viscosity of the fluid and the size of the substrate to be coated. High viscosity fluid or larger substrates typically required a larger puddle to ensure full coverage of the substrate during the high-speed spin step. After the dispense step it is common to accelerate to a relatively high speed to thin the fluid to near its final desired thickness. Typical spin speeds in this step range from 1500-6000 RPM, depending on the properties of the fluid as well as the substrate. This step can take from 10 seconds to several minutes. The combination of spin speed and time selected for this step will generally define the final film thickness. In general, higher spin speeds and longer spin times create thinner films. The spin coating process involves a large number of variables that tend to cancel and average out during the spin process and it is best to allow sufficient time for this to occur. A separate drying step is sometimes added after the high speed spin step to further dry the film without substantially thinning it. This can be advantageous for thick films since long drying times may be necessary to increase the physical stability of the film before handling. Without the drying step, problems can occur during handling, such as pouring off the side of the substrate when removing it from the spin bowl. In this case, a moderate spin speed of about 25% of the high-speed spin will generally suffice to aid in drying



the film without significantly changing the film thickness. Each program on a spin coater may contain up to ten separate process steps. While most spin processes require only two or three, this allows the maximum amount of flexibility for complex spin coating requirements.



Figure 2-1 Schemes depicting the spin coating process.

Ease of fabrication and processing are the obvious advantages. The disadvantage of spin coating is that it is an inherent batch (single substrate) process and therefore relatively low throughput compared to roll-to-roll processes. Faster drying times can also lead to lower performance for some particular nano-technologies (small molecule OFETs for example) which require time to self-assemble and/or crystallize. Finally, the material usage is typically very low at around 10% or less with the rest being flung off the side and wasted. Whilst this is not usually an issue for research environments it is clearly wasteful for manufacturing.



2.1.2 3D printing

3D printing, also known as additive manufacturing, is a process used to synthesize a three-dimensional object. Generally 3D printing is the process of successive layers of material forming via computer control to create an object. These objects can be of almost any shape or geometry, and are produced from a 3D model or other electronic data base.

Early Additive Manufacturing (AM) equipment and materials were developed in the 1980s. Generally there are two AM fabricating methods of a three-dimensional plastic model with photo-hardening polymer, where the UV exposure area is controlled by a mask pattern or the scanning fiber transmitter. The term 3D printing originally referred to a process employing standard and custom inkjet print heads. The technology used by most 3D printers to date fused deposition modeling, a special application of plastic extrusion, including microcasting and sprayed materials, the technologies all share the common theme of sequential-layer material addition/joining throughout a 3D work envelope under automated control. In addition, sacrificial and support materials had also become more common, enabling new object geometries.

There are essentially three stages in the 3D printing process. Initially, the product



was first designed and draw with computer software such as CAD or Solidwork. The commands then insert into the printer. Subsequently, the ejected product, in the form of common PLA or ABS polymer is transported to sequential-layer joining throughout a 3D work envelope under automated control. The output product will then process a filing and finishing. Eventually, the product is available for application.

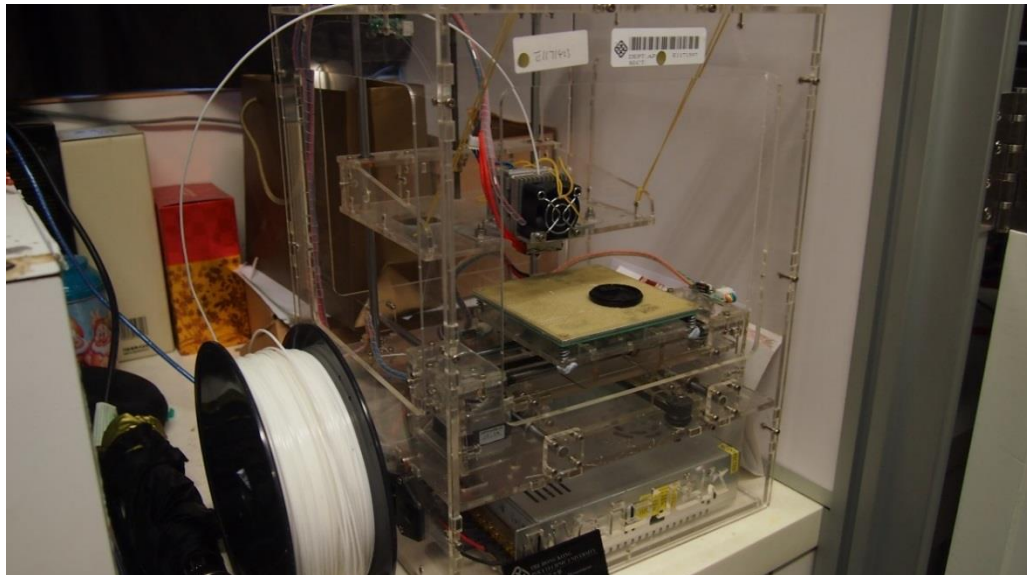


Figure 2-2 A photograph of the in house 3D printer.

3D printing provides a wide variety of manufactured products, including customizable products and even an individual's personal designs. It producing a more quickly go from just a design to an actual prototype, with speed for a large number of end products at ease.

One of the most innovative products of 3D printing is the manufacturing of



customizable human body parts or organs. While these usages are still experimental, the potential advantages are huge. Providing quick and reliable building and replacing critical organs have almost no chance of donor rejection as the organs will be built using the patients' unique characters and DNA.

However, it also inherent a few limitations, currently, 3D printers only manufacture products out of plastic, resin, certain metals, and ceramics. 3D printing of products in mixed materials and technology, such as circuit boards, are still under development.

Also 3D printing limited with the size of the products that they can create. Ultimately, large items, such as houses and building, could be created by using 3D printers.

2.2 Characterization

The phosphors and composites have been characterized using several common techniques to acquire information on their structural and luminescent properties.



2.2.1 Scanning electron microscopy

Scanning electron microscopy (SEM) operates through focusing electron beam over the surface of a specimen in a high vacuum chamber. The morphologies of composites were obtained using JEOL-JSM 6335F field-emission scanning electron microscope.



Figure 2-3 A photograph of SEM in the laboratory.

The field emission system works by ejecting electrons from the Ti filament by an external high voltage, 5kV. The electric field lowers the potential barrier between the vacuum energy level and the electrons, allowing them to tunnel through the barrier. Secondary electrons, backscattered electrons, are produced when the electrons interact



with the specimen. Hence, high-resolution images, specific morphological properties such as distribution of elements and components can be obtained. Nonconducting material may not be analyzed by SEM directly, and an abnormal contrast may be resulted from the uneven distribution of negative charges building up gradually from bombardment by the high-energy electron beam. A Layer of gold (~10-20 nm in thickness) is coated onto the sample to enhance the emission of secondary and backscattered electrons as well as to eliminate the charging effect.

2.2.2 Vibrating sample magnetometer

A vibrating sample magnetometer (VSM) operates on Faraday's Law of induction, which demonstrated the changing of magnetic field will produce an electric field. This electric field can be measured and give rise to information about the changing magnetic field. A VSM is used to measure the magnetic behavior of magnetic materials. It operates by first placing the sample to be studied in a constant magnetic field. If the sample is magnetic, this constant magnetic field will magnetize the sample by aligning with the field its corresponding magnetic domains, individual magnetic spins. The Figure 2-4 show the VSM employed.

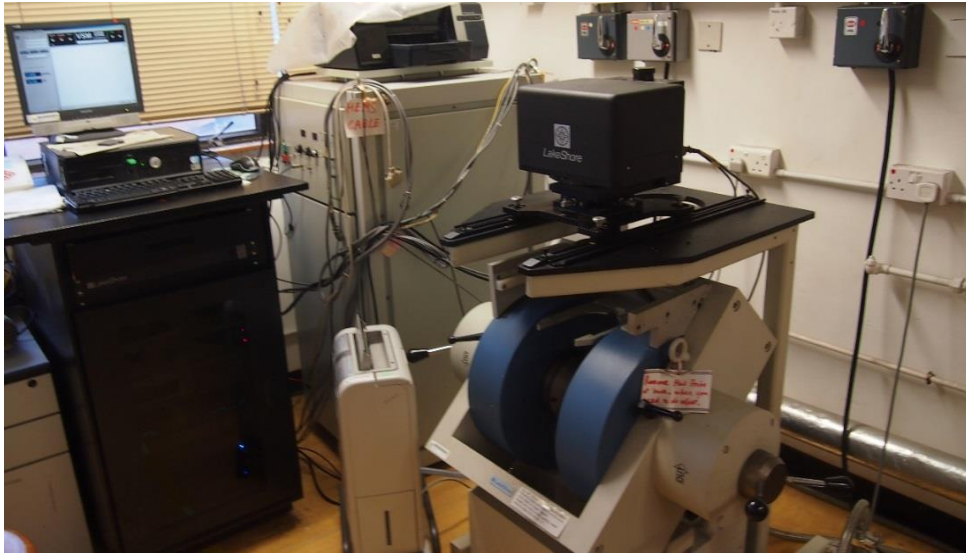


Figure 2-4 A photograph of VSM in the laboratory.

The stronger the magnetic field, the larger the magnetization will be. The magnetic dipole moment of the sample will create a magnetic field around the sample, sometimes called the magnetic stray field. As the sample is moved up and down, this magnetic stray field is changing as a function of time and can be sensed by a set of pick-up coils.

As the magnetic stray field moves up and down, will cause an electric field in the pick-up coils according to Faraday's Law of Induction. This current will be proportional to the magnetization of the sample. The greater the magnetization, the greater the induced current is.

The induction current is amplified by an amplifier, with the whole system is



connected to a computer interface. Under a controlling and monitoring software, the system can give details on the sample's ability of magnetized and how its magnetization depends on the strength of the constant magnetic field.

2.2.3 Luminescent spectroscopy

The luminescence spectroscopy measures the energy levels of the luminescence centers, which are related to the physical nature of the center, and estimate the energetic and dynamic processes that the center undergoes. The luminescence properties of a phosphor are usually characterized by its excitation and emission spectra, brightness, and decay time.



Figure 2-5 A photograph of PL measurement system in the laboratory.

The fundamental concepts of luminescence are discussed in Chapter 1. The relationship between the wavelength and the intensity of the emitted light from a sample excited by an appropriate excitation light source of constant energy, an excitation spectrum is obtained. The dependence of photoluminescence intensity on the frequency or wavelength of the exciting light refers to an excitation spectrum. Simultaneous study of excitation spectra in phosphor yields valuable information about the energy spectrum of matter.



2.2.4 Spectrometer

The detector used for the USB4000 is a charge transfer device (CCD) that has a fixed well depth (capacitor) associated with each photodetector (pixel).



Figure 2-6 A photograph of spectrometer in the laboratory.

A spectrometer is an apparatus to measure an optical emission spectrum. A spectrum recorded by the spectrometer that shows intensity as a function of wavelength, of frequency, of time decay. The Ocean Optics USB4000 Spectrometer includes an advanced detector and powerful high-speed electronics to provide both a high spectral response and high optical resolution. The result is a compact, flexible system, with no moving parts, a few triggering options, a dark-level correction during temperature change. It is responsive from 200-1100 nm and can be configured with various Ocean Optics optical bench accessories, light sources and sampling optics, to create application-specific systems for thousands of absorbance, reflection and



emission applications.

Basic operator of the detector used for the USB4000 is a charge transfer device (CCD) that has a fixed well depth (capacitor) associated with each photodetector (pixel). The first step in detection process is to direct light through a fiber optic cable into the spectrometer through a narrow aperture known as an entrance slit. The slit vignettes the light and they enter the spectrometer. In most spectrometers, the divergent light is then collimated by a concave mirror and directed onto a grating. The grating disperses the spectral components of the light at slightly varying angles, which is then focused by a second concave mirror and imaged onto the detector.

Once the light is imaged onto the detector, the photons are then converted into electrons which are digitized and read out through a USB. The software then interpolates the signal based on the number of pixels in the detector and the linear dispersion of the diffraction grating to create a calibration that enables the data to be plotted as a function of wavelength over the given spectral range. This data can then be used and manipulated in countless spectroscopic applications.



2.2.5 Spectroradiometer

The design of Spectroradiometer includes spectrally based photometric and calorimetric measurements, source spectral power distribution, dominant wavelength and correlated color temperature quick and simple. The measurement can be a cosine receptor for irradiance/ illuminance. The essential components of a Spectroradiometer consist input optics that gather the electromagnetic radiation from the source, a monochromator separating light into its component wavelengths and a detector, and a control and logging system to define data and store it.



Figure 2-7 A photograph of spectroradiometer in the laboratory.



2.2.6 AC magnetic field system

A self-designed lab-made AC magnetic field system which can generate a magnetic field strength of 3.5 kOe with 400 Hz was set up to investigate and characterization of MIL. It consists of 4 main parts: (i) a high speed brush motor, which is used to generate rotation of the magnet; (ii) a NdFeB axial magnetized magnet with the remanence of 0.6 T; (iii) a PWM modulator to control the RPM of the motor from 0 to 22000, which in turn the frequency of magnetic field measurements and (iv) a couple of carjacks to adjust the distance of the composites from the magnet. The frequency of the magnetic field is countered by a hall probe, counter as the magnet rotates. The corresponding magnetic field strength with distance relationship is recorded precisely with a hall probe, thickness gauge and an optical carjacks.

A longitudinal AMF is prepared in a similar way. It was set up to investigate the performances and characteristics of the wafer sized MIL display. A sample holder is driven by a motor. Simulate the AC magnetic field with 50 Hz.

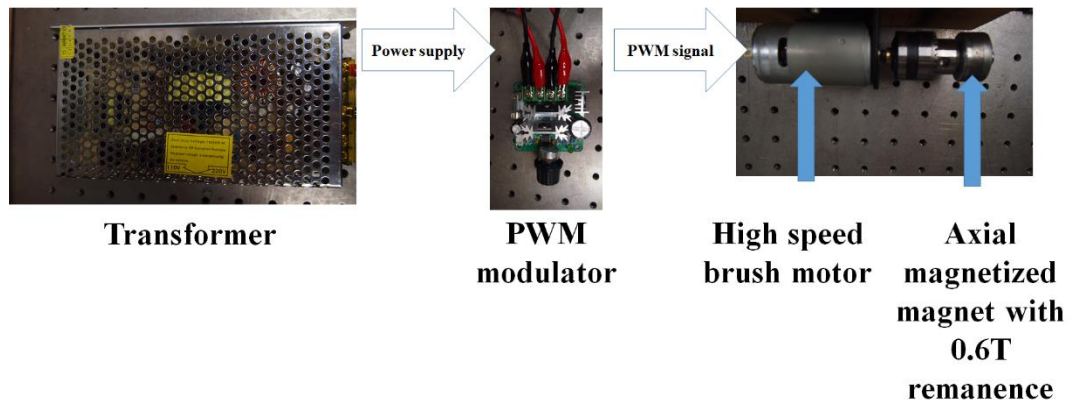


Figure 2-8 A schematic of homemade AC magnetic field system in the laboratory.

Chapter 3 Observation of Magnetic induced luminescence

In this chapter, the mechanism of the magnetic induced luminescence (MIL) via strain-mediated coupling is presented. Then, the facile fabrication method of MIL composite laminates is demonstrated. The relationships between MIL intensity and amplitude or frequency of magnetic field are investigated. Moreover, the transient response of MIL and optical performance are discussed. This work has been featured in Frontispiece, and highlighted as "Materials: Magnetic opportunities" by Chief



Editor, Dr. Oliver, Graydon in "News and Views", Nature Photonics, 9, 558 (2015).

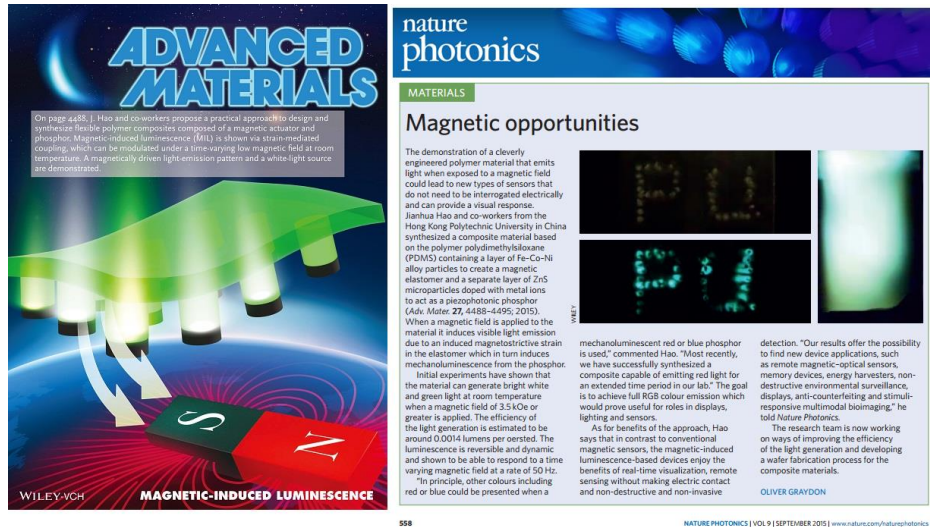


Figure 3-1 Frontispiece of Advanced Materials and highlighted by Nature Photonics.

3.1 Mechanism of MIL

Wang proposed piezophotonic effect, which is a three-way coupling among piezoelectricity, luminescence and semiconductor behavior (Figure 3-1 shows). [23]

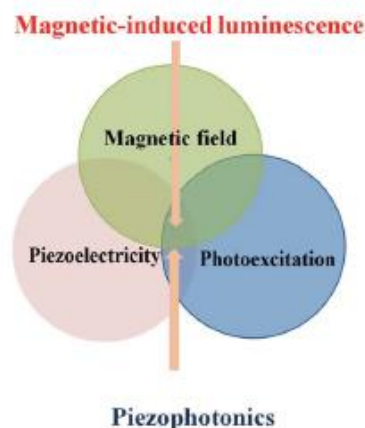
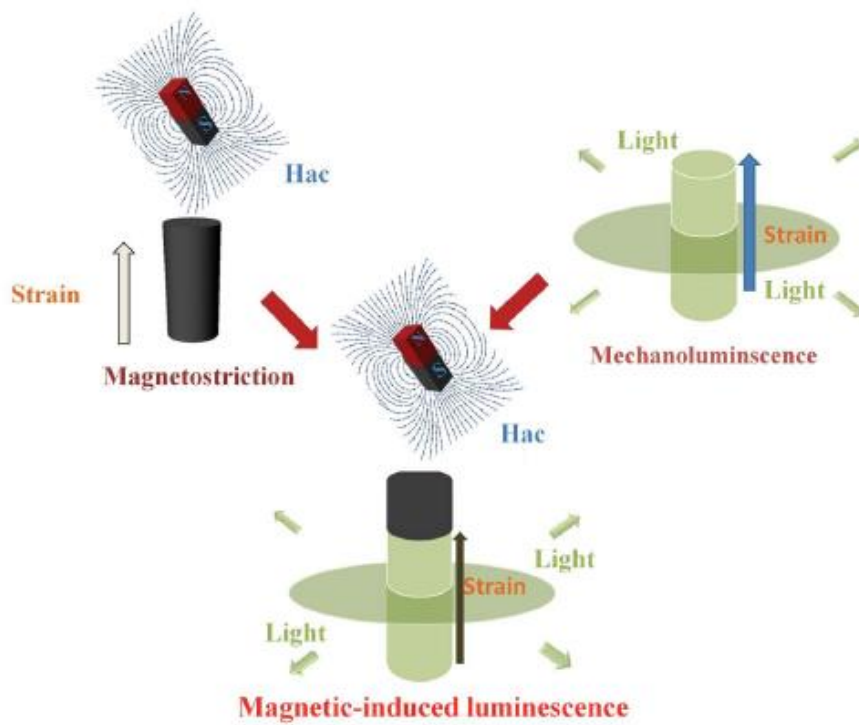


Figure 3-2 Schematic diagram illustrating the field of piezophotonics and MIL.

In this work, we have proposed a practical approach to design and fabricate composite laminate systems composed of magnetic actuator and phosphor materials. The novel MIL phenomenon has first been observed from the flexible composite laminates via strain-mediated coupling, resulting in the green and white light emissions by the naked eyes.



[35]

Figure 3-3 MIL effect based on strain-mediated magnetoluminescent coupling in two phases of magnetic elastomer and mechanoluminescence phosphor.

Figure 3-2 depicts a strategy of practical approach to realize MIL in this work,



namely strain-mediated magnetoluminescent coupling in two phases where the magnetic and photon parameters arise in separate but intimately connected phases. Such MIL is a result of the product of the magnetostrictive (magnetic/mechanical) effect from the magnetic phase and mechanoluminescence (mechanical/luminescent) effect in the phosphor one. According to previous studies, the total luminescence intensity of mechanoluminescence is proportional to the strain and its rate of change, which is written as strains (σ).

$$I_T = \sigma \frac{\partial \sigma}{\partial t}$$

It is apparent that the static DC magnetic field is unable to excite the luminescence because of $\partial H/\partial t = 0$.

For alternative magnetic field, the magnetic field can be given as,

$$H = H_0 \sin \omega t = \sqrt{2} H_{rms} \sin \omega t,$$

H_0 is the maximum value of the magnetic field

Assume that an external magnetic field (H) is applied to the two phases system and the strain coupled is given as (σ). A magnetostrictive coefficient in a magnetic-phase can then be described by



$$c = \frac{\partial H}{\partial \sigma}$$

In our cases, the emission intensity from our composite triggered by magnetic field can be therefore expressed as:

$$I = c\sigma \frac{\partial H}{\partial t}$$

For some magnetic elastomer maintaining the linear relationship of σ and H with correlation coefficient k under certain operation range, the equation can be rewritten

$$I = ckH \frac{\partial H}{\partial t} dt$$

The total luminescence intensity of MIL can be approximately by integrating the equation when taking

$$I_T = \int_0^T ckH \frac{\partial H}{\partial t} dt$$

Solving for a period T give,

$$I_T = \frac{1}{2} ckH_{rms}^2 \quad (1)$$

Hence, the total luminescence intensity of MIL is proportional to the magnetic field coupling and correlation coefficient. Additionally, MIL intensity will depend on the amplitude and frequency of the input magnetic field. It should be noticed that this novel equation is valid only in a low frequency magnetic field excitation. As there may



be mechanical damping or photon quenching from the phosphor occur, which will be discussed in later chapter.

Figure 3-2 shows that the MIL composite laminates are multiphase rods consisted of the composite of metal-ion-doped ZnS microparticles mixed to polydimethylsiloxane (PDMS) and another composite of magnetic Fe–Co–Ni alloy particles mixed to PDMS. ZnS is chosen as phosphor host here because of its excellent piezoelectricity. Previous studies have proven that the piezoelectric potential generated is able of triggering the luminescent center of metal-ion dopants. Resulting light emissions when the flexible composites of metal-ion-doped ZnS microparticles embedded in PDMS are stimulated by external strain. The structure of the laminates composite of MIL consists of multiphase rods consisted of the composite. Each rod consisted of the composite phase of metal-ion-doped ZnS microparticles mixed to PDMS and another phase of the composite of MR elastomer with soft magnetic Fe–Co–Ni alloy particles mixed to PDMS. The novel MIL phenomenon has first been observed from the flexible composite laminates via strain-mediated coupling, resulting in the green and white light emissions.



3.2 Fabrication of flexible MIL composite laminates

The flexible phosphor composite was made of metal ion-doped ZnS particles and PDMS. Metal ion-doped ZnS powders (green: ZnS: Al, Cu (GGS42) or white: ZnS: Al, Cu, Mn (GG73), Global Tungsten & Powders Co.) were homogeneously mixed into a PDMS.

Acrylonitrile butadiene styrene (ABS) mold composed of 25 holes, each with a diameter of 1 mm and a depth of 5 mm was made via 3 D printing,

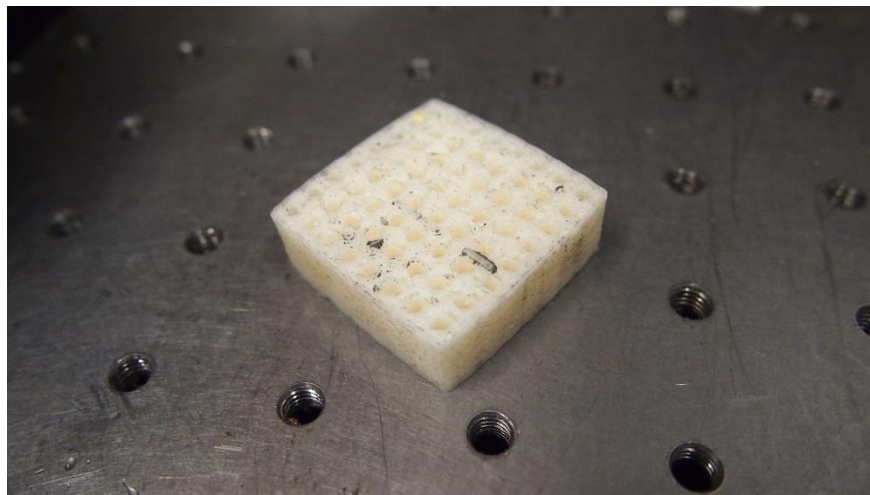


Figure 3-4 3-D printed ABS mold.

Simultaneously, another mold was fabricated by polymethyl methacrylate (PMMA), also consists of 25 elements, each with a diameter of 0.5 mm and a length of 3 mm.

Then, ZnS: Al, Cu/ ZnS: Al, Cu, Mn microparticles with the average size of 23 μm were uniformly mixed. The PDMS consists of base and crosslink at a weight ratio of



10:1. Consequently, metal ion-doped ZnS based powders (70 wt. %) and the PDMS host (30 wt. %) comprise the flexible phosphor composite. The mixture was poured into the PMMA mold.

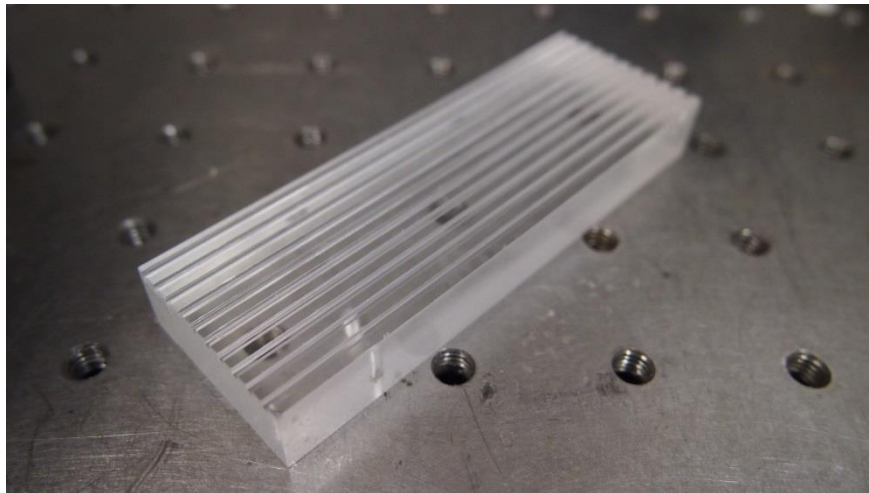


Figure 3-5 PMMA mold for fabrication of the MIL phosphor phase.

After curing the composite at 70 °C for 2 h, the rods were extracted and inserted into each hole of the ABS mold which half filled with magnetic responsive polymer. The MR elastomer consists of magnetic Fe–Co–Ni alloy particles (75 wt. %) with the average size of 100 μm embedded in uncured PDMS host (25 wt. %). Then, the samples were degassed for 30 min to ensure good adhesion between the ML phase and the Fe–Co–Ni alloy particle-doped uncured PDMS. After degassing, the mold was put into the oven at 110 °C for 24 h to cure the polymer. After removal of the ABS mold, multiphase composites with magnetic actuator phase and mechanoluminescence



phosphor phase can be obtained.

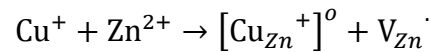
3.3 Results and discussion

3.3.1 Relationship between MIL and frequency of magnetic field

When applying a magnetic field with the frequency of 26–50 Hz, the luminescence spectra of Al, Cu-doped ZnS, and Al, Cu, Mn-doped ZnS phosphors combined with MR elastomer are shown in Figure 3-3 and Figure 3-4. From Figures 3-3 and 3-4 we can see that the obtained MIL emission profiles are quite similar to the previous observation from PL, EL, and ML spectra from the metal-ion doped ZnS phosphors. [34, 97] When the magnetic field induced a strain from the MR elastomer and give rise to a piezoelectric field in the metal-ion-doped ZnS, the carriers in the luminescent center are excited to a higher energy level. Luminescence is then induced by the electron–hole (e–h) recombination. ZnS ML capacity process a non-symmetric crystal structure, such that during deformation, a piezoelectric field was induced inside. This piezoelectric field then excited theses charge carrier in the luminescent center and as photon emission as they relax. The “luminescent center” means the metal ions



doped in the ZnS crystal. It can be regarded as a defect state. It is inside the energy band gap of the ZnS host. For example, luminescent centers were introduced by doping Cu⁺ ions that replace Zn²⁺ ions in the host lattice. Due to a non-equivalent substitution, two kinds of defects can be simultaneously created as described by equation.



The Cu⁺ related defects carrying one negative charge act as the trapping centers of hole. And correspondingly, the Al³⁺ related defects carrying one positive charge acts as the trapping centers of electron, to participate in the trap-related luminescent processes.

As in Figure 3-3, the dominant peak is seen at 509 nm, while in Figure 3-4 measured from Al, Cu, Mn-doped ZnS, there are two main peaks centered at 525 nm and 588 nm. The luminescence intensity of MIL varies with frequency when it ranges from 10 Hz to 50 Hz, shown in Figure 3-5. It is noticeable that the MIL intensity increases linearly when increasing f , which is consistent with the proposed MIL model in the low frequency range as discussed.

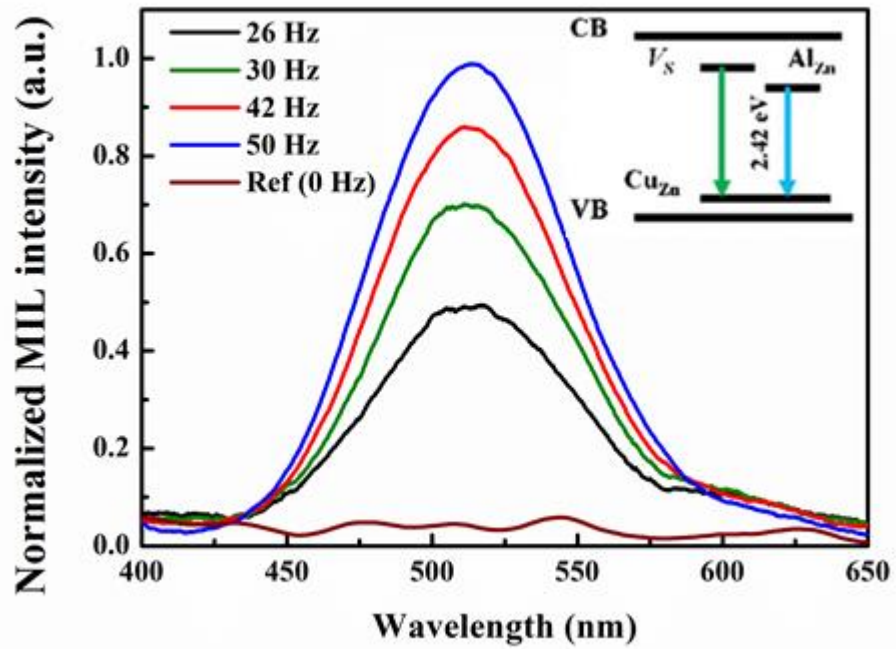


Figure 3-6 Emission spectra of ZnS: Al, Cu phosphor based MIL composite under AMF of various frequencies.

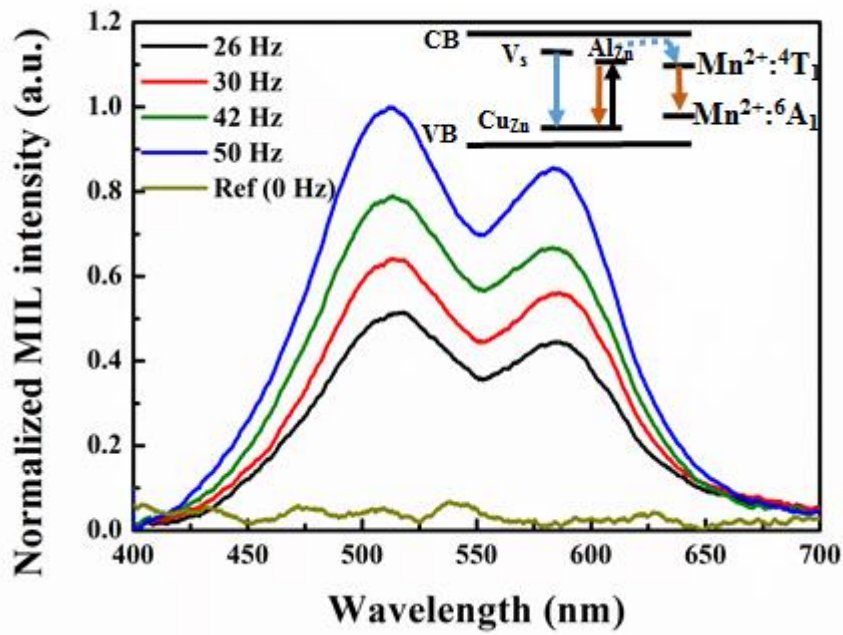


Figure 3-7 Emission spectra of ZnS: Al, Cu, Mn phosphor based MIL composite under AMF of various frequencies.

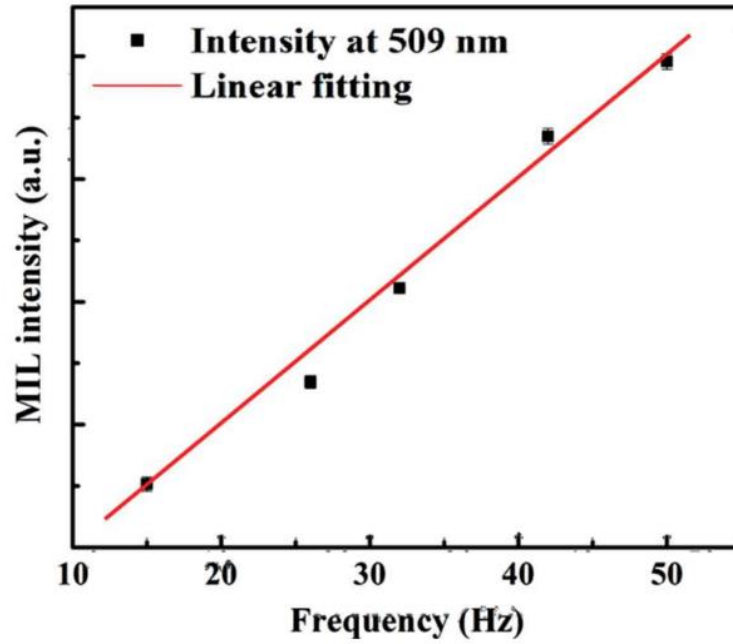


Figure 3-8 A linear relation between luminescence intensity of ZnS: Al, Cu phosphor based MIL and low frequency of magnetic field.

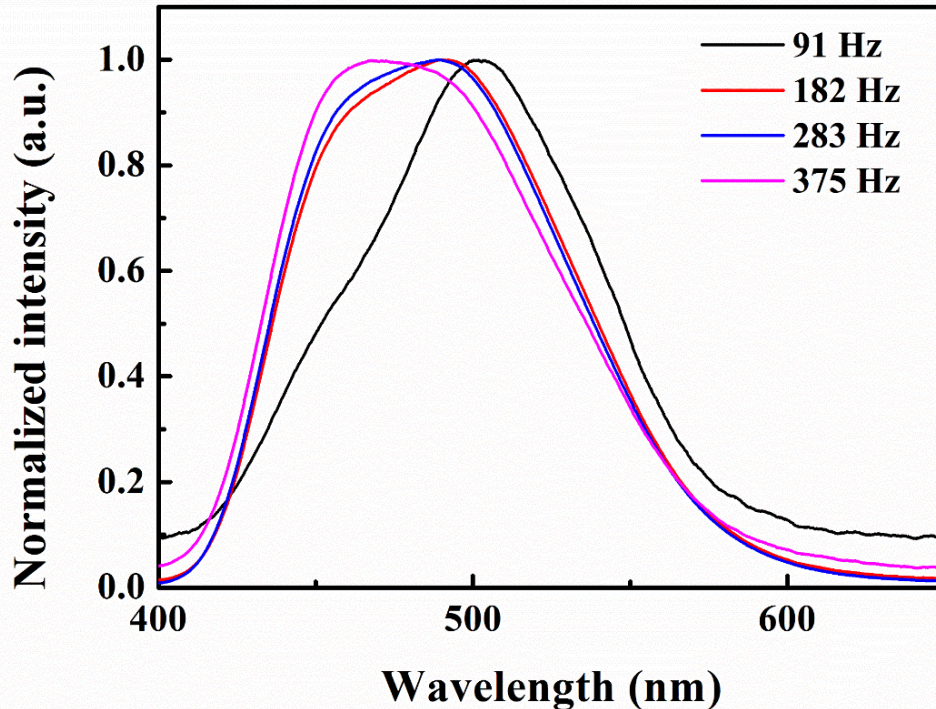


Figure 3-9 Emission spectra of ZnS: Al, Cu phosphor based MIL under a high frequency of AMF.

In order to obtain blue color MIL, we tested the ZnS: Al, Cu phosphor based MIL composite at high frequency of alternative magnetic field. In this measurement, AMF with maximum frequency of 366 Hz was initially switched on and retained at $H_{rms}=2.5$ kOe at room temperature then decrease the frequency of AMF gradually. When the frequency varied from 91 Hz to 375 Hz, the peak of the emission intensity has a shifted from 509 nm to 472 nm, as shown in Figure 3-6. The color change from green



to blue can be observed by naked eyes. The peak of the emission spectra at 91 Hz is located about 500 nm (green) while the peak of the emission spectra at 366 Hz shift to lower wavelength and it is peaked at 472 nm (blue). This spectral blue shift of MIL is consistent with blue EL enhancement at higher electrical frequencies. The reason for the spectral shift is difficult to describe in detail at the current stage. A tentative explanation of this phenomenon is proposed based on the presence of two different phases of the MIL materials, resulting in two emission sites. We purposed the mechanism based on figure 3.4, the MIL peak observed corresponding to the transition between Al_{Zn} and Cu_{Zn} , as it is under a low frequency magnetic field excitation. The deeper charge carriers in these two sites be excited. Therefore, only emission at 2.42 eV be observed and the green emission dominated.

The V_s to Cu_{Zn} transition can occur only when the charge carrier injection rate increases with the existence of the remnant piezo-potential. Such that charge carrier can obtain more energy to commence this shallower charge traps donor acceptor type recombination. This can happen only due at a high frequency magnetic stimuli. Result in primary blue emissions.

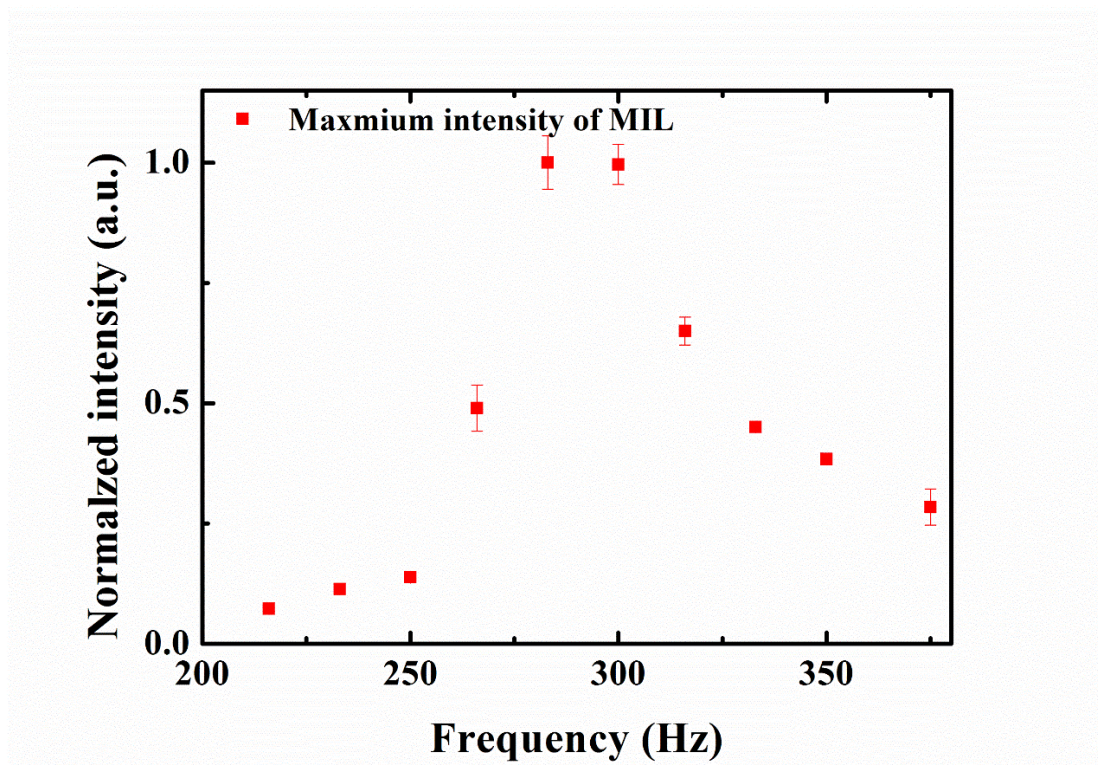


Figure 3-10 Intensity of ZnS: Al, Cu phosphor based MIL under a high frequency of AMF.

To further investigate the influence of high frequency of magnetic field on the blue MIL intensity, Figure 3-7 shows the spectrum of ZnS: Al, Cu phosphor with frequency changed from 200 Hz to 400 Hz. The MIL emission wavelength at 472 nm first increased with increasing frequency and then reached a saturated value at 250 Hz. As the magnetic field frequency increases beyond 300 Hz, the intensity of MIL reduced sharply with increasing frequency of magnetic field. It was first suspected to



be the physical dimension of the MIL composite caused various respond delay. Therefore, another MIL composite with different dimension was tested under the same condition. The result turned out to be the same that its maximum intensity also reached around 250 Hz and decayed afterward with the increasing frequency of AMF. It is therefore deduced that photon quenching occurs.

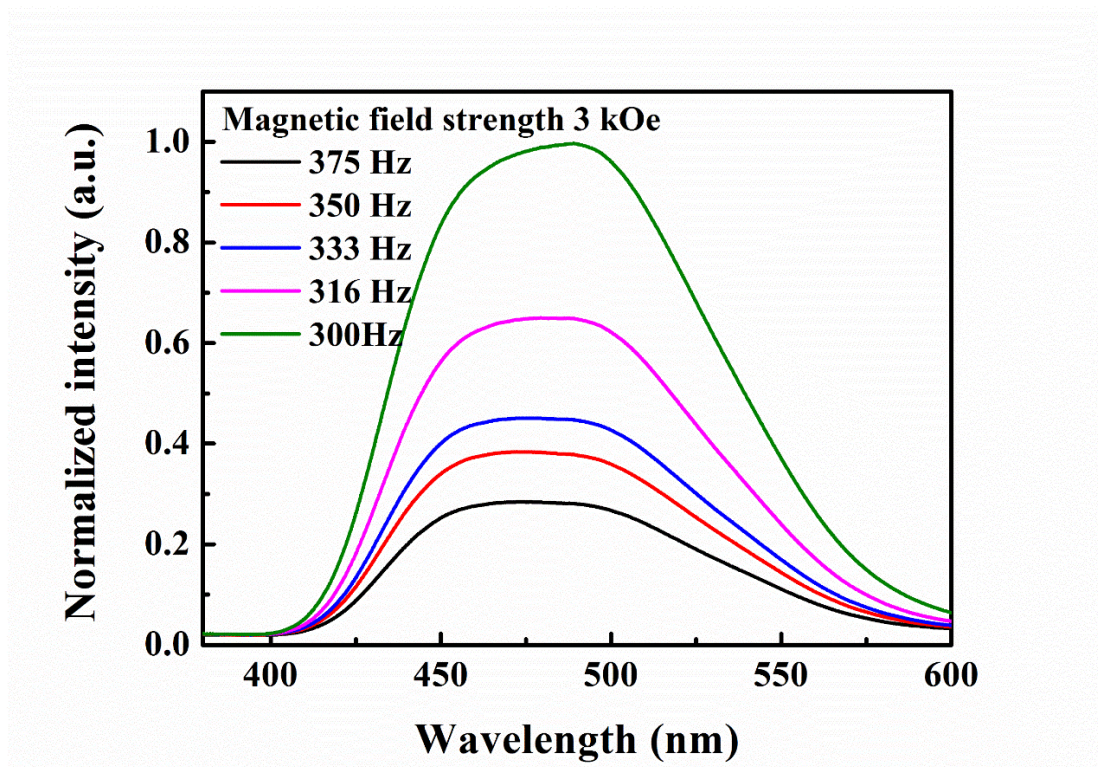


Figure 3-11 Emission spectra of ZnS: Al, Cu phosphor coupled MIL under a high frequency AMF.

One explanation for the suspected photon quenching process is via the direct



dipole interaction of photons with electronic states of two conduction bands. It is the first time such a MIL demonstration showing how such a high-frequency affect the peak wavelength of emission and the area under the emission spectra, as the previous studies of MIL/ML focuses on the magnitude of strain induced onto a sample. [17, 18, 22, 26, 34, 42, 98] And previously Xu et al also demonstrated photon quenching via mechanical stimuli on a ML sample. [99]

Furthermore, results above showed that the emission intensity of MIL depends on both amplitude and frequency of the applied AMF. A rise in the amplitude of the AMF results in an increase in the intensity of the emission spectra without altering the shape of the spectrum, while a rise in the excitation frequency up to 220 Hz, producing two effects. The MIL spectrum blue shifted from 500 nm to 472 nm with the frequency of AMF varying from 50 Hz to 366 Hz. It is suspected in the phosphor, contain a polycrystalline structure caused defects (stacking faults) that introduce localized states with higher energy emissions. Such a variety of peak wavelength is suspected to be due a mechanism of stark effect, band-filling of these charge carriers, and a charge screening effect of the carrier distribution of and the internal electric dipole the present within the phosphor. A blue shift of the emission peak also occurs when increasing the



injection level, high injection frequency as in our case, occurs when there already exists a built-in piezoelectric field and the injected carriers are gradually screening its effect. The other reason contrariwise deduced the blue emission to the transition from the conduction band edge to the t_2 state. On the ground of these arguments, the composite did not show blue ML due to insufficient frequency to excite the blue energy level. That implies the optical properties of the composite can be alternated simply via adjusting the application of frequency of the AMF which open a door to numerous application involving MIL or ML. Figure 3-8 illustrated the spectrum shift and intensity changes with frequency of AMF changes.

3.3.2 Relationship between MIL and magnetic field strength

Under a low frequency of magnetic field, white light emitted from Al, Cu, Mn-doped ZnS based MIL composite, which contains two main peaks. They centered at 525 nm and 588 nm. It is interesting to investigate the relationship between MIL spectrum and magnetic field strength. Theory calculation indicates that the MIL intensity increases linearly with increasing square of magnetic field strength. Experimental results also verified this property shown in Figure 3-9 and Figure 3-10.



When AMF applied to the MIL composite, the magnitude of strain induced by the magnetostriction of MR elastomer is enhanced with increasing magnetic field strength. Hence, more charge carriers are detrapped when increasing the magnitude and frequency of AMF, resulting in the enhancement of e–h recombination and MIL. There are two mechanisms involved in these two emission peaks. The origin of these two peaks can be described as follow. Briefly, after the magnetic field induced a stress onto the phosphor, a piezopotential arise inside the ZnS crystal. For 503 nm, a donor acceptor recombination occur as this piezopotential detrapped the charge carriers in the copper and aluminum occupied zinc site. The recombination of these charge carriers give rise to the emission. For the 580 nm emission, the large piezopotential enable the detrapped charge carrier to obtain enough energy to accelerate and become hot electrons. They impact and excited manganese ions to emit its characteristic light

Importantly, the linear relationship of MIL intensity versus low frequency range and H_{rms}^2 should benefit to developing novel MIL-based magnetic sensors when considering that good linear relationship between the output and input signals is preferred in practical application.

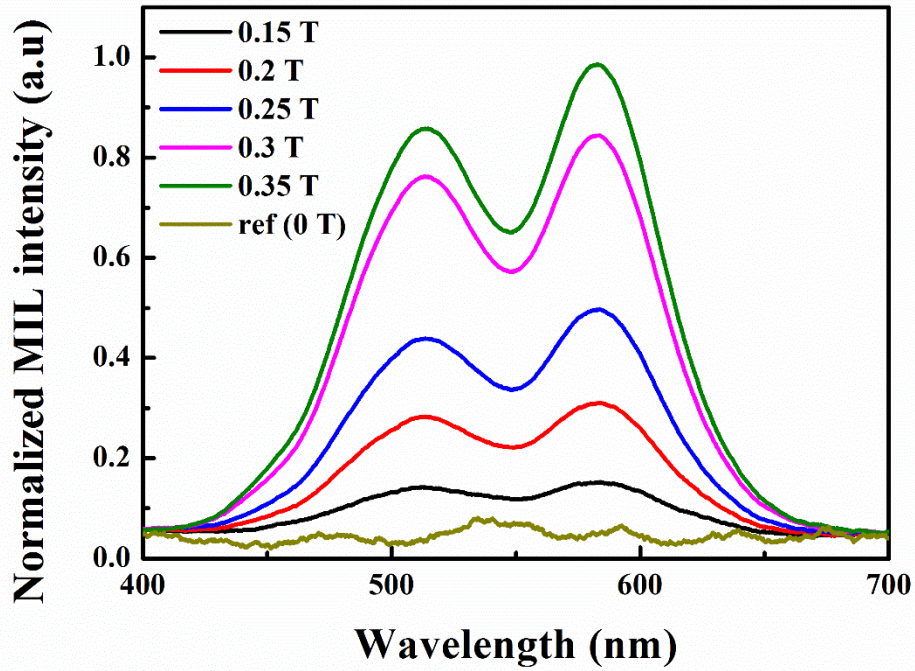


Figure 3-12 Emission spectra of ZnS: Al, Cu, Mn phosphor coupled MIL under various strength of AMF.

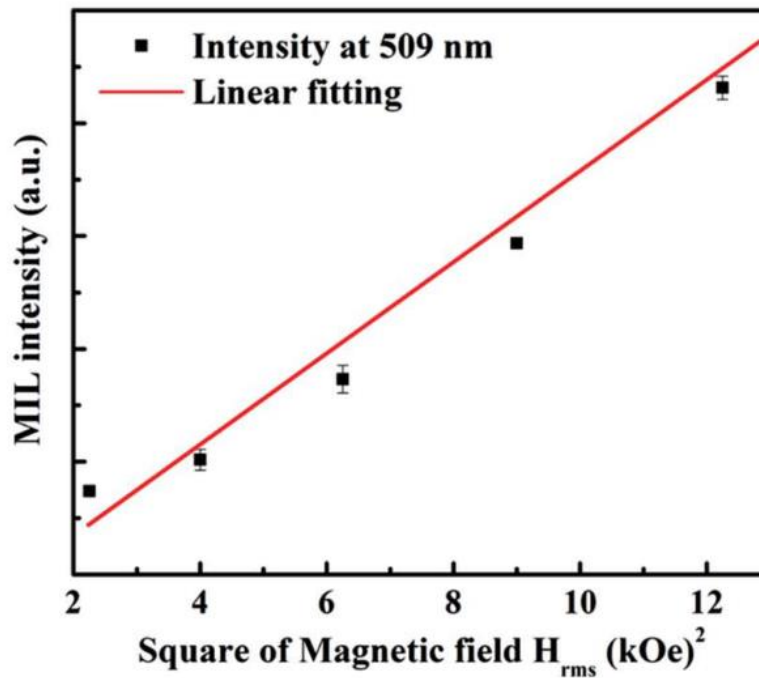


Figure 3-13 Intensity of ZnS:Al, Cu phosphor coupled MIL under various strength of AMF.

3.3.3 Transient response of MIL

The transient characteristic of MIL from the Al, Cu-doped ZnS based MIL composite was studied. AMF with the frequency of 50 Hz was initially switched on and retained at 3.5 kOe for 30 s and subsequently switched off. In response to the switching cycle of from 0 to 3.5 kOe, MIL intensity peaked at 509 nm rises until its saturated value, when the AMF is switched off and then begins to fall towards zero when the field strength decreased from the maximum value of 3.5 kOe to 0 as expected.



Figure 3-11 shows the transient response of MIL.

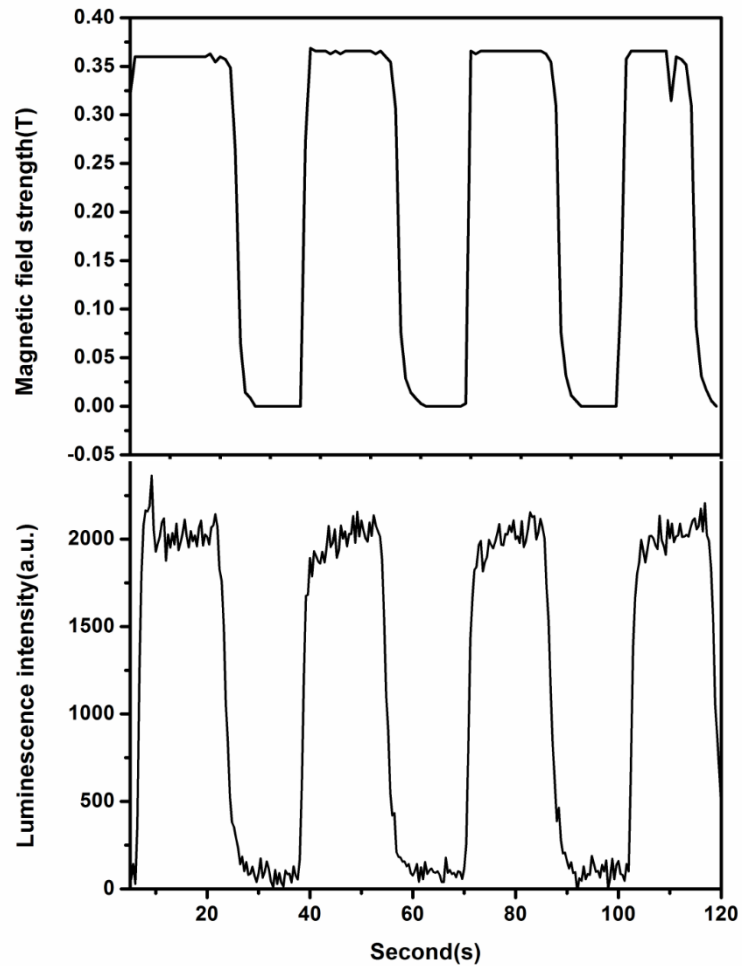


Figure 3-14 Transient response of green MIL from the Al, Cu-doped ZnS

phosphor composite.

Figure 3-12 shows the transient response of MIL in one cycle. The rising and falling edges of MIL respond the changes in can be fitted as exponential growth and decay functions, respectively. The time constant for rise and fall are determined to be



2.85 s and 3.15 s, respectively. The time constants are determined by following the equation describing the MIL intensity

$$I = \alpha\beta\sigma\lambda \frac{\partial H}{\partial t} (1 - e^{-t/\Gamma})$$

Such that by fitting these data obtain from experiments, the time constants therefore can be calculated.

It should be pointed out the rise time serves as the response time of the MIL phosphor composite in the device applications. Since AMF are employed, the composite should experience tensile and compressive strains in one cycle, it would induce piezoelectric potential with opposite polarity in the metal-ion-doped ZnS. Such effect may result in the different response of luminescence at the rising and falling edges, which has been studied in our previous reports. [18, 19]

Another MIL emission peak at 580nm should have a transient should have a similar relaxation time. Firstly, the decay times obtained are strongly depend on the decay time of the applied magnetic field. Secondly, the time constant of impulsive deformation of ZnS:Mn phosphor 580 nm emitting phosphor according to previous studies is around 0.02 s. This is negligible when compare with the decay time of our magnetic field. Such that it is believe that the relaxation time is strongly depend on the



setup of the magnetic field instead.

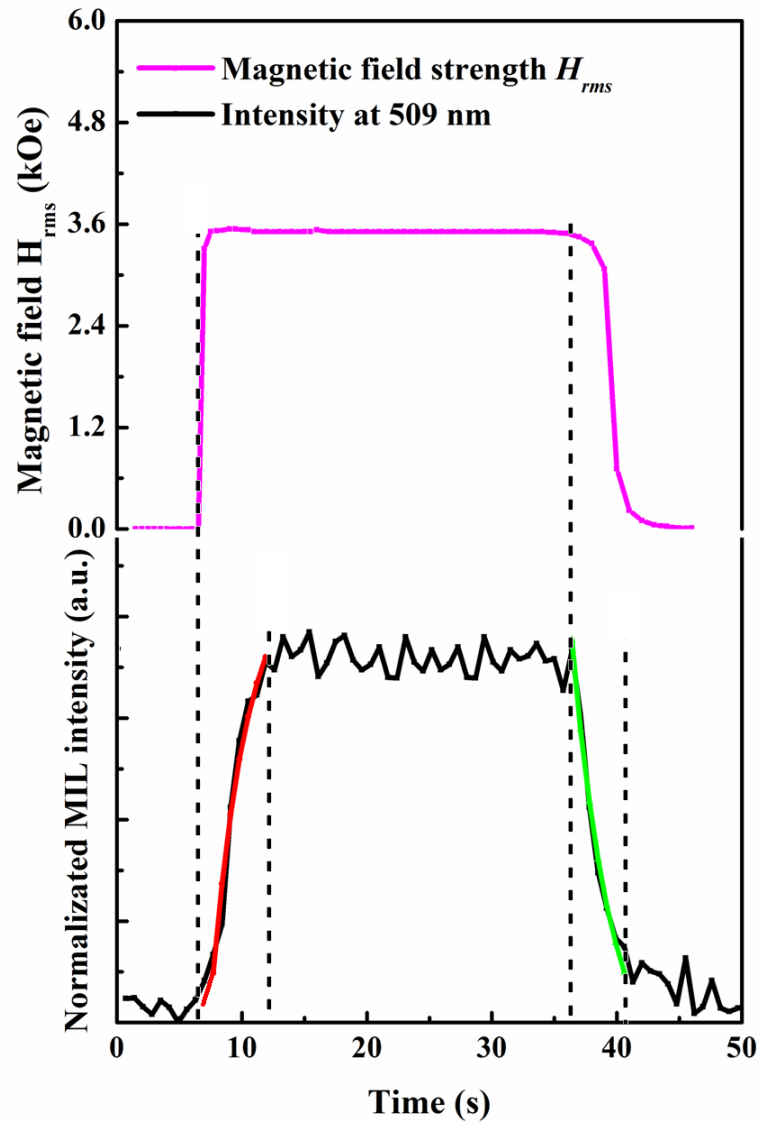


Figure 3-15 Enlarged graphs of a single cycle. The rising and falling edges of MIL can be fitted to exponential growth (red) and decay (green) functions.



At any rate, the obtained result shown in Figure 3-12 demonstrates the modulation of the luminescence in reversible and dynamical manners with time-varying magnetic field applied to MIL composites, which should be very promising to design and make new concepts of magnetic-luminescence devices.

3.3.4 CIE of MIL

The conventional Commission Internationale de L'Eclairage (CIE) diagram of the observed green and white light emissions has been investigated, which was shown in Figure 3-13. The CIE coordinates are found to be (0.3462, 0.3735) and hence the CCT is determined to be 5027 K, indicating the obtained MIL phosphor composite emits a somewhat cool white color. The bottom left of Figure 3-14 demonstrated the blue shift from green to blue of CIE values as the frequency of the AMF varies. It not only implies the controllable emission properties from AMF but as the emission spectra increases to a higher energy level, new applications can be imposed and a discussion on MIL coupling with PL will be presented in the next chapter.

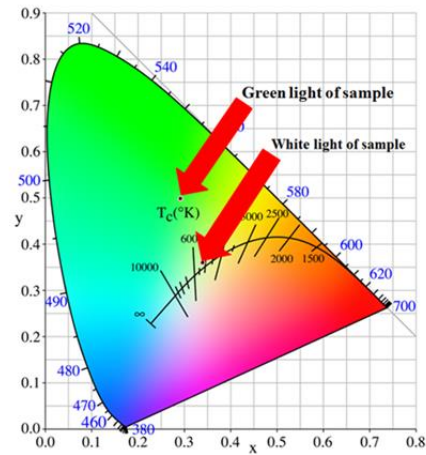


Figure 3-16 CIE diagram showing the green and white lights of the obtained MIL-based pattern and light source.

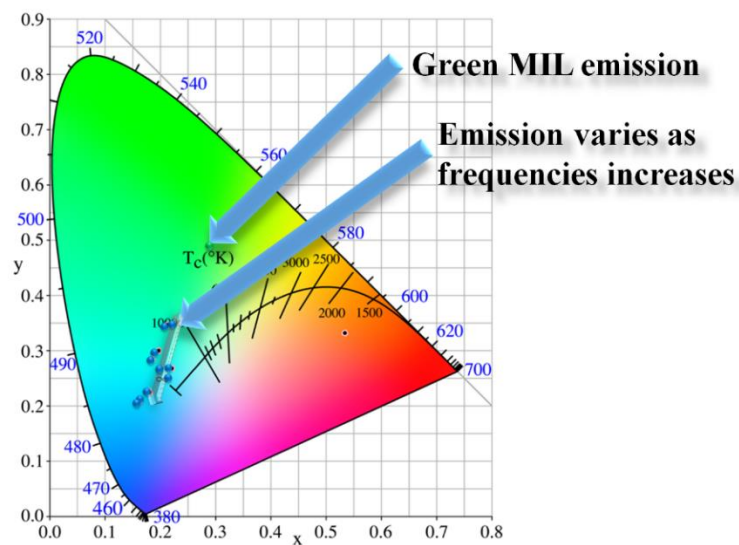


Figure 3-17 CIE diagram showing the green and tunable blue lights of the obtained MIL-based pattern and light source.



Chapter 4 MIL coupling with photoluminescence

To expand the emission spectrum of MIL and shed more light on MIL's potential application, two phosphors are utilized to further expand the emission spectra. Yttrium aluminium garnet (YAG: Ce) has been recognized as a prominent wide band gap semiconductor for PL applications due to its unique optical properties. It is usually used in LED phosphor and display applications. High quality YAG: Ce shows an emission spectrum in the near-yellow region with high intensity. When incorporated with the blue emission of MIL discussed in the previous chapter, a white tunable MIL emission is recognized.

Calcium strontium sulfide doped with divalent europium ($(\text{Ca}_{1-x}\text{Sr}_x) \text{S} : \text{Eu}$) powder typically emits over a wide range of the visible spectrum. The aims of this strategy for MIL induced simultaneous persistence luminescence result tricolor (RGB) luminescence and a prolonged reddish emission.



4.1 Composite fabrication

4.1.1 White MIL composites fabrication

Similar to the previous chapter, ABS and PMMA mold were employed, but with a diameter of 1 mm and a length of 3 mm. Then, YAG: Ce and ZnS: Cu/ZnS: Al, Cu microparticles with weight ratio of 5:3 were uniformly mixed in PDMS and poured into the PMMA mold. The concentration of YAG: Ce particles have been optimized in preliminary tests, to emit the closest CIE value of white light. After curing the composite at 70 °C for 2 h, the rods were extracted and inserted into each hole of the ABS mold, which half filled with uncured MR elastomer. The MR elastomer also consists of magnetic Fe-Ni-Co microparticles embedded in uncured PDMS in weight ratio of 2.5:1. Then, the samples were degassed for 30 min to ensure good adhesion between the luminescence phase and MR elastomer with good structural integrity. The mold was put into oven to 110 °C for 24 h. Finally, the ABS mold was removed, multiphase composites with magnetic sensitive composite and ML phosphor composite is obtained.



4.1.2 RGB MIL composite fabrication

A new ABS mold with the same dimensions discussed in the previous section is used, with the same PMMA mold. ZnS: Cu/ZnS: Al, Cu microparticles were uniformly mixed in PDMS with a weight ratio of 7:3 and poured into the PMMA mold. After curing the composite at 70 °C for 2 h, the rods were extracted. These rods intended to exhibit simultaneous persistent luminescence was further coated with ((Ca_{1-x}Sr_x) S: Eu) microparticle doped PDMS and cured the composite for 12 h at 70 °C. They were extracted and one end of the rods was coated with the MR elastomer of Fe-Ni-Co microparticles mixed to PDMS with weight ratio of 2.5:1. The mold was put into oven to 110 °C for 24 h to cure the polymer after degassing. After removal of the ABS mold, multiphase composites with magnetic sensitive and ML phosphor able to emit tunable simultaneous persistence red color, blue and green was obtained.

4.1.3 RGB MIL wafer sized composite display fabrication

The ZnS: Cu/ZnS: Al, Cu microparticles was uniformly mixed with a weight ratio of 8:2 in PDMS, which base to curing agent ratio at 20:1, the mixture then spin-coated onto a SiO₂ substrate to obtain a ML thick film, then cured at 110 °C for 2 h. A



mixture of uncured PDMS and persistence luminescence phosphor (weight ratio of 1:1) was screen printed onto the desired area of the thick film. After extraction, the polymer film was rod coated with stiffer PDMS, with base to curing agent ratio at 5:1 on both sides. The polymer film then en-caped with MR elastomer, which consisted Fe-Ni-Co microparticles embedded into PDMS with a weight ratio of 5:1 by means of a PTFE mold. After degassing for 30 mins, the mold was put into oven to 70 °C for 24 h to cure the polymer. After removal of the mold, multiphase composites with magnetic actuator composite and ML phosphor composite was obtained.

4.2 Results and discussion

In this chapter, a brief discussion of the morphology of the MIL coupling with PL composite is presented. Then the mechanism underlying MIL inducing white luminescence and simultaneous persistence luminescence will be given. Green light and a specific warm white of the MIL phenomenon under low frequency will be demonstrated. Finally, a much wider range of color emission generated by high frequency magnetic field will be presented.



4.2.1 Morphology of MIL multicolor display composite

In order to observe prolonged persistence luminescence at high frequency of magnetic field, the design of the MIL persistence luminescence converter of polymer, magnetic particle, and phosphor should be optimized to reach a compromise between elastic module, magnetic permeability, and MIL luminescence. The mixing ratio between phosphor and polymer and thickness of the active layer plays a key role in the composite fabrication. If the composite was not well prepared, neither MIL nor long persistence luminescence emission can be observed.

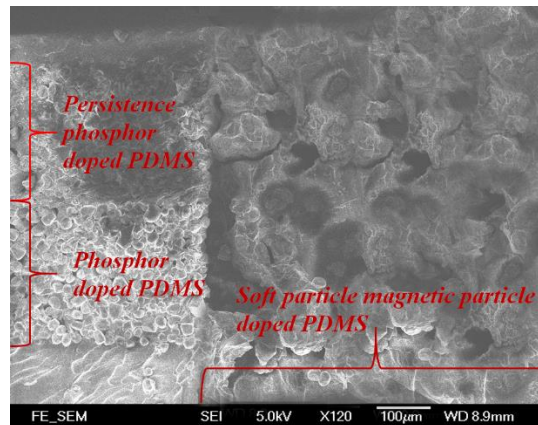


Figure 4-1 SEM images of the synthesized PDMS polymer composite laminate consisted of Fe–Co–Ni alloy particle-based magnetic elastomer, metal-ion-doped ZnS microparticle-based mechanoluminescence phosphor and Persistence phosphor.



To show the possibility of MIL induced simultaneous persistence luminescence composite, and demonstrate a display of tunable red luminescence emission via MIL. Both ML phosphor and simultaneous persistence luminescent material were mixed into a soft organic polymer matrix PDMS. In here as shown in Figure 4-1, a wafer-sized, flexible display was introduced. Different from the previous chapter, the design required a more delicate balance between the three components employed. The weight ratio of the three components of polymer, magnetic particle, and phosphor are further optimized to reach a compromise between elastic module, magnetic permeability, luminescence intensity, and other requirements in this hybrid structure. In the light of these conditions, the requirement for luminescence polymer matrix material has to be as soft as possible to optimize the magneto-elastic ratio. It is a delicate balance between the maximum magnetization of the whole composite and its mechanical strength. Also, the combination of two or more luminescence material sources is a useful concept for the manufacture of various optical devices, which has a promising application of standalone, connection free device display-related applications with environmental adjustable optical properties and prolonged afterglow.



Here, a new design of longitudinal AMF instead of a rotating one, a higher loading content of the Fe-Ni-Co particle was incorporated into the MR elastomer. In order to induce the optimized strain required, the magnetic and elastic properties of the MR polymer were first measured in experiments by applying a magnetic field along the axial direction along the length of the samples. As prior discussed, to obtain wafer scale MIL multicolor display, the first priority is to enhance the MIL intensity in order to stimuli the persistence phosphor. Therefore, the structure of the ML phosphor doped PDMS was further modified. Optimize the structure so that it can sustain high frequency and large stress. Various techniques to produce wafer size composite are reported in a number of literatures. [100, 101] Aforementioned, the structure–property relationship and thickness play an important role in the composite, exhibiting a compromise between flexibility and luminescence intensity. As a rule of thumb, the size and concentration of the MIL phosphor doped into the polymer matrix must be carefully elevated. In principle, a higher amount of phosphor yields a higher intensity, but result in weaker ductility and uniformity. So that prolonged MIL and the subsequent induced simultaneous persistence luminescence is impossible under any given magnetic field. On the other hand, adding low-weight ratio phosphor



microparticles to a composite decreases the Young's modulus of the composite, as the composite with a low concentration of phosphor particles becomes more ductile but dimmer. Such inappropriate design will result in a more flexible material with reduced strain delivered to phosphor phase. One preparation technique to produce a composite film structure with the filling of the active layer of PDMS in the pores of one or two support layer. With active luminescence layer with a lower concentration of crosslinker, and filled with ML phosphor in highest weight ratio, and coated it with persistence luminescence phosphor. Then one or two supporting layers with high young modulus PDMS was rod coated onto the active layer. This supporting layer not only provides the structural integrity of the active layer structure. A multi-directional stress was applied to the active layer and induced an enhanced MIL emission. As a result, MIL activated simultaneous persistence luminescence is accomplished.

4.2.2 Mechanism for persistence luminescence via MIL

Consider Figure 4-2, when applied external magnetic fields on the MIL composite, two MIL emission spectra peaked at 509 nm arisen from the piezoelectric potential of metal-ions doped ZnS.

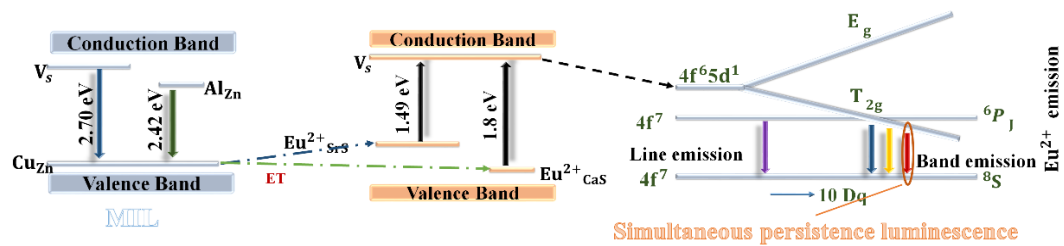


Figure 4-2 Schematic showing the coupling between MIL with simultaneous persistence luminescence.

The band structure of semiconductors changed under strain actuation from MR elastomer. This 509 NM MIL emission in turn excite and the emission spectrum of (Ca_{1-x}Sr_x) S: EU shows one instead of three major features; the red emission of (640 nm), however the broad emission band (350 to 550 nm) which characteristic of the case host and an additional peak at 580 nm is absent. Comparing with the excitation under 350 nm, the characteristic broadband emission of with the maximum at 640 nm is corresponds to the Laporte allowed transition from the 4f⁶5d¹ to the 4f⁷ levels. The shape and the band position were found to be independent of the concentration of Eu. The intensity of the band decreases in here is expected to be risen from concentration quenching of Eu, such that only a single narrow band is observed. As discussed prior, a long decay is ascribed to the afterglow when the AMF is turned off. It is noticeable that the excitation spectrum does not show any significant changes from the 509 nm



with 500 nm.

In every experiment, persistence phosphor coated MIL display was magnetic field by means of AMF in a constant field strength or frequency. The new mechanism of MIL induced simultaneous persistence luminescence via stress management. The MIL luminescence spectra of Al, Cu, doped ZnS phosphors combined with $(Ca_{1-x}Sr_x)S:Eu$ MIL composite (509 nm + 640 nm) is shown in Figure 4-3.

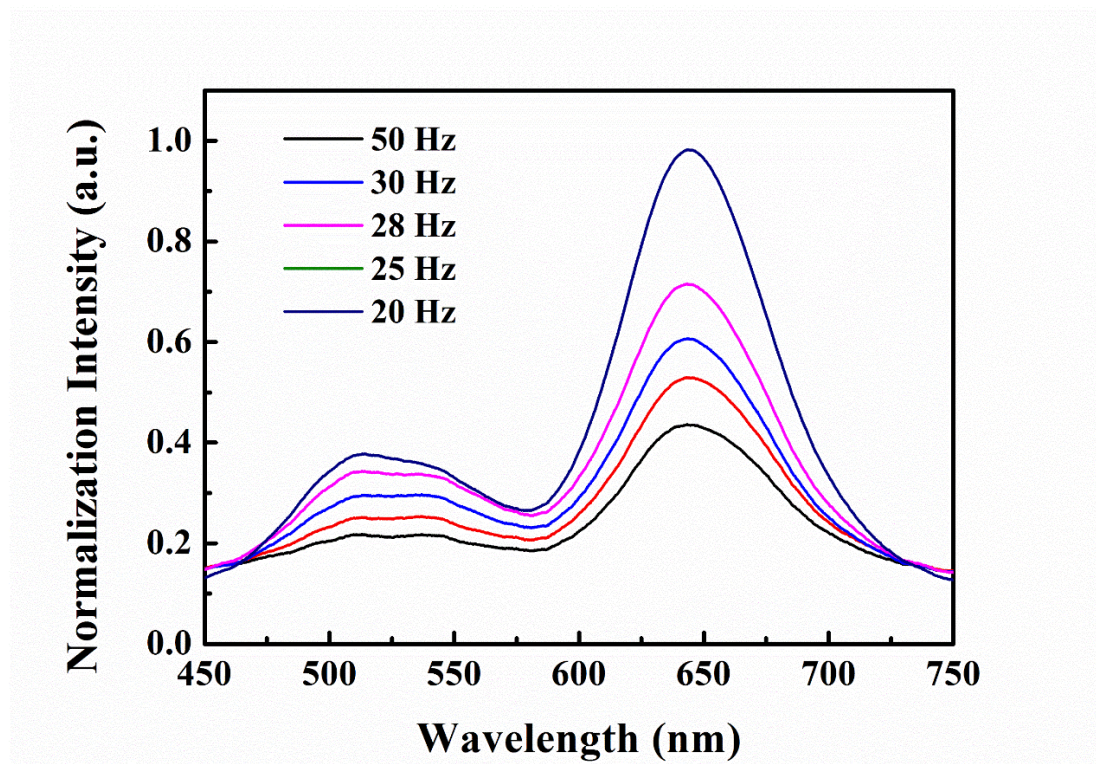


Figure 4-3 Emission spectra of persistence luminescence excited by MIL under a low frequency of AMF.



On the whole, the obtained MIL/PL emission profiles shares similarity to the previously observed green to white emission spectra from the corresponding phosphors. In Figure 4-3 the dominant peak is seen at 640 nm. It is noticeable that the MIL intensity increases linearly when increasing frequency of magnetic field strength. The magnitude of strain is enhanced with an increase of magnetic field strength. Importantly, the linear relationship of MIL intensity versus low frequency range should benefit to developing novel MIL-based magnetic sensors when considering that good linear relationship between the output and input signals is preferred in practical application.

4.2.3 Transient response

Figure 4-4 demonstrate the dependent of AMF frequency and field strength excitation, the modulation of the rise time of the persistence luminescence and the intensity with various frequencies of AMF applied to MIL composites, the graph study the photo-stimulated emission time (PST) as a function of excitation (509 nm) power, where PST is defined as the time required to release the electrons from the deeper traps using 509 nm excitation.[46]

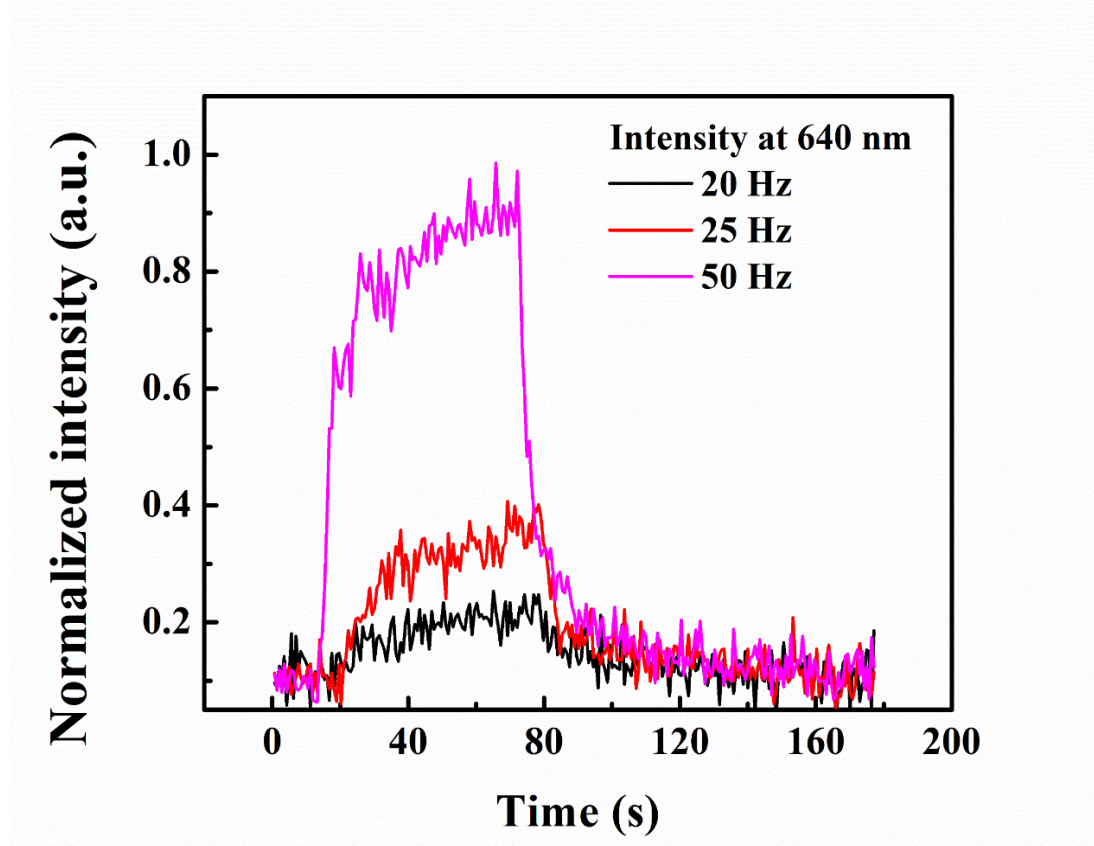


Figure 4-4 Enlarged graphs of a single cycle of simultaneous persistence luminescence via MIL excitation of various frequencies of AMF.

It was observed that as the frequency of the AMF decrease, the intensity of MIL is decreased. The PST becomes longer due to less photons are available to excite the electrons in the traps. The MIL intensity also dictates the intensity of the simultaneous persistence luminescence.

Figure 4-5 shows the transient characteristic of MIL from the persistence



luminescence/metal ions doped ZnS green-phosphor-based composite. In this measurement, biaxial AMF with a frequency of 50 Hz was initially switched on and retained at $H_{rms} = 1.2$ kOe for 1 min and subsequently switched off.

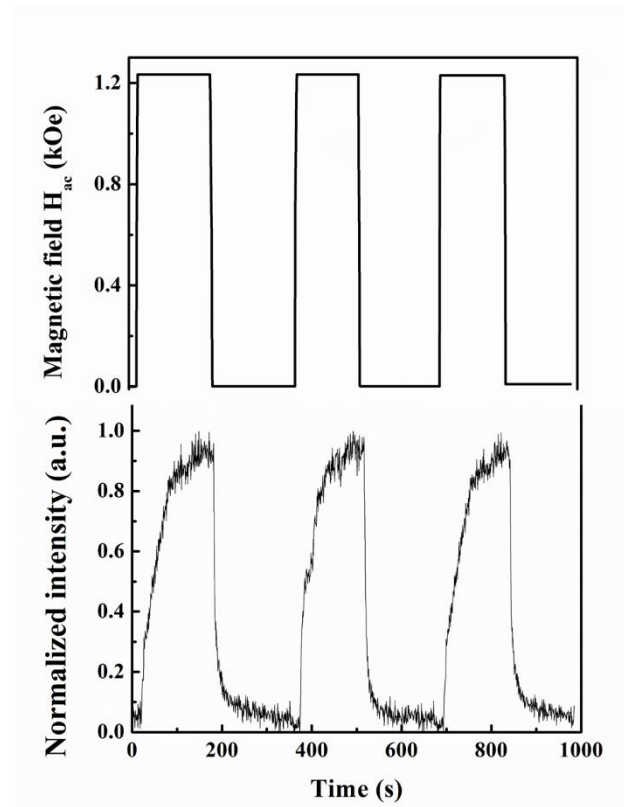


Figure 4-5 Transient characteristics of persistence luminescence via MIL excitation from the Al, Cu-doped ZnS green-phosphor based composite.

In response to the switching cycle of magnetic field from 0 to 1.2 kOe, MIL induced persistence luminescence intensity peaked at 640 nm with intensity rising



when the AMF switches on. And then begins to decay when the AMF is decreased from the maximum value of to 0 as expected. The length of irradiation time (charging time), with MIL at 509 nm, did affect the duration of the afterglow. To ascertain the effect of the charging time on the duration of the afterglow three charging times were studied, (not shown here). A charging time of 1.5 min was found to give the longest duration of the afterglow (The time taken for the emission to subside without irradiation and the sample is placed in the dark) for the same samples (120 s and 250 s). This optimal charging time ensures the complete lowing of the traps. It is interesting to notice that using longer charging times produced shorter duration of the afterglow, which can be attributed to the saturation of shallow traps for a given intensity of MIL, and with the subsequent release of the electrons occurring in the same time frame as the charging process. This results the desired reddish simultaneous persistence luminescence.

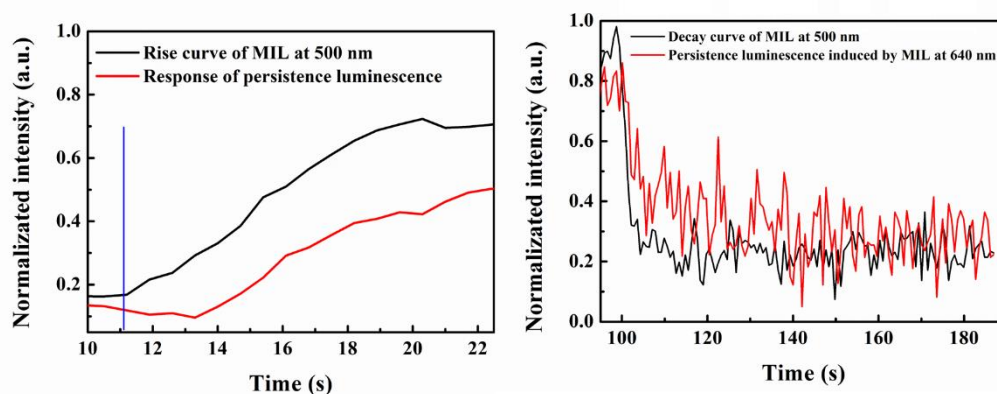


Figure 4-6 The rising and falling edges of MIL and persistence luminescence. The Blue line is when the AMF activated.

To shed more light on the properties of the simultaneous persistence tunable MIL, Figure 4-6 enlarged a section of the charging of the persistence phosphor with the MIL, and de-trapping from the shallow traps at room temperature. The data show the increase in the intensity of the photo-stimulated emission as a function of time. There is approximately exponential increase in the MIL intensity and a few millisecond delays of the MIL induced persistence luminescence under time-varying amplitude of AMF. As described the photo-stimulated emission proceeds via two steps: the storage of energy by MIL excitation followed by the release of the stored energy via red color emission. According to the fitting curves (not shown), the rise time constant of MIL and persistence luminescence are determined to be 7.7 s^{-1} and 14.28 s^{-1} , respectively.



It should be pointed out the rise time serves as the response time of the MIL phosphor composite in the device applications. Moreover, this novel type of display will highly depend on the constant coupling of MIL with persistence luminescence. Also, the persistent phosphor show a prolonged decay (~ 1 min) compares with ML (~ 10 s). [35] As expected, the persistence luminescence intensity was found to increase with the increasing AMF field strength, contributions of MIL intensity increase. In addition to the experimental test results showed that persistence luminescence decay rates under MIL are no significant differences from normal PL decay rates.

To visualize the color dependence on the AMF frequency, CIE color coordinates that represent the simultaneous persistence luminescence colors from the composites under various frequencies was shown in Figure 4-7. Two behaviors can be observed. First, the color varied according to the AMF frequency; this occurs because the CIE coordinates of the multi-component light are linear combinations of the individual coordinates. Second, the red color shift was associated with increasing frequency due to the intensity of MIL emission.



promising for practical applications in science and engineering. In here, a demonstration is done to shed light of this interesting property, the emission spectra of this composite, compare with the spectra of the blue emission under the same condition, imply that various yellow colors are arise from the excitation from MIL under a sufficient level of frequency of AMF.

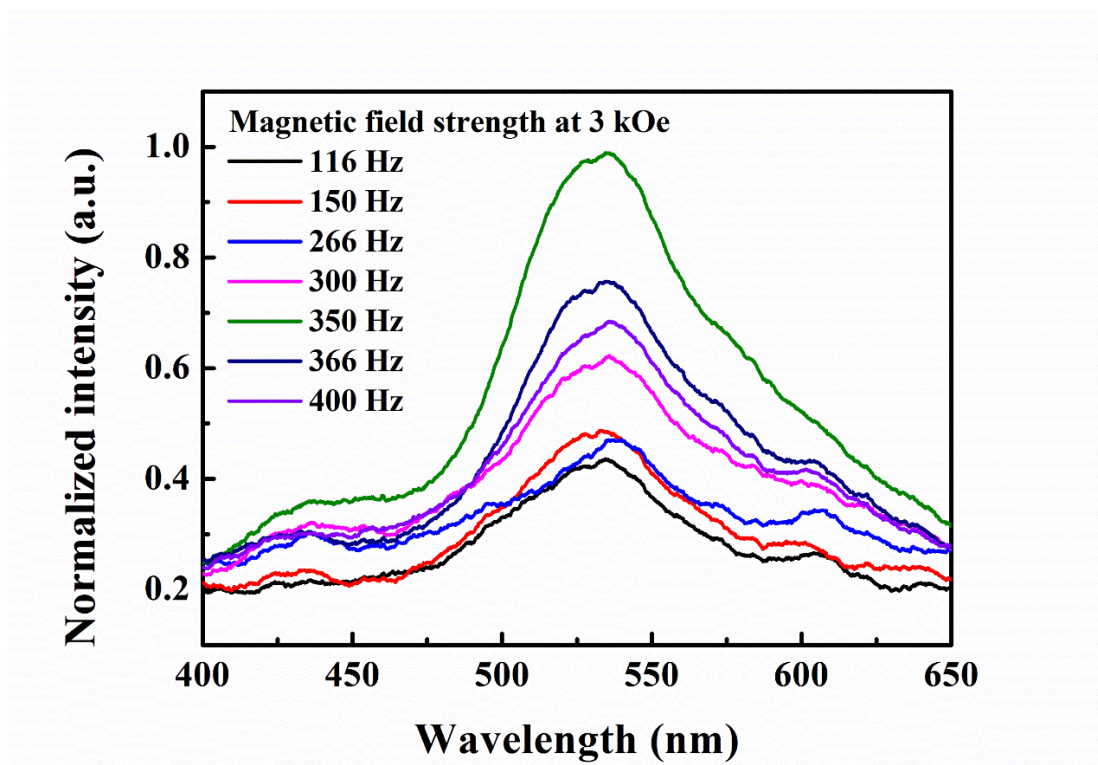


Figure 4-8 Emission spectra of YAG: Ce phosphor coupled with MIL excitation under a high frequency AMF.

The frequency of AMF modulates the wavelength of MIL. It demonstrates the



capability of a tunable white emission. It was discussed in chapter 1 that three excitation bands appear with peak wavelengths at 233, 340, 470 nm for YAG: Ce crystal. There is one electron in the 4f state of Ce^{3+} , and the ground state of Ce^{3+} is split into $^2F_{7/2}$ and $^2F_{5/2}$. The major excited spectrum peak locates at 472 nm, which matches the blue emission of MIL very well. As shown in Figure 4-8, the emission peak locates at about 535 nm, which can combine the blue light of the high frequency stimulated MIL to yield a white emission. It is well known that the emission at 535 nm is attributed to the 5d–4f transition of Ce^{3+} , which depends strongly on the crystal field.[102]

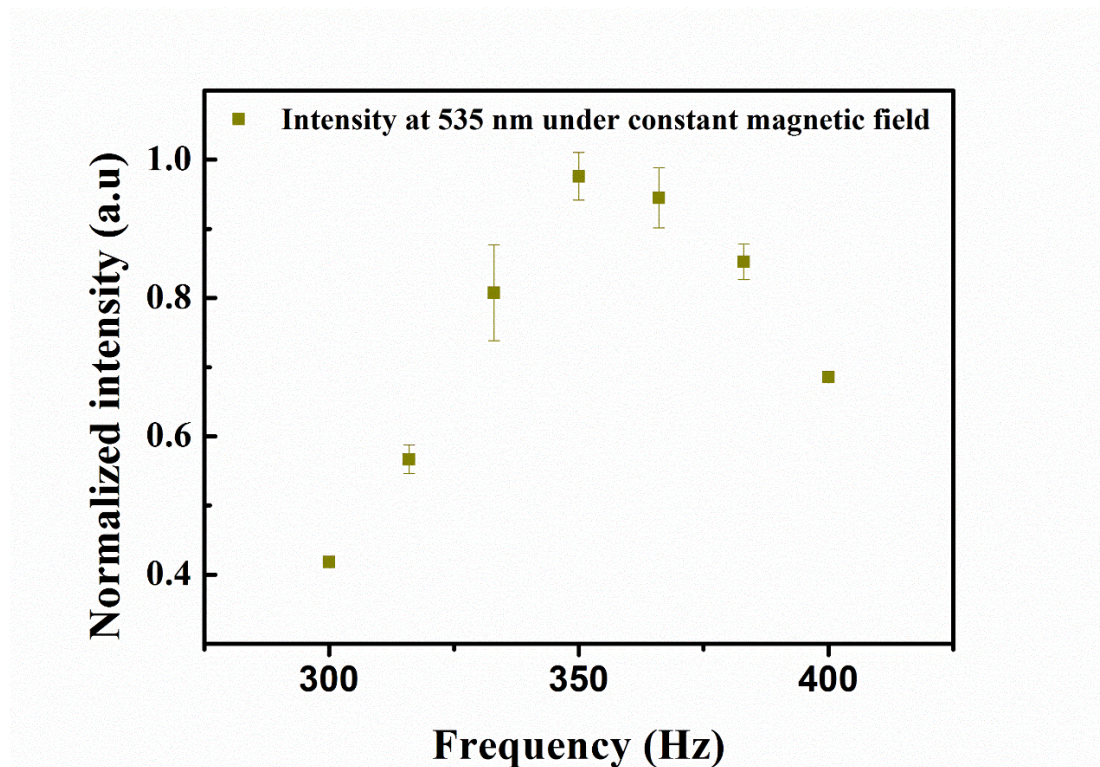


Figure 4-9 Normalized intensity of YAG: Ce phosphor coupled MIL excitation under a high frequency AMF.

Figure 4-9 show the trend of the intensity of luminescence of the 535 nm PL via MIL excitation. It roughly follows the trends from that of blue MIL emission. The principle of the luminescence conversion as ZnS: Al, Cu phosphor doped PDMS is homogeneously mixed with luminescence converter consisting of YAG: Ce powder and form a MIL composite. When excited by high frequency AMF, the blue emission is partially emitted at 535 nm yellowish emission via PL coupling. This combination



forms a warm white (6028 K) emitting MIL at the optimum frequency.

4.2.5 Demonstration of MIL

In order to show the potential of MIL phenomena for potential applications such as display and white lighting, we have made patterned arrays as illustrated in Figure 4-10.

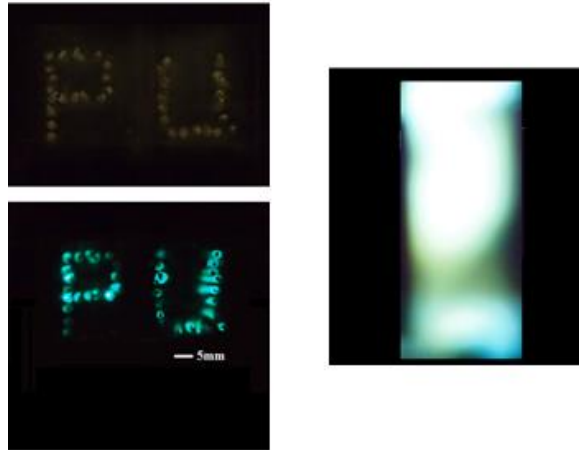


Figure 4-10 Displaying green colored logo “PU” representing the abbreviation for the Hong Kong Polytechnic University from MIL materials driven by low magnetic field without (upper) and with a magnetic field (lower), White color emission of MIL light source. [35]

In the measurements, the magnetic field of $H_{\text{rms}} = 3.5$ kOe with a frequency of



50 Hz were employed at room temperature. With ZnS: Al, Cu doped base MIL composites, displaying green colored logos “PU” representing the abbreviation for the Hong Kong Polytechnic University as shown in the photograph in Figure 4-10. In addition, the right side of Figure 4-10 illustrates white-light emission from MIL made by ZnS: Al, Cu, Mn based composites. Both green letters and bright white source can be seen by the naked eyes. As the samples are all handmade and as a proof of concept. The resolution is around $0.5 \text{ mm} \times 0.5 \text{ mm}$. Moreover, without the regards of fabrication method, the MIL composite’s resolution only limited by the sizes of these particles doped into the polymer matrix. In present, lab based ML phosphor and magnetostrictive material are with size of 50-100 nm.

In order to show the potential of applying tuning and incorporation of MIL phenomena with other PL material potential applications, a patterned RGB array was fabricated and illustrated in Figure 4-11. In the demonstration, the magnetic field of $H_{\text{rms}} = 2.5 \text{ kOe}$ with the frequency of 250 Hz was employed at room temperature. Also With Al, Cu-doped ZnS-based MIL composites (screen/spin) coated with $(\text{Ca}_{1-x}\text{Sr}_x) \text{S}:\text{Eu}$ doped PDMS, the red colored logo of the Hong Kong Polytechnic University as shown in the photograph of tricolor in Figure 4-11. Both dynamic demonstrations can



be reversible and seen by the naked eyes.

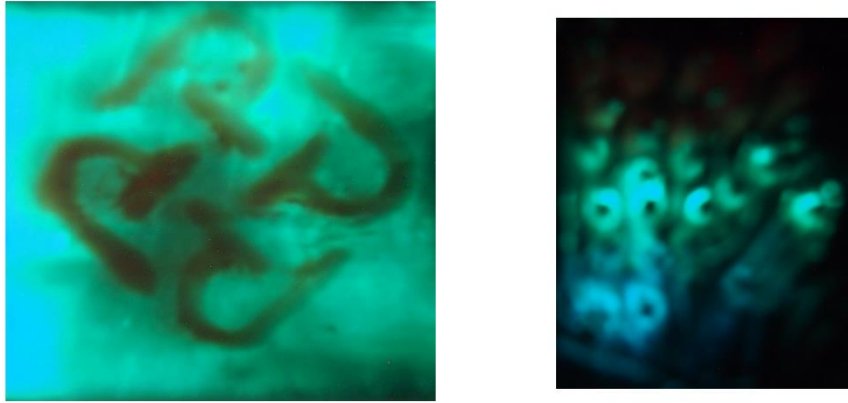


Figure 4-11 Photograph of MIL light source under uniaxial magnetic field of the red color logo representing the Hong Kong Polytechnic University (left) and displaying red, green and blue colored MIL matrix under high frequency AMF (right).

Figure 4-12 presents the tune-ability of green to white emission under varying frequency of AMF. It shows a MIL sample mixed with YAG: Ce changed color with increasing AMF frequency. The MIL induced luminescence images from our samples with varying color from 116 Hz and 400 Hz. As the AMF frequency increased, the brightness increased until 250 Hz, then decreases again.

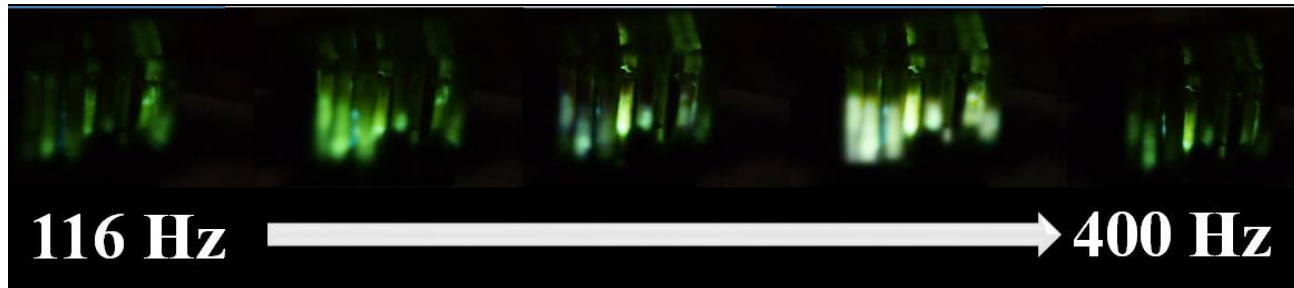


Figure 4-12 Photographs of the MIL for color tuning under various AMF frequencies and field strength of 2 kOe.

4.2.6 Performance and efficiency

A new term is defined as the MIL efficiency as the composite is driven by magnetic field such that, it is light emission output divided by magnetic field input strength in the unit of lm/Oe.

The gathered emission efficiencies recorded as the following table.

| Luminescence type | CIE | CCT | Luminance (cdm ⁻²) | Efficiency |
|---------------------|------------------|------|--------------------------------|------------|
| White MIL | (0.3427, 0.3735) | 5027 | 19 | 0.0013 |
| High Freq. Blue MIL | (0.1885, 0.2018) | n/a | 28 | 0.0025 |
| Low Freq. MIL Green | (0.2893, 0.4884) | n/a | 21 | 0.0014 |
| PL coupled white | (0.3443, 0.3427) | 6028 | 24 | |
| PL coupled red | (0.5897, 0.2981) | n/a | 15 | |

Table 1 Performance parameters of the emissions based on MIL composite.

The intensity of the MIL display design is comparable to commercial night light



with around 5 lm, which should be very promising to design and make new concepts of tricolor MIL devices or display. An external quantum efficiency (ZEQE) of (69.5 ± 5) % was obtained in the as-prepared persistence luminescence phosphor without further optimization or purification of raw materials (for both excitation at a wavelength of 500 nm and 509 nm).



Chapter 5 Conclusion and future work

The present research is on the realization of magnetic induced luminescence from flexible magnetic composite laminates via strain-mediated coupling. The samples have been characterized by various instruments to explore their properties in different aspects.

5.1 Conclusion

The main objectives of the presented work are to investigate a novel MIL phenomenon from the magnetic composite laminates via strain-mediated coupling. A practical approach to design and fabricate composite laminate systems composed of magnetic actuator and phosphor materials has been proposed. Structure, magnetic, and elastic characterizations of the magnetic elastomer and luminescent dependent on the amplitude and frequency of the magnetic field as well as CIE, CCT, luminance, and power efficiency have been tested. The main conclusion can be briefly described as follows:

A facile polymer package method has been used to fabricate the magnetic



composite laminates. Multiphase rods consisted of the composite of metal-ion-doped ZnS micro particles mixed to PDMS and another composite of magnetic Fe–Co–Ni alloy particles mixed to PDMS were fabricated. Physical properties of the multiphase composite are important to the magnetic responsive luminescence. A compromise between magnetic permeability, elastic module and luminescence was investigated. It is found that the magnetic behavior of the Fe–Co–Ni alloy + PDMS composite can be approximately considered as linear with no significant hysteresis because of negligible coercive field ($H_c \approx 9$ Oe). The maximum values of stress and strain are 0.45 MPa and 4.4%, respectively under the external DC magnetic field of 3.5 kOe. The Young's modulus for the sample is calculated to be 70 MPa under a zero magnetic field. When an alternating magnetic field acts on the sample, the transient strain produced in Fe–Co–Ni + PDMS side delivers to the metal-ion-doped ZnS PDMS side and subsequently generates light.

Relationships between the luminescence of the magnetic composite laminates and the amplitude and frequency of the AMF have been investigated. When applying an AMF, the Al, Cu doped ZnS phosphors combined with Fe–Co–Ni alloy microparticle + PDMS emits bright green light and its luminescence spectrum peaks



at 509 nm, which can be explained from the donor–acceptor (D–A) recombination of $\text{Al}_{\text{Zn}} \rightarrow \text{Cu}_{\text{Zn}}$. While the Al, Cu, Mn-doped ZnS phosphor composite emits white light with two main peaks at 525 nm and 588 nm. No emission peak shifts with varying magnetic amplitude or frequency in our experiment. When the frequency of the magnetic field varies from 26-50 Hz or the magnitude of magnetic field strength increases from 2.0 to 3.5 kOe, the MIL intensity increases linearly with either f or H_{rms}^2 , which is consistent with the proposed MIL model. This result also accords with the variation tendency of strain, which is enhanced by an increase in the strength of the magnetic field. This is due to that more charge carriers are detrapped when increasing the magnitude and change rate of the magnetic field, resulting in the enhancement of e-h recombination and MIL. The response time of the MIL phosphor composite has also been measured. The rise time (τ_r) and the fall time (τ_f) are determined to be 2.85 s and 3.15 s, respectively. The results show that the MIL can be modulated reversible and dynamical manners with time-varying magnetic field.

The device performance parameters, including CIE, CCT, luminance, and power efficiency have been tested. Under the magnetic field of $H_{\text{rms}} = 3.5$ kOe and the frequency of 50 Hz, green colored logo “PU” is demonstrated from Al, Cu-doped



ZnS-based MIL composites. On the other hand, white light emits from Al, Cu, Mn-doped ZnS-based composites. CIE coordinates are found to be (0.3462, 0.3735) and hence the CCT is determined to be 5027 K, indicating the obtained white MIL phosphor composite emits a somewhat cool white color. The luminance for green and white MIL is 21 and 19 cd/m² respectively. By analogy with EL, we have defined the new type MIL efficiency as $\eta \approx \text{light emission output} / \text{magnetic field input strength}$ in the unit of lm Oe⁻¹. The MIL efficiency is calculated to be 0.0014 and 0.0013 lm/Oe for green and white color severally. Moreover, RGB colors are realized from the MIL system with optimizing structure and test condition. The blue light color is obtained from the phosphor composite under a high magnetic frequency of ~250 Hz and magnetic field strength of 3.5 kOe. On the other hand, the long persistence material (Ca_{1-x}Sr_x) S: Eu and YAG: Ce were mixed to PDMS and combined with the magnetic composite laminate separately to emit red and white light color by energy transfer from the blue MIL induced by magnetic field.

This work represents the first demonstration of MIL luminescent in low magnetic field strength and room temperature. The proof-of-concept MIL devices have been demonstrated with RGB and white color emission, which can be



modulated in reversible and dynamical manners. Our results not only provide a new family member in both phosphor and magnetic materials to observe the novel MIL phenomenon, but also offer the new possibility to find prospective device applications, such as remote magnetic-optical sensor, memory devices, energy harvester, nondestructive environmental surveillance, and stimuli-responsive multimodal bioimaging.

5.2 Suggestions for future work

Recently, research on the magnetic inducing strain material has experienced a rapid expansion in recent decades, namely, magnetic shape memory alloy, Terfenol-D and ferrofluid pending continuous and vibrant growth of this field. Several key challenges need to be addressed. First, a more compact design is required for MIL to be realized in terms of response time, a magnitude of strain induction and stress induced. Second a finer particle size, higher brightness and more sensitive to strain induction is desired for the controlled synthesis of ML phosphors. The spatial resolution of luminescence of MIL of present work can be greatly improved with various method such as micropatterning technology employed during the fabrication



process, or localized magnetic moment. So that sensitivity and emission intensity can be enhanced, as well as stability and repeatability. We conclude these findings in Figure 5-1.

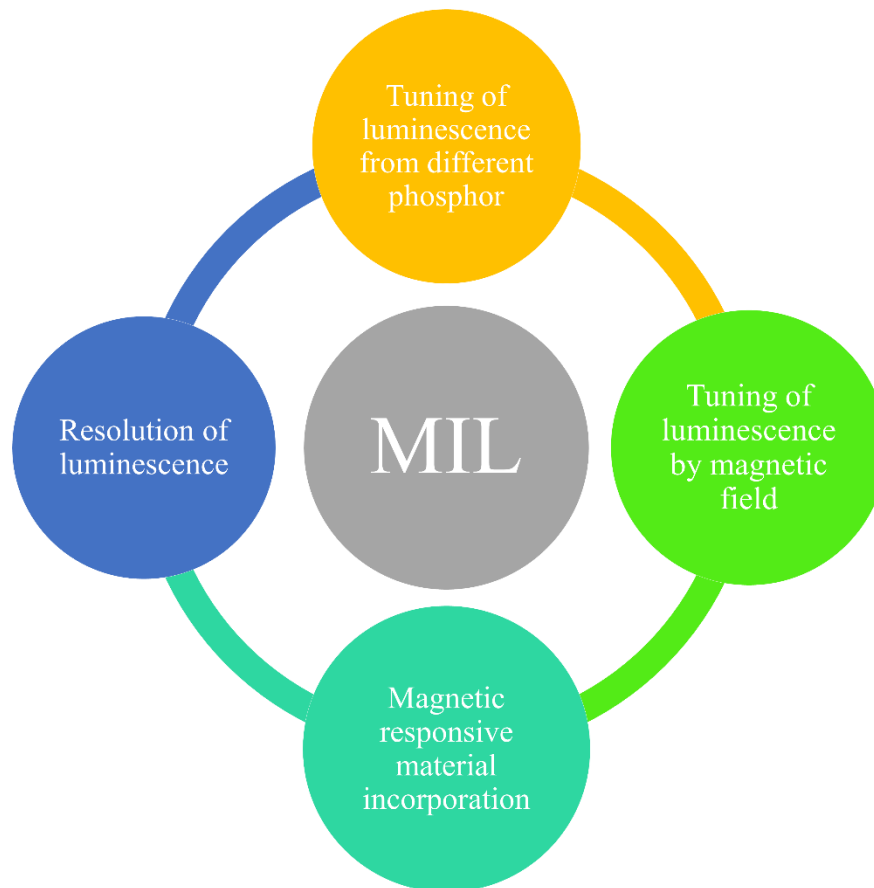


Figure 5-1 Schematic showing the prospect of future MIL investigation.

Such a new type of composite is capable of sensing or converting a dynamic magnetic action without the need of using a power unit to the composite. The composite performance parameters, including CIE, luminance, and power efficiency have been tested. Our results not only provide a new property and new family member



in both phosphor and magnetic materials to observe the novel MIL phenomenon, but also offer the new possibility to find prospective applications, such as remote magnetic-optical sensor, memory devices, energy harvester, nondestructive environmental surveillance, and stimuli-responsive multimodal bio and mechanical imaging.



References

1. Sailor, M.J. and Lee, E.J., Surface chemistry of luminescent silicon nanocrystallites. *Advanced Materials*, 1997. **9**(10): pp. 783-793.
2. Pan, D., Zhang, J., Li, Z., and Wu, M., Hydrothermal route for cutting graphene sheets into blue-luminescent graphene quantum dots. *Advanced Materials*, 2010. **22**(6): pp. 734-738.
3. Lima, N.B.D., Gonçalves, S.M.C., Júnior, S.A., and Simas, A.M., A Comprehensive Strategy to Boost the Quantum Yield of Luminescence of Europium Complexes. *Scientific Reports*, 2013. **3**: p. 2395.
4. Bredol, M., Kynast, U., and Ronda, C., Designing luminescent materials. *Advanced Materials*, 1991. **3**(7-8): pp. 361-367.
5. Feldmann, C., Jüstel, T., Ronda, C.R., and Schmidt, P.J., Inorganic luminescent materials: 100 years of research and application. *Advanced Functional Materials*, 2003. **13**(7): pp. 511-516.
6. Bai, G., Tsang, M.K., and Hao, J., Tuning the luminescence of phosphors: beyond conventional chemical method. *Advanced Optical Materials*, 2015.



- 3(4): pp. 431-462.
7. Ziemelis, K., Display technology: Glowing developments. *Nature*, 1999. **399**(6735): pp. 408-411.
 8. Bourzac, K., Quantum dots go on display. *Nature*, 2013. **493**(7432): p. 283.
 9. Dong, Z., Zhang, X., Gao, H., Luo, Y., Zhang, C., Chen, L., Zhang, R., Tao, X., Zhang, Y., and Yang, J., Generation of molecular hot electroluminescence by resonant nanocavity plasmons. *Nature Photonics*, 2010. **4**(1): pp. 50-54.
 10. Jha, P. and Chandra, B.P., Survey of the literature on mechanoluminescence from 1605 to 2013. *Luminescence*, 2014. **29**(8): pp. 977-93.
 11. Pust, P., Weiler, V., Hecht, C., Tücks, A., Wochnik, A.S., Henß, A.-K., Wiechert, D., Scheu, C., Schmidt, P.J., and Schnick, W., Narrow-band red-emitting Sr[LiAl₃N₄]:Eu²⁺ as a next-generation LED-phosphor material. *Nat Mater*, 2014. **13**(9): pp. 891-896.
 12. Zhu, H., Lin, C.C., Luo, W., Shu, S., Liu, Z., Liu, Y., Kong, J., Ma, E., Cao, Y., Liu, R.-S., and Chen, X., Highly efficient non-rare-earth red emitting phosphor for warm white light-emitting diodes. *Nat Commun*, 2014. **5**.
 13. Huang, X., Solid-state lighting: Red phosphor converts white LEDs. *Nat*



- Photon*, 2014. **8**(10): pp. 748-749.
14. Eddingsaas, N.C. and Suslick, K.S., Mechanoluminescence: Light from sonication of crystal slurries. *Nature*, 2006. **444**(7116): pp. 163-163.
 15. Zuo, Z., Pan, D., Jia, Y., Tian, J., Zhang, S., and Qiao, L., Enhanced magnetoelectric effect in magnetostrictive/piezoelectric laminates through adopting magnetic warm compaction Terfenol-D. *Journal of Alloys and Compounds*, 2014. **587**: pp. 287-289.
 16. Terasaki, N., Yamada, H., and Xu, C.-N., Ultrasonic wave induced mechanoluminescence and its application for photocatalysis as ubiquitous light source. *Catalysis Today*, 2013. **201**: pp. 203-208.
 17. Jeong, S.M., Song, S., Joo, K.-I., Kim, J., Hwang, S.-H., Jeong, J., and Kim, H., Bright, wind-driven white mechanoluminescence from zinc sulphide microparticles embedded in a polydimethylsiloxane elastomer. *Energy Environ. Sci.*, 2014. **7**(10): pp. 3338-3346.
 18. Chen, L., Wong, M.-C., Bai, G., Jie, W., and Hao, J., White and green light emissions of flexible polymer composites under electric field and multiple strains. *Nano Energy*, 2014.



19. Zhang, Y., Gao, G., Chan, H.L., Dai, J., Wang, Y., and Hao, J., Piezotronic effect-induced dual-mode light and ultrasound emissions from ZnS:Mn/PMN-PT thin-film structures. *Advanced Materials*, 2012. **24**(13): pp. 1729-35.
20. Chandra, B., Chandra, V., and Jha, P., Models for intrinsic and extrinsic fracto-mechanoluminescence of solids. *Journal of Luminescence*, 2013. **135**: pp. 139-153.
21. Chandra, B.P., Baghel, R.N., Luka, A.K., Sanodiya, T.R., Kuraria, R.K., and Kuraria, S.R., Strong mechanoluminescence induced by elastic deformation of rare-earth-doped strontium aluminate phosphors. *Journal of Luminescence*, 2009. **129**(7): pp. 760-766.
22. Chandra, B.P., Mahobia, S.K., Jha, P., Kuraria, R.K., Kuraria, S.R., Baghel, R.N., and Thaker, S., Transient behaviour of the mechanoluminescence induced by impulsive deformation of fluorescent and phosphorescent crystals. *Journal of Luminescence*, 2008. **128**(12): pp. 2038-2047.
23. Wang, Z.L., Piezotronic and Piezophototronic Effects. *Journal of Physical Chemistry Letters*, 2010. **1**(9): pp. 1388-1393.



24. Wang, Z.L., Piezopotential gated nanowire devices: Piezotronics and piezophotonics. *Nano Today*, 2010. **5**(6): pp. 540-552.
25. Corrado, C., Jiang, Y., Oba, F., Kozina, M., Bridges, F., and Zhang, J.Z., Synthesis, Structural, and Optical Properties of Stable ZnS:Cu,Cl Nanocrystals. *Journal of Physical Chemistry A*, 2009. **113**(16): pp. 3830-3839.
26. Chandra, B.P., Xu, C.N., Yamada, H., and Zheng, X.G., Luminescence induced by elastic deformation of ZnS:Mn nanoparticles. *Journal of Luminescence*, 2010. **130**(3): pp. 442-450.
27. Wang, X., Yamada, H., Nishikubo, K., and Xu, C.-N., Electrostrictive properties of Pr-doped BaTiO₃-CaTiO₃ ceramics. *Japanese journal of applied physics*, 2006. **45**(2R): p. 813.
28. Sohn, K.S., Seo, S.Y., Kwon, Y.N., and Park, H.D., Direct observation of crack tip stress field using the mechanoluminescence of SrAl₂O₄:(Eu,Dy,Nd). *Journal of the American Ceramic Society*, 2002. **85**(3): pp. 712-714.
29. Zhang, H., Yamada, H., Terasaki, N., and Xu, C.-N., Blue light emission from stress-activated CaYAl₃O₇: Eu. *Journal of The Electrochemical Society*, 2008. **155**(5): pp. J128-J131.



30. Peng, D., Ju, Q., Chen, X., Ma, R., Chen, B., Bai, G., Hao, J., Qiao, X., Fan, X., and Wang, F., Lanthanide-Doped Energy Cascade Nanoparticles: Full Spectrum Emission by Single Wavelength Excitation. *Chemistry of Materials*, 2015. **27**(8): pp. 3115-3120.
31. Zhang, Y. and Hao, J., Metal-ion doped luminescent thin films for optoelectronic applications. *Journal of Materials Chemistry C*, 2013. **1**(36): pp. 5607-5618.
32. Peng, D.F., Chen, B., and Wang, F., Recent Advances in Doped Mechanoluminescent Phosphors. *Chempluschem*, 2015. **80**(8): pp. 1209-+.
33. Xu, C.-N., Zheng, X.-G., Watanabe, T., Akiyama, M., and Usui, I., Enhancement of adhesion and triboluminescence of ZnS: Mn films by annealing technique. *Thin Solid Films*, 1999. **352**(1): pp. 273-277.
34. Jeong, S.M., Song, S., Lee, S.K., and Ha, N.Y., Color manipulation of mechanoluminescence from stress-activated composite films. *Advanced Materials*, 2013. **25**(43): pp. 6194-200.
35. Wong, M.C., Chen, L., Tsang, M.K., Zhang, Y., and Hao, J.H., Magnetic-Induced Luminescence from Flexible Composite Laminates by Coupling



- Magnetic Field to Piezophotonic Effect. *Advanced Materials*, 2015. **27**(30): pp. 4488-4495.
36. Zhang, H., Terasaki, N., Yamada, H., and Xu, C.-N., Development of mechanoluminescent micro-particles $\text{Ca}_2\text{MgSi}_2\text{O}_7:\text{Eu,Dy}$ and their application in sensors. *Thin Solid Films*, 2009. **518**(2): pp. 610-613.
37. Kher, R., Dhoble, S., Pandey, R., Upadhyay, A., and Khokhar, M., Impulsive excitation of mechanoluminescence in gamma-irradiated $\text{CaSO}_4:\text{Eu}$ phosphors. *Radiation Effects & Defects in Solids*, 2011. **166**(1): pp. 63-66.
38. Zhang, J.-C., Xu, C.-N., Kamimura, S., Terasawa, Y., Yamada, H., and Wang, X., An intense elastico-mechanoluminescence material $\text{CaZnOS}:\text{Mn}^{2+}$ for sensing and imaging multiple mechanical stresses. *Optics express*, 2013. **21**(11): pp. 12976-12986.
39. Chandra, B., Development of mechanoluminescence technique for impact studies. *Journal of Luminescence*, 2011. **131**(6): pp. 1203-1210.
40. Fontenot, R.S., Hollerman, W.A., Bhat, K.N., and Aggarwal, M.D., Comparison of the triboluminescent properties for europium tetrakis and $\text{ZnS}:\text{Mn}$ powders. *Journal of Theoretical and Applied Physics*, 2012. **6**(1): pp. 1-9.



41. Terasaki, N., Zhang, H., Imai, Y., Yamada, H., and Xu, C.-N., Hybrid material consisting of mechanoluminescent material and TiO₂ photocatalyst. *Thin Solid Films*, 2009. **518**(2): pp. 473-476.
42. Wang, X., Zhang, H., Yu, R., Dong, L., Peng, D., Zhang, A., Zhang, Y., Liu, H., Pan, C., and Wang, Z.L., Dynamic pressure mapping of personalized handwriting by a flexible sensor matrix based on the mechanoluminescence process. *Advanced Materials*, 2015. **27**(14): pp. 2324-31.
43. Munoz-Garcia, A.B. and Seijo, L., Ce and La Single- and Double-Substitutional Defects in Yttrium Aluminum Garnet: First-Principles Study. *Journal of Physical Chemistry A*, 2011. **115**(5): pp. 815-823.
44. Mirhosseini, R., Schubert, M.F., Chhajed, S., Cho, J., Kim, J.K., and Schubert, E.F., Improved color rendering and luminous efficacy in phosphor-converted white light-emitting diodes by use of dual-blue emitting active regions. *Optics Express*, 2009. **17**(13): pp. 10806-10813.
45. Pan, Z., Lu, Y.-Y., and Liu, F., Sunlight-activated long-persistent luminescence in the near-infrared from Cr³⁺-doped zinc gallogermanates. *Nat Mater*, 2012. **11**(1): pp. 58-63.



46. Liu, F., Yan, W., Chuang, Y.-J., Zhen, Z., Xie, J., and Pan, Z., Photostimulated near-infrared persistent luminescence as a new optical read-out from Cr³⁺-doped LiGa₅O₈. *Scientific Reports*, 2013. **3**: pp. 1554.
47. Pan, Z., Lu, Y.Y., and Liu, F., Sunlight-activated long-persistent luminescence in the near-infrared from Cr³⁺-doped -doped zinc gallogermanates. . *Nat Mater*, 2012. **11**(1): pp. 58-63.
48. Rodríguez Burbano, D.C., Rodríguez, E.M., Dorenbos, P., Bettinelli, M., and Capobianco, J.A., The near-IR photo-stimulated luminescence of CaS:Eu²⁺/Dy³⁺-nanophosphors. *J. Mater. Chem. C*, 2014. **2**(2): pp. 228-231.
49. Chen, W., Wang, Y., Zeng, W., Han, S., Li, G., Guo, H., Li, Y., and Qiang, Q., Long persistent composite phosphor CaAl₂O₄:Eu²⁺,Nd³⁺/Y₃Al₅O₁₂:Ce³⁺: a novel strategy to tune the colors of persistent luminescence. *New Journal of Chemistry*, 2016. **40**(1): pp. 485-491.
50. Wondraczek, L., Batentschuk, M., Schmidt, M.A., Borchardt, R., Scheiner, S., Seemann, B., Schweizer, P., and Brabec, C.J., Solar spectral conversion for improving the photosynthetic activity in algae reactors. *Nat Commun*, 2013. **4**: p. 2047.



51. Lin, J., Huang, Y., Bando, Y., Tang, C., and Golberg, D., BN tubular layer-sheathed CaS:Eu²⁺ nanowires as stable red-light-emitting nanophosphors. *Chem. Commun.*, 2009(43): pp. 6631-6633.
52. Fujio, Y., Xu, C.-N., Nishibori, M., Teraoka, Y., Kamitani, K., Terasaki, N., and Ueno, N., Development of highly sensitive mechanoluminescent sensor aiming at small strain measurement. *Journal of Advanced Dielectrics*, 2014. **04**(02): p. 1450016.
53. Pamme, N., Magnetism and microfluidics. *Lab on a Chip*, 2006. **6**(1): pp. 24-38.
54. Wang, S.X., Sun, N.X., Yamaguchi, M., and Yabukami, S., Sandwich films: Properties of a new soft magnetic material. *Nature*, 2000. **407**(6801): pp. 150-151.
55. Osaka, T., Takai, M., Hayashi, K., Ohashi, K., Saito, M., and Yamada, K., A soft magnetic CoNiFe film with high saturation magnetic flux density and low coercivity. *Nature*, 1998. **392**(6678): pp. 796-798.
56. Gavrilă, H. and Ionita, V., Crystalline and amorphous soft magnetic materials and their applications- status of art and challenges. *Journal of Optoelectronics*



- and Advanced Materials(Romania)*, 2002. **4**(2): pp. 173-192.
57. Li, X. and Takahashi, S., Synthesis and magnetic properties of Fe–Co–Ni nanoparticles by hydrogen plasma–metal reaction. *Journal of Magnetism and Magnetic Materials*, 2000. **214**(3): pp. 195-203.
58. Azinheira, J., Reis, L., and Ribeiro, A., Influence of the Wave Form on the Material Response Delay. *Shock and Vibration*, 2014. **2014**.
59. Bertotti, G., General properties of power losses in soft ferromagnetic materials. *Magnetics, IEEE Transactions on*, 1988. **24**(1): pp. 621-630.
60. Philippova, O., Barabanova, A., Molchanov, V., and Khokhlov, A., Magnetic polymer beads: Recent trends and developments in synthetic design and applications. *European polymer journal*, 2011. **47**(4): pp. 542-559.
61. White, S.R., Sottos, N.R., Geubelle, P.H., Moore, J.S., Kessler, M.R., Sriram, S.R., Brown, E.N., and Viswanathan, S., Autonomic healing of polymer composites. *Nature*, 2001. **409**(6822): pp. 794-797.
62. Langer, R. and Tirrell, D.A., Designing materials for biology and medicine. *Nature*, 2004. **428**(6982): pp. 487-492.
63. Eerenstein, W., Mathur, N.D., and Scott, J.F., Multiferroic and magnetoelectric



- materials. *Nature*, 2006. **442**(7104): pp. 759-765.
64. Rodríguez, C., Barrio, A., Orue, I., Vilas, J.L., León, L.M., Barandiarán, J.M., and Fdez-Gubieda Ruiz, M.L., High magnetostriction polymer-bonded Terfenol-D composites. *Sensors and Actuators A: Physical*, 2008. **142**(2): pp. 538-541.
65. Rolfs, K., Chmielus, M., Guldbakke, J.M., Wimpory, R.C., Raatz, A., Petry, W., Müllner, P., and Schneider, R., Key Properties of Ni-Mn-Ga Based Single Crystals Grown with the SLARE Technique. *Advanced Engineering Materials*, 2012. **14**(8): pp. 614-635.
66. Rani, R.J., Pandi, R.S., Seenithurai, S., Kumar, S.V., Muthuraman, M., and Mahendran, M., Structural, Thermal and Magnetic Characterization of Ni-Mn-Ga Ferromagnetic Shape Memory Alloys. *American Journal of Condensed Matter Physics*, 2012. **1**(1): pp. 1-7.
67. Murray, S.J., Marioni, M., Allen, S.M., O'Handley, R.C., and Lograsso, T.A., 6% magnetic-field-induced strain by twin-boundary motion in ferromagnetic Ni-Mn-Ga. *Applied Physics Letters*, 2000. **77**(6): p. 886.
68. Yamahata, C., Lotto, C., Al-Assaf, E., and Gijs, M.A.M., A PMMA valveless



- micropump using electromagnetic actuation. *Microfluidics and Nanofluidics*, 2004. **1**(3): pp. 197-207.
69. Huang, T.-C., Du, M.-J., Kang, Y.-C., Peng, R.-H., Chen, K.-H., Lin, Y.-H., Tsai, T.-Y., Lee, C.-C., Chen, L.-D., and Chen, J.-L., 120% Harvesting Energy Improvement by Maximum Power Extracting Control for High Sustainability Magnetic Power Monitoring and Harvesting System. *Ieee Transactions on Power Electronics*, 2015. **30**(4): pp. 2262-2274.
70. Yang, J.Y., Dong, X.Y., Zheng, Y.Z., Ni, K., Chan, C.C., and Shum, P.P., Magnetic Field Sensing With Reflectivity Ratio Measurement of Fiber Bragg Grating. *Ieee Sensors Journal*, 2015. **15**(3): pp. 1372-1376.
71. Wilhelm, C., Elias, F., Browaeys, J., Ponton, A., and Bacri, J.-C., Local rheological probes for complex fluids: Application to Laponite suspensions. *Physical Review E*, 2002. **66**(2): p. 021502.
72. Graydon, O., Materials: Magnetic opportunities. *Nat Photon*, 2015. **9**(9): pp. 558-558.
73. Daniel-da-Silva, A.L., Carvalho, R.S., and Trindade, T., Magnetic hydrogel nanocomposites and composite nanoparticles—a review of recent patented



- works. *Recent patents on nanotechnology*, 2013. **7**(2): pp. 153-166.
74. Carlson, J.D. and Jolly, M.R., MR fluid, foam and elastomer devices. *Mechatronics*, 2000. **10**(4–5): pp. 555-569.
75. Thevenot, J., Oliveira, H., Sandre, O., and Lecommandoux, S., Magnetic responsive polymer composite materials. *Chem Soc Rev*, 2013. **42**(17): pp. 7099-116.
76. Chappert, C., Fert, A., and Van Dau, F.N., The emergence of spin electronics in data storage. *Nat Mater*, 2007. **6**(11): pp. 813-823.
77. Pleasants, S., Magnetic fluids: Magnetic-field sensor. *Nat Photon*, 2014. **8**(3): pp. 168-168.
78. Olsson, R.T., Azizi Samir, M.A.S., Salazar Alvarez, G., BelovaL, StromV, Berglund, L.A., IkkalaO, NoguesJ, and Gedde, U.W., Making flexible magnetic aerogels and stiff magnetic nanopaper using cellulose nanofibrils as templates. *Nat Nano*, 2010. **5**(8): pp. 584-588.
79. Torchilin, V.P., Multifunctional, stimuli-sensitive nanoparticulate systems for drug delivery. *Nat Rev Drug Discov*, 2014. **13**(11): pp. 813-827.
80. Meng, J., Xiao, B., Zhang, Y., Liu, J., Xue, H., Lei, J., Kong, H., Huang, Y.,



- Jin, Z., Gu, N., and Xu, H., Super-paramagnetic responsive nanofibrous scaffolds under static magnetic field enhance osteogenesis for bone repair in vivo. *Scientific Reports*, 2013. **3**: p. 2655.
81. Bonmassar, G., Lee, S.W., Freeman, D.K., Polasek, M., Fried, S.I., and Gale, J.T., Microscopic magnetic stimulation of neural tissue. *Nat Commun*, 2012. **3**: p. 921.
82. Xia, K., Vanner, M.R., and Twamley, J., An opto-magneto-mechanical quantum interface between distant superconducting qubits. *Scientific Reports*, 2014. **4**: p. 5571.
83. Böse, H. and Röder, R., Magnetorheological elastomers with high variability of their mechanical properties. *Journal of Physics: Conference Series*, 2009. **149**(1): p. 012090.
84. Mietta, J.L., Ruiz, M.M., Antonel, P.S., Perez, O.E., Butera, A., Jorge, G., and Negri, R.M., Anisotropic magnetoresistance and piezoresistivity in structured Fe₃O₄-silver particles in PDMS elastomers at room temperature. *Langmuir*, 2012. **28**(17): pp. 6985-96.
85. Ginder, J.M., Clark, S.M., Schlotter, W.F., and Nicholas, M.E.,



- Magnetostrictive phenomena in magnetorheological elastomers. *International Journal of Modern Physics B*, 2002. **16**(17n18): pp. 2412-2418.
86. Mitumata, T., Ikeda, K., Gong, J.P., Osada, Y., Szabó, D., and Zrínyi, M., Magnetism and compressive modulus of magnetic fluid containing gels. *Journal of Applied Physics*, 1999. **85**(12): pp. 8451-8455.
87. Breulmann, M., Cölfen, H., Hentze, H.P., Antonietti, M., Walsh, D., and Mann, S., Elastic Magnets: Template - Controlled Mineralization of Iron Oxide Colloids in a Sponge-like Gel Matrix. *Advanced Materials*, 1998. **10**(3): pp. 237-241.
88. Lu, Y., Yin, Y., Mayers, B.T., and Xia, Y., Modifying the surface properties of superparamagnetic iron oxide nanoparticles through a sol-gel approach. *Nano letters*, 2002. **2**(3): pp. 183-186.
89. Cheng, J.Y., Ross, C., Chan, V.H., Thomas, E.L., Lammertink, R.G., and Vancso, G.J., Formation of a cobalt magnetic dot array via block copolymer lithography. *Advanced Materials*, 2001. **13**(15): pp. 1174-1178.
90. Ma, H., Jen, A.Y., and Dalton, L.R., Polymer- Based Optical Waveguides: Materials, Processing, and Devices. *Advanced materials*, 2002. **14**(19): p.



1339-1365.

91. Gdovinová, V., Tomašovičová, N., Éber, N., Tóth-Katona, T., Závíšová, V., Timko, M., and Kopčanský, P., Influence of the anisometry of magnetic particles on the isotropic–nematic phase transition. *Liquid Crystals*, 2014. **41**(12): pp. 1773-1777.
92. Evans, B.A., Shields, A.R., Carroll, R.L., Washburn, S., Falvo, M.R., and Superfine, R., Magnetically actuated nanorod arrays as biomimetic cilia. *Nano Letters*, 2007. **7**(5): pp. 1428-1434.
93. Evans, B.A., Fiser, B.L., Prins, W.J., Rapp, D.J., Shields, A.R., Glass, D.R., and Superfine, R., A Highly Tunable Silicone-Based Magnetic Elastomer with Nanoscale Homogeneity. *Journal of magnetism and magnetic materials*, 2012. **324**(4): pp. 501-507.
94. Jolly, M.R., Carlson, J.D., Muñoz, B.C., and Bullions, T.A., The magnetoviscoelastic response of elastomer composites consisting of ferrous particles embedded in a polymer matrix. *Journal of Intelligent Material Systems and Structures*, 1996. **7**(6): pp. 613-622.
95. Halsey, T.C. and Toor, W., Fluctuation-induced couplings between defect



- lines or particle chains. *Journal of statistical physics*, 1990. **61**(5-6): pp. 1257-1281.
96. Kallio, M., *The elastic and damping properties of magnetorheological elastomers*. 2005: VTT Technical Research Centre of Finland.
97. Huang, J., Yang, Y., Xue, S., Yang, B., Liu, S., and Shen, J., Photoluminescence and electroluminescence of ZnS: Cu nanocrystals in polymeric networks. *Applied physics letters*, 1997. **70**(18): pp. 2335-2337.
98. Chandra, B.P., Chandra, V.K., Mahobia, S.K., Jha, P., Tiwari, R., and Haldar, B., Real-time mechanoluminescence sensing of the amplitude and duration of impact stress. *Sensors and Actuators A: Physical*, 2012. **173**(1): pp. 9-16.
99. Tu, D., Xu, C.-N., Fujio, Y., and Yoshida, A., Mechanism of mechanical quenching and mechanoluminescence in phosphorescent CaZnOS:Cu. *Light: Science & Applications*, 2015. **4**(11): p. e356.
100. Mamedov, A.A., Kotov, N.A., Prato, M., Guldi, D.M., Wicksted, J.P., and Hirsch, A., Molecular design of strong single-wall carbon nanotube/polyelectrolyte multilayer composites. *Nat Mater*, 2002. **1**(3): p. 190-194.



101. Yano, H., Sugiyama, J., Nakagaito, A.N., Nogi, M., Matsuura, T., Hikita, M., and Handa, K., Optically Transparent Composites Reinforced with Networks of Bacterial Nanofibers. *Advanced Materials*, 2005. **17**(2): pp. 153-155.
102. Yang, Z., Li, X., Yang, Y., and Li, X., The influence of different conditions on the luminescent properties of YAG:Ce phosphor formed by combustion. *Journal of Luminescence*, 2007. **122–123**: pp. 707-709.